이학박사 학위논문

Theoretical and Computational Study on Dynamically Heterogeneous Systems

동력학적 불균일성을 갖는 계에 대한 이론 및 전산모사 연구

2015년 8월

서울대학교 대학원
화학부 물리화학 전공
김 소 리

Theoretical and Computational Study on Dynamically Heterogeneous Systems

동력학적 불균일성을 갖는 계에 대한 이론 및 전산모사 연구

지도교수 정 연 준

이 논문을 이학박사 학위논문으로 제출함

2015년 7월

서울대학교 대학원

화학부 물리화학 전공

김 소 리

김소리의 이학박사 학위논문을 인준함

2015년 6월

위 원 장	이 상 엽	(인)
부위원장	정 연 준	(인)
위 원	신 석 민	(인)
위 원	석 차 옥	(인)
위 원	성 봉 준	(인)

Contents

List of Figures

List of Tables

Abstract

Dynamic heterogeneity has gained much attention for describing distinctive properties of the supercooled liquids. In this thesis, dynamically heterogeneous systems are investigated using computational methods.

First, the dimensional dependence of dynamic heterogeneity in the supercooled liquid systems using kinetically constrained models (KCMs) is investigated. Higher dimensional generalization of 1-dimensional East model and its variation with an embedded probe particle are used as a representative fragile liquid system. We investigate the upper critical dimension of our model system using the fractional scaling behavior of the Stokes-Einsten relation. In contrast to previous simulation studies on the hard sphere model and theoretical studies based on the mean field approach, our study suggests that the East model has an infinite upper critical dimension.

Second, the dynamic heterogeneity in the fragile-to-strong crossover model of the supercooled liquids is studied using the model that linearly interpolates between the strong-liquid and the fragile-liquid by an asymmetry parameter b. We investigate fractional Stokes-Einstein relations observed in this model. When b is fixed, the system shows a constant power law exponent under the temperature change, and the exponent has the value between the strong liquid

and the fragile liquid values. We find a smooth transition of the exponent from 0.66 to 0.73 as b is decreased.

Lastly, the dynamic heterogeneity and its length scale found in the coarse-grained ionic liquid model system is numerically investigated. Cations and anions composing the ionic liquids are modeled as two spheres with positive charges and a single sphere with a negative charge, respectively. To study the effect of the charge distributions on the cations, two schematic models with different charge distributions are used and the model without charge is also considered as a counterpart. All three models show significant increase of the dynamic heterogeneity as the temperature is lowered. The dynamic heterogeneity is quantified via the well-known four-point susceptibility, $\chi_4(t)$, which measures the fluctuation of time correlation functions. The dynamic correlation length is calculated by fitting the dynamic structure factor, $S_4(k,t)$, with the Ornstein-Zernike form. Obtained time and length scales exhibit power law relations at low temperatures, similar to various supercooled liquid models. Especially, the model systems with charge show unusual crossover behaviors which is not observed in the uncharged model system. We ascribe the crossover behavior to the enhanced cage effect caused by charges on the particles.

Keywords: Dynamic heterogeneity, Kinetically constrained models, Stokes-Einstein relation, Room-temperature ionic liquids, Monte-Carlo simulation, Molecular dynamics simulation

Student Number: 2008-20308

Chapter 1

Overview

1.1 Supercooled liquids and glass transition

Supercooled liquids can be formed when the temperature of a material is rapidly cooled down below the melting temperature. Preserving their liquid structures, the supercooled liquids are considered to be in a metastable state. The properties of the supercooled liquids are distinguished compared to normal liquid states: (1) extremely slow dynamics (high viscosity), (2) stretched exponential form of the correlation function, (3) heterogeneous dynamics, and so on.[1–9] The supercooled liquids can be classified into two groups, which are strong and fragile liquids, depend on the functional form of the relaxation times. This terminology is first proposed by Angell.[1] Strong materials have the relaxation times which grow with a lowering temperature, T, in an Arrhenius fashion, $\tau = \tau_0 \exp(E/T)$, where E is an effective energy barrier of relaxation process. For strong liquids, E is constant under the temperature change. Fragile materials show different temperature dependence on the relaxation time that the effective energy barrier is growing as the temperature

is lowered. This is called super-Arrhenius behavior. Various functional forms have been proposed to describe the growing relaxation times of the fragile liquids based on the different theoretical processes: (1) Vogel-Fulcher-Tamman (VFT) formula: $\tau = \tau_0 \exp(A/(T - T_0))$,[10] (2) Mode coupling theory (MCT) : $\tau \propto (T - T_0)^{-\gamma}$,[11] (3) facilitation picture : $\tau = \tau_0 \exp(B(1/T - 1/T_o)^2)$,[12] where A and B are fitting parameters.

When the supercooled liquids are cooled further, the dynamics of the materials are so slow that the system becomes like amorphous solids, which is called glass. This change of state is considered as a glass transition and this is why the supercooled liquids are often called the glass formers. However, the existence of the glass transition is in a long debate because proper order parameter related to the glass transition has not been found. Furthermore, observed glass transition temperature, T_g, is not a fixed quantity, but T_g depends on the cooling rate. There are different views which insist that the glass transition is a real physical thermodynamic phase transition or it is simple crossover behavior. Many theoretical scenarios related to the glass transition have been proposed, which will be shown in the next section.

1.2 Theories

Theories related to the glass transition could be classified into two groups: thermodynamic view and dynamical view. The origins of the thermodynamic view are often attributed to Goldstein[13] and to Adam & Gibbs.[10] Energy landscape theory and Adam-Gibbs theory are well known related theories.[10,13–15] In this view, as the temperature is decreased, the system is trapped in the

basin and it takes a long time to overcome the barrier and relax. The number of the metastable states that the system can visit is defined as N_m. Then, the configuration entropy can be written by $S_c = \log N_m$. At $T = T_g$, the system can not evolve to other basins so that $N_m = 1$ and $S_c = 0$. In the Adam-Gibbs theory,[10] the relation between S_c and τ is as follows: $\tau = \tau_0 \exp(A/TS_c)$, where A is constant. In this sense, the relaxation times diverge when $T = T_g$. In the thermodynamic view, glass states can be regarded as liquids which have infinitely long relaxation times. Although the thermodynamic approach has successfully explained some parts of physical properties of the liquids, there are many unexplained exceptions such that thermodynamic approach may not regarded as the most fundamental theory to describe the glass transition.

Meanwhile, dynamical view attributes the distinctive properties of the supercooled liquids to kinetics. In this approach, heterogeneous dynamics found in the supercooled liquids play a key role for describing the properties of the supercooled liquids.[16–19] In contrast to thermodynamics which pertain to the mean values, dynamical view concentrates on the fluctuation of dynamic quantities. In many studies, inhomogeneously distributed local dynamics, so-called dynamic heterogeneity, have been observed. Clustering of fast and slow regions is getting stronger as the temperature of the system is lowered. This clustering behavior is found to be transient in time and the characteristic time scale of clustering is often called the lifetime of the dynamic heterogeneity. The lifetime of dynamic heterogeneity and the length scale of the cluster becomes longer at lower temperatures. Growing length scales and their relation to timescales in glass-forming liquids are intriguing and important subject to investigate.[20–25] Various physical aspects have been explained with this view, including well-

known violation of Stokes-Einstein relation.[22,26,27]

In spite of the various theoretical and numerical studies performed in the past, intense research on the supercooled liquids and the glass transition is ongoing in search of the most regorous first-principle theory. Because of extremely slow dynamics of the supercooled liquids at low temperatures, it is hard to investigate glass forming systems in experiments and simulation studies.

1.3 Outline of the thesis

In this thesis, dynamically heterogeneous systems are studied using computer simulations and statistical mechanical theories. Especially, the dynamics of the supercooled liquids system and the RTILs model will be discussed. Approaching with dynamical view, KCMs will be introduced to describe the supercooled liquids in Chapter 2. In Chapter 3 and Chapter 4, two intriguing subjects will be examined, which are the dimensional dependence of the East model and the fragile-to-strong crossover behavior in 1-dimensional KCMs. Also, the effect of charge distributions on the heterogeneous dynamics of RTILs will be discussed using the theoretical method that has originally been proposed for explaining the behavior of the supercooled liquids, in Chapter 5. Lastly, the conclusion of the thesis is sketched in Chapter 6.

1.4 Dynamic heterogeneity in kinetically constrained models and specific issues

In the first part of this thesis, the computational model systems called kinetically constrained models (KCMs) are proposed utilizing dynamical view. In an effort to describe the glassy dynamics, KCMs focus on the dynamic behavior of the supercooled liquids. In this approach, thermodynamics plays a very limited role, while the local kinetic rules govern the relaxation process. Detailed description of various KCMs will be shown in Chapter 2. We use KCMs to investigate specific issues on the supercooled liquids. First, the results of the study on the upper critical dimension and dimensional dependence of the dynamic heterogeneity of the KCMs will be shown. The upper critical dimension is the lowest dimension above which the mean-field theory is correct. It has been argued that the upper critical dimension of the supercooled liquid would be 8, from the theoretical and simulation approaches.[28–31] However, our simulation result strongly supports the fact that the upper critical dimension of the East model which is one of the cooperative KCMs is infinite. Detailed contents and simulation results will be followed in Chapter 3. Second, the crossover behavior of 1-dimensional KCMs is investigated. Using the model that linearly interpolates between the strong and the fragile-liquid like behavior, we observe a smooth transition of the power law exponent of fractional Stokes-Einstein relation. The results are shown in Chapter 4.

1.5 Dynamic heterogeneity in room-temperature ionic liquids

In the second part of the thesis, among the numerous systems that shows heterogeneous dynamics, the simple toy model of room-temperature ionic liquids (RTILs) are investigated via molecular dynamics simulations. Due to the considerable size difference between cations and anions, RTILs exist in a liquid phase near the room temperature. The size difference also results in heterogeneous dynamics, similar to the model systems of the supercooled liquids. The evidences of dynamic heterogeneity have been found through theoretical and experimental studies.[4,27,32,33] We use coarse-grained ionic liquid model systems to study the effect of charge distributions on the dynamic heterogeneity. Particularly, we adopt the four-point density correlation functions to analyze the time scale and the length scale of the dynamic heterogeneity. Related scaling laws are examined and the power law exponents are also calculated. We confirm that the effect of charge is realized by enhanced cage effect resulting the crossover behavior at intermediate time and length scales. The simulation results are shown in Chapter 5.

Chapter 2

Introduction to Kinetically Constrained Models

2.1 General features of kinetically constrained models

One of the distinctive features of the supercooled liquids is growing viscosity (or relaxation time) at low temperature. In many theoretical and computer simulation studies, it has been known that the origin of this slowing down is dynamical, while thermodynamics plays a very limited role. For example, molecular dynamics simulation on the supercooled liquids system shows that the radial distribution functions in different temperatures are similar to each other.[34] In the view that the local dynamics plays an important role to the interesting properties of glass formers, simple theoretical models, called kinetically constrained models (KCMs), have been proposed.[35,36]

KCMs are simple lattice models designed to describe supercooled liquids. KCMs usually have simple and trivial thermodynamic properties. However, the

system is controlled by kinetic constraints which reflects local dynamics of real systems. The lattice sites, which usually have binary value $n_i = 0, 1$ where i is an index of lattice site, can be regarded as a coarse-grained local domain of a dense molecular system. In the realistic system, the energetic interactions between molecules would be very weak beyond certain molecular length scale, but the kinetic interactions between the local domains can not be ignored, which contributes to the local restrictions in the dynamics. In this basis, the lattice sites in KCMs typically do not interact with other lattice sites. KCMs aim to answer the question that how much we can understand the glassy behavior without invoking the effect of equilibrium structures. Generally, KCMs use local constraints, but they can lead to cooperative and hierarchical relaxation mechanisms.

Historically, various versions of KCMs have been introduced in many computational studies. The KCMs can be classified into two groups, which are conservative (particle based) and non-conservative (field based) models. Conservative KCMs are lattice gases where the variable n_i represent the presence or the absence of particles with $n_i = 1$ or $n_i = 0$, respectively. The particle can jump into the neighboring site under the kinetic constraint which generally requires minimum number of vacancies around the site i. The total number of particle, $N_p = \sum_i^{N_s} n_i$, is conserved, where N_s is the number of sites. Most commonly used conservative KCMs are triangular lattice gas models[37,38] and the Kob-Andersen model.[39] In non-conservative KCMs, the lattice sites can be regarded as a coarse-graining of local areas that are not energetically interacting with neighboring areas. In most cases, the lattice sites have binary values representing sparse (mobile) or dense (immobile) sites with $n_i = 1$ or

$n_i = 0$, respectively. Note that sparse states are called excitation in some context. The value of each site can be viewed as a mobility field, so that sometime non-conservative KCMs are called field-based KCMs. Typically, the kinetic constraint of non-conservative KCMs requires a minimum number of neighboring sparse state to change the configuration, n_i, of site i. Representative models of non-conservative KCMs are the Fredrickson-Andersen (FA) model[40] and the East model.[41]

As described above, the key property of all KCMs is that there should be empty or mobile sites for the system to undergo changes in configuration. The underlying physical basis is that there should be mobile regions around the local area when the particles reorganize their local structures. As the concentration of free volume (mobile region) is decreased, the relaxation time of system would increase, reflecting the low temperature condition of the supercooled liquids. Another important condition for the KCMs is the satisfaction of the detailed balance. With this condition, the equilibrium trajectories with the Boltzmann distribution can be generated. Because there is no energetic interactions, randomly distributed configuration guarantees the equilibrium state. Furthermore, static phase transitions are not possible in the simplest case, which satisfies the purpose of KCMs: the exclusion of non-trivial thermodynamic transition.

2.2 Spin facilitated models

Non-conservative KCMs are often called spin facilitated models (SFMs) because the condition of lattice sites can be expressed with two state spins. We especially review SFMs with the FA model and the East model.[40,41] These

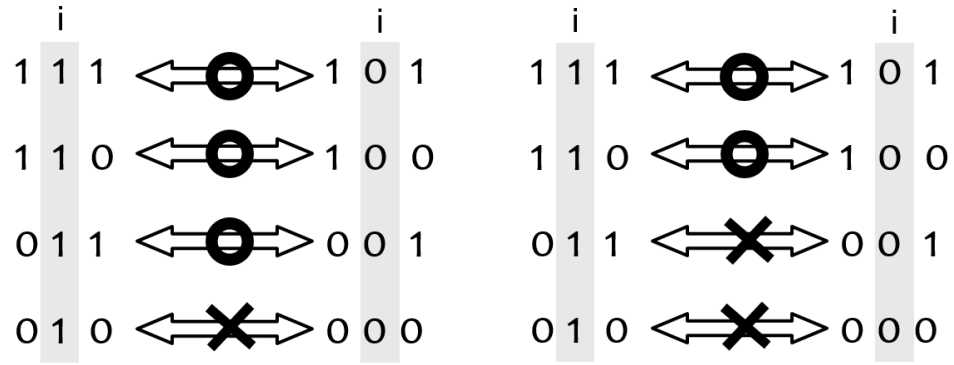

Figure 2.1: The illustration of facilitation rule for (a) 1-dimensional FA model and (b) 1-dimensional East model. For the FA model, the spin at the site i can change its configuration if there is at least one active spin at the neighbor sites. In contrast, the East model only accounts the configuration of left site.

models are representative models of non-cooperative and cooperative models, respectively. As we will see in the following paragraph, non-cooperative models show Arrhenius behavior, while cooperative models show super-Arrhenius slowing down. In both models, the liquid is described as a lattice of spins that can either take value of 1 or 0. The spin state 1 can be regarded as an mobile region and 0 is for an immobile region. Spins in the system can undergo flipping transition when a certain constraint is satisfied under the condition of detailed balance. The FA model is the simplest version that requires only one adjacent active spin. The East model incorporates directional facilitation: a spin can undergo a flipping transition only if there is an adjacent active spin to a pre-specified direction, say, to the East direction. This facilitation rule is illustrated in Fig.2.1.

The FA model and the East model can be extended to higher dimensional

model simply by taking high dimensional lattice structure. Here, we show the facilitation rule of the models in the dimension d. Hamiltonian of these systems are

$$H = \sum_{i=1}^{N} n_i \quad (n_i = 0, 1), \tag{2.1}$$

where n_i represents state of coarse-grained liquids. The total number of lattice sites in the system, $N = L^d$, is dependent on the spatial dimension d, where L is the length of simulation box. The system has periodic boundary conditions for all the directions. Because of simplicity of Hamiltonian, the equilibrium concentration of excitations

$$c =< n_i >= \frac{1}{1 + \exp(1/T)}, \tag{2.2}$$

can be easily obtained, where T is a reduced temperature.

Even though each site in the system does not have energetic interactions, there are kinetic constraints on the sites that regulate transition between different states. These constraints are reflected on the local dynamic rules which depend on the site i as well as its neighbors. The flipping rates, $k_i^{\pm}$, depend on the configurations of local area via the facilitation function, $f_i(\{n_{\mathbf{x}}\}) = f_i(n_1, n_2, ..., n_N)$. The local dynamics obey following conditions

$$n_i = 0 \quad \underset{k_i^-}{\overset{k_i^+}{\rightleftharpoons}} \quad n_i = 1, \tag{2.3}$$

where

$$k_i^+ = e^{-1/T} f_i(\{n_{\mathbf{x}}\}), \tag{2.4}$$

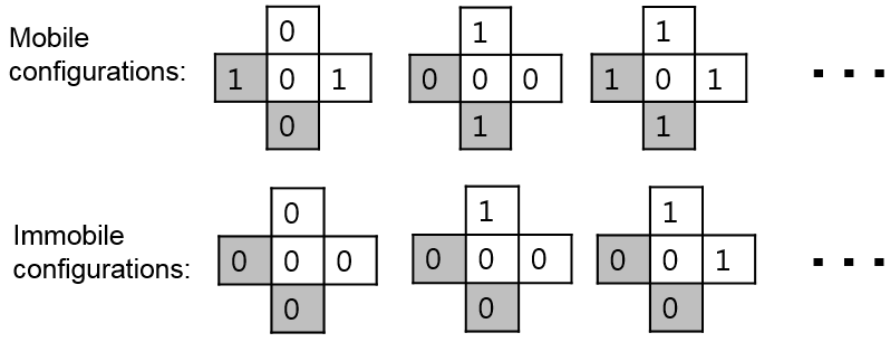

Figure 2.2: The illustration of mobile configurations and immobile configurations for 2-dimensional East model. Note that at least one active spin has to be in the negative direction of neighboring site.

$$k_i^- = f_i(\{n_{\mathbf{x}}\}). \tag{2.5}$$

Higher dimensional generalizations of the FA model and the East model can be modeled with following facilitation function:

$$[f_i(\{n_{\mathbf{x}}\})]_{\mathrm{FA}} = 1 - \prod_{l=1}^{d}(1 - n_{\mathbf{x}_i+\delta l\widehat{\mathbf{u}}_l})(1 - n_{\mathbf{x}_i-\delta l\widehat{\mathbf{u}}_l}), \tag{2.6}$$

$$[f_i(\{n_{\mathbf{x}}\})]_{\mathrm{East}} = 1 - \prod_{l=1}^{d}(1 - n_{\mathbf{x}_i-\delta l\widehat{\mathbf{u}}_l}), \tag{2.7}$$

where d is spatial dimension of the system and $\widehat{\mathbf{u}}_l$ is a unit vector of lth dimension. Controlling the flip of chosen lattice, this functions govern the local dynamics of the system. To perform a transition to another state in the East model, at least one of the neighbors have to be excited state at proper direction. The examples of mobile configurations and immobile configurations of 2-dimensional East model are illustrated in Fig.2.2. It is often called the East

model and the north-or-east-or-front (NEF) model for $d = 1$ case and $d = 3$ case, respectively.

Precisely speaking, the multi-dimensional FA model that we considered is one of the m-constrained FA models, called FA-m model. m is the minimum number of neighboring excitation required to change the configuration of site i. In this sense, multi-dimensional FA model we discussed can be expressed FA-1. Generally, The FA-m models are considered on hyper-cubic lattices of dimension d with the condition, $2 \leqslant m \leqslant d$. When $m \geqslant 2$, the models show cooperative nature, distinguished from original FA model. This can be seen easily with the example, $m = d = 2$. The configuration that the two lows of the system are immobile sites can not be relaxed, even if an infinite time is passed.

In the same manner, the East model is a cooperative model. The lattice site in the East model requires an excitation in the left side (within our notation: n_{i-1}) so that the lattice site at the end of left direction can not change its configuration when the open boundary condition is used. The directional nature of the constraint makes the relaxation mechanism cooperative, which results in extremely slow dynamics at low temperature (low concentration of the excitations). The directional facilitation of the East model is undoubtedly a strong constraint. However, directional movement of the excitation has reasonable physical origins. First, as we discussed before, there should be mobile region nearby for a region to become mobile in the next time step. Second, the direction of a displacement is preserved by the movements of the new mobile region to a certain extent.[42] This feature is often called string-like motion, which has also been found in the off-lattice model systems.[43–45]

Fig.2.3 shows the trajectory of the 1-dimensional FA model and the East

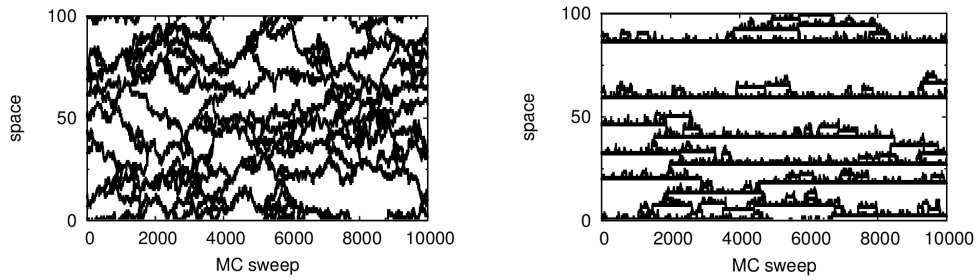

(a) (b)

Figure 2.3: The example of the trajectory of (a) the 1-dimensional FA model and (b) the 1-dimensional East model. x-axis and y-axis are time and space, respectively. The active spin is represented with black square, while inactive spin is white. The excitation line in the FA model travels in both way, while there is a clear hierarchical transition in the East model.

model at the same temperature. The comparison of two trajectories clearly shows how the hierarchical facilitation rule affects the transition of the excitation line in the East model. As we observed, the small difference of facilitation rule affects the properties of the system heavily.

In spite of its simplicity, KCMs have been recognized as useful models to describe the dynamic properties of the supercooled liquids. Especially, the FA and the East model show the properties of strong and fragile liquids, respectively. Fig.2.4 shows the temperature dependence of the relaxation time in the FA model and the East model from $d = 1$ to $d = 4$. In Fig.2.4, T_g is defined as a temperature that the relaxation time, τ/τ_0, of each system is 10^{12} MCS. Note that the relaxation time of the FA models shows an Arrhenius behavior, while the relaxation time of the East models shows a super-Arrhenius behavior which is a distinctive property of the fragile liquids. The difference between two models comes from different relaxation process.

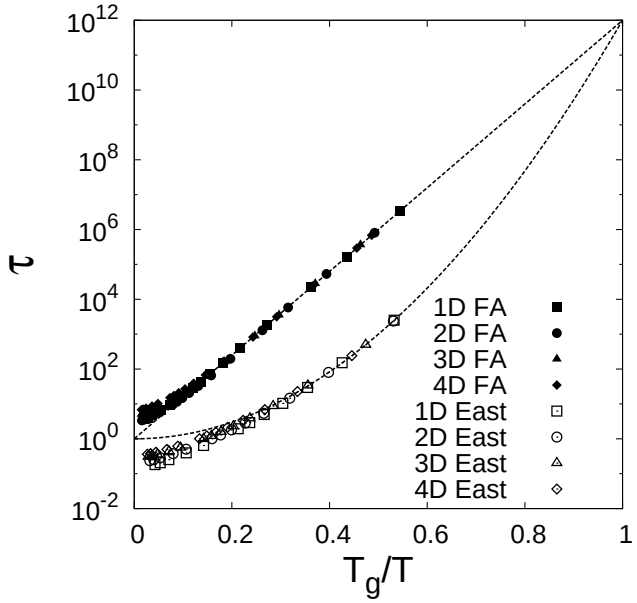

Figure 2.4: Angell plot of higher dimensional models of the FA model and the East model. The FA models exhibit Arrhenius temperature dependence, while the East models show super-Arrhenius behavior. The glass transition temperature T_g is defined as a temperature that the relaxation time over τ_0 is equal to 10^{12} MCS. The East modes are fitted to exponential inverse squared temperature, $\tau = \tau_0 \exp(B/T^2)$, where τ_0 and B are fitting parameters.

The relaxation process in the FA model is simple. From the Hamiltonian of the system, we know that the average distance between the nearest active spin is $l_{eq} \sim c$. The relaxation time would be the same for the time that excitation line comes from distance l_{eq}. Furthermore, the local diffusivity of the excitation is proportional to c: $D_{\text{diff}} \sim c$ As a result, the relaxation time for the FA model is $\tau \sim l_{eq}^2/D_{\text{diff}} \sim l_{eq}^2/c \sim c^{-3}$. At low temperature, c is proportional to $\exp(1/T)$ so that $\tau \sim \exp(3/T)$. However, the facilitation rule of the East model has a hierarchical nature that the relaxation time can not be expressed in a simple

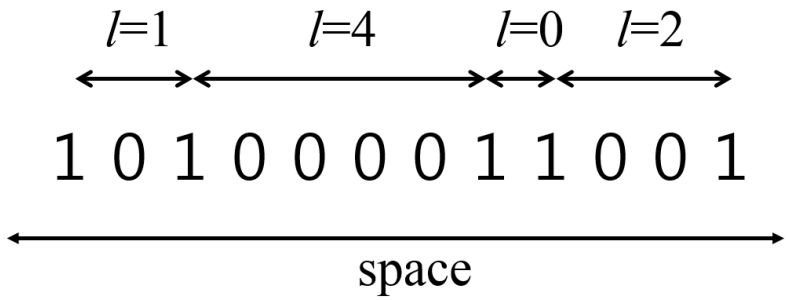

Figure 2.5: Example of the configuration in the East model is shown. Distance between the nearest two excitations is defined as l and it is shown in the figure.

scaling relation between the concentration c. Instead, the relaxation time of the East model can be expressed as a following form: $\tau = \tau_0 \exp(B/T^2)$.[46,47] This can be derived easily considering effective barrier of relaxation process. Note that in the East model case, relaxation process can only take place when there is a mobile site on the left. Now, we can think about effective energy barrier when the separated distance between two excitations is l, Fig.2.5. For a length $l = 0$, there is no dynamical constraint and the excitation can relax freely. The time scale for this process would be $t_0 \sim 1$. For a length $l = 1$, the excitation can relax with following process:

$$101 \rightarrow 111 \rightarrow 110 \rightarrow 100 \tag{2.8}$$

During the process, the immobile site between two excitation should be excited. This will take timescale as $t_1 \sim \exp(1/T)$ and the effective energy barrier, ΔE,

is 1. We can extend the situation for lengths $l = 2$ and $l = 3$:

$$1001 \rightarrow 1101 \rightarrow 1111 \rightarrow 1110 \rightarrow 1100 \rightarrow 1000 \tag{2.9}$$

$$\begin{aligned} &10001 \rightarrow 11001 \rightarrow 11101 \rightarrow 10101 \rightarrow 10111 \rightarrow \\ &10110 \rightarrow 10100 \rightarrow 11100 \rightarrow 11000 \rightarrow 10000 \end{aligned} \tag{2.10}$$

The smallest number of the excitation that the process requires is 2 for both processes involving the energy barrier $\Delta E = 2$. Generally, a length l and the energy barrier are related with following equation: $2^{\Delta E-1} \leq l < 2^{\Delta E}$. For a process that has the energy barrier of ΔE, the timescale of relax process would be $t_{\Delta E} \sim \exp(\Delta E/T)$.[48] In equilibrium, excitations are distributed at random, $P(l) = c_{eq}\exp(-c_{eq}l)$, and the average distance between two excitation is $l_{\mathrm{eq}} = 1/c_{\mathrm{eq}} \sim \exp(1/T)$. Using the approximation that $\Delta E \sim \ln l_{\mathrm{eq}}/\ln 2$, the timescale for asymmetric relaxation process can be obtained:

$$\tau \sim \exp\left(\frac{\ln l_{\mathrm{eq}}}{T\ln 2}\right) = \exp(B/T^2), \tag{2.11}$$

where $B = 1/\ln 2$. In more rigorous theoretical study, $B = 1/2\ln 2$ is proposed.[47] For higher dimensional East model, it has been proved that the timescale would be $\tau = \tau_0\exp(1/2d\ln 2T^2)$ where d is spatial dimension.[47]

Although there is a limitation that the KCMs can not capture the detailed molecular structures, KCMs are useful and successful tools to describe the intriguing features of the supercooled liquids. In the following chapters, the simulation results using the KCMs, especially the East model, will be shown.

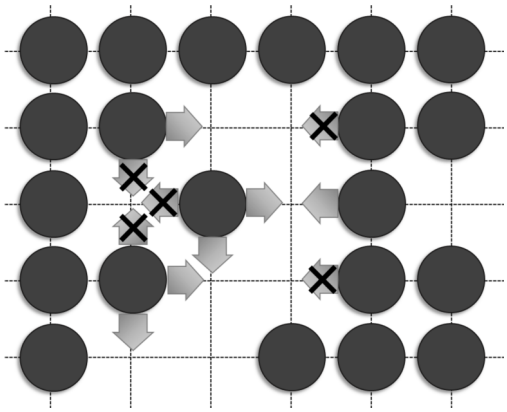

Figure 2.6: Typical configuration of Kob-Andersen model is shown. Each arrow shows possible and impossible movements of particles.

2.3 Kinetically constrained lattice gases

In conservative KCMs, the total particle number is conserved. A particle at site i attempts a jump to empty neighboring sites j at a fixed rate. The resulting dynamics preserves the number of particles, and so detailed balance is satisfied. There is no energy difference between each configurations. However, the dynamic rule requires certain number of empty neighbors for the movement of particles. In most cases, there is no energetic values for the sites that the temperature of system can not be defined. Instead of the temperature, total density can be varied, and effective temperature can be defined like $-\log(1-\rho) \equiv 1/T$. Reduced free volume at low temperature is reflected in this scheme.

Kob-Andersen (KA) model, triangular lattice gas (TLG) models are representative models of conservative KCMs. Those models are kinetically constrained lattice gas models.[37–39] The first conservative KCM is the KA model which has cooperative dynamics. KA model can be constructed in a hyper-

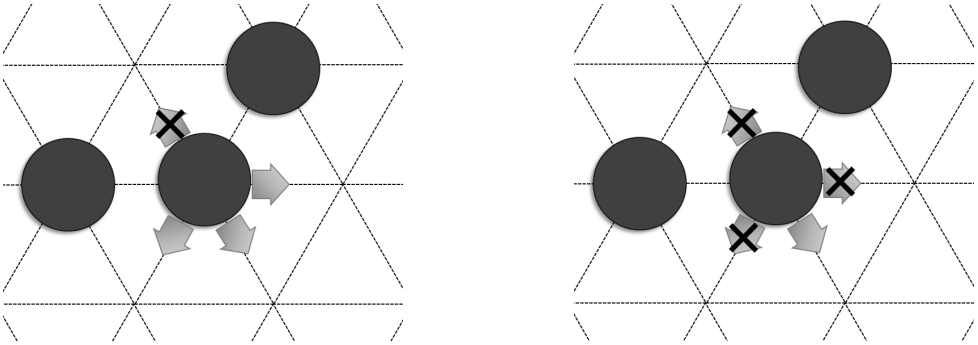

Figure 2.7: Typical configurations of trianglular lattice gas models are shown. Each arrow shows possible and impossible movements of particles. (a) (1)-TLG model. (b) (2)-TLG model.

cubic lattce. A particle in a KA model can jump into neighboring site only if both the initial and final position at least m of its neighboring sites are empty. The original KA model had $m = 3$ in 3-dimension. Generally, KA-m models can be defined within the condition, $2 \leq m \leq d$. If m is larger than spatial dimension d, there exists frozen particles at any density similar to the FA-m models. Typical configuration of KA-2 model is shown in Fig.2.6. The arrows show possible and impossible movements of particles.

Two other KCMs on triangular lattices were introdued. For the (1)-TLG, a particle can move from site i to a neighboring site j if there is at least one empty site on the mutual neighboring site of i and j. See Fig.2.7(a) for example configuration. For the (2)-TLG, a particle can move from site i to a neighboring site j if two mutual neighboring sites are empty, Fig.2.7(b). Note that (1)-TLG is a non-cooperative KCM, while (2)-TLG is a cooperative KCM. Furthermore, the effective temperature dependence of models show that (1)-TLG and (2)-

TLG can be regarded as strong and fragile liquids, respectively.

Chapter 3

Dimensional Dependence of Dynamic Heterogeneity in the East Model

3.1 Introduction

The East model describes the behavior of a fragile supercooled liquid with the heterogeneous dynamics. The model has a simple and insightful facilitation rule that controls the dynamics of the system. Using the East model, the theoretical approach to the description on the glassy behavior is possible and various simulation studies show the important physical properties such as the super-Arrhenius behavior of the relaxation time, the fractional Stokes-Einstein relation (SER), $D \sim \tau^{-1+\omega}$, and the increasing dynamic length scale at low temperatures.[26,49–53] Even in the higher dimensions, the asymmetric and extremely hierarchical facilitation rule makes the system behave like a fragile liquid. As a result, the heterogeneous and hierarchical dynamics would be preserved irrespective of the spatial dimension.[50]

Meanwhile, previous theories based upon the mode-coupling theory and the field theory predict that the upper critical dimension, d_u, of the liquids is

8.[28–30] Based on the result, the critical behavior of the liquids would follow the mean-field theory and the strong fluctuations of the dynamic variables would vanish at $d > d_u = 8$. Recent computational study of the hard sphere system seems to support this idea.[54] Charbonneau et al. showed that the violation exponent, ω, of the Stokes-Einstein relation is 0 in $d > d_u$.

The existence of a finite upper critical dimension is an unexpected phenomenon in the East model. Because the mean-field like characteristics are not found in the East model, which could be inferred from the structure of the facilitation rule. In this chapter, we investigate if there is a finite upper critical dimension and there is a crossover behavior in $d = 8$. To answer the questions, we first show the calculation of the violation exponent of the Stokes-Einstein relation up to $d = 10$. Further, the dimensional dependence of the dynamic heterogeneity will be illustrated using the decoupling of the mean persistence time and the mean exchange time. Finally, the mean exchange time of the enduring kinks and the mean waiting times between neighboring kinks are calculated to verify the time scale that is coupled to the diffusive behavior of the probe particle.

3.2 Method

We use kinetically constrained models (KCMs) to describe the supercooled liquids. Especially, higher dimensional generalizations of the East models are used.[49] The East model is a two state lattice model with a dynamic constraint.

The Hamiltonian of the system is defined,

$$H = \sum_{i=1}^{N} n_i \quad (n_i = 0, 1). \tag{3.1}$$

$n_i = 0$ represents the dense state while $n_i = 1$ represents the sparse state. $n_i = 1$ states are called the up-spins or the excitations which implies that local dynamics is faster than $n_i = 0$ sites. There are no energetic interactions between the neighbor lattices. However, there are kinetic constraints that control the dynamics of the system. The flipping rates of the lattice site, $k_i^{\pm}$, are defined, $k_i^+ = e^{-1/T} f_i(\{n_{\mathbf{x}}\})$ and $k_i^- = f_i(\{n_{\mathbf{x}}\})$. Note that $f_i(\{n_{\mathbf{x}}\})$ is a facilitation function that regulates the flipping events,

$$f_i(\{n_{\mathbf{x}}\}) = 1 - \prod_{l=1}^{d} (1 - n_{\mathbf{x}_i - \delta \widehat{\mathbf{u}}_l}), \tag{3.2}$$

where d is the spatial dimension and $\widehat{\mathbf{u}}_l$ is a unit vector of lth dimension. For the higher dimensions, there should be at least one excitation on the positive direction along the axis. We use the continuous-time Monte Carlo algorithm and the Monte Carlo with absorbing Markov chains method for low temperature.[55,56] To check the finite size effect, we increase the size of the system until the physical quantities differ less than 1%. Total simulation times are set to be 50$\sim$100 times of the relaxation time. Temperature of the system is varied to have over 6 orders in the relaxation times. Physical quantities are averaged over 10$\sim$$10^3$ independent trajectories.

3.3 Results and discussion

3.3.1 Upper critical dimension and fractional Stokes-Einstein relation

We first investigate the upper critical dimension of the East model. The upper critical dimension is defined as the lowest dimension that satisfies the SER. To obtain the power law exponent, ω, we calculate the structural relaxation times and the diffusion constants up to $d = 10$. We use the mean persistence time of the system, $\tau_{\rm per} = \langle t_{\rm per} \rangle$, for the relaxation time. $t_{\rm per}$ is the waiting time that first flip occurs from the randomly chosen time.[26] Varying the temperature, the mean persistence time shows super-Arrhenius behavior for all dimensions, Fig.3.1(a). At fixed temperature, it decreases when the dimension is increased. Further, $\ln(\tau_{\rm per})$ is well fitted to the quadratic fuction,[12,42,56]

$$\ln(\tau_{\rm per}/\tau_0) = J^2(1/T - 1/T_0)^2. \tag{3.3}$$

τ_0, J and T_0 are the fitting parameters. T_0 is the onset temperature above which the dynamics is thought to be heterogeneous and τ_0 is the relaxation time at onset temperature. In our model, J^2 is inversely proportional to the spatial dimension, $J^2 \propto 0.7/d$, Fig.3.1(b). The fitting supports that the dynamics in the East model is hierarchical.[42] Our result is similar to the result of Ashton et al., $J^2 \sim 0.8$.[56] Theoretical study predicts a coefficient of $1/T^2$ as b/d, where b is $1/(2\log 2) \sim 0.721$.[47] The discrepancy between the simulation results may come from the different definition of the relaxation times.

The probe particles are inserted to calculate the diffusion constants. The

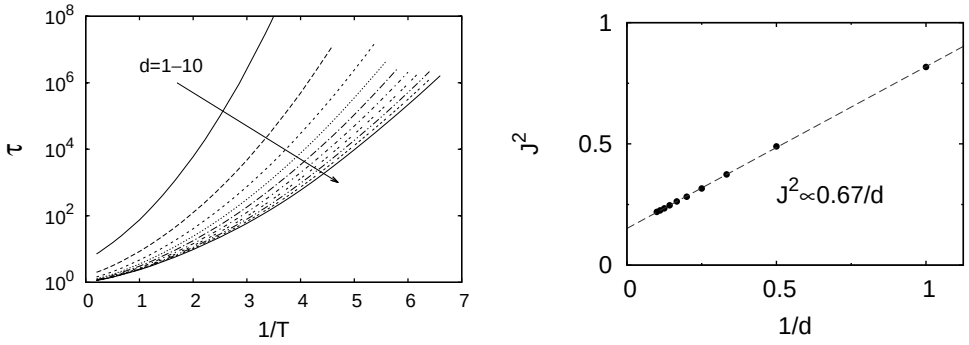

(a) (b)

Figure 3.1: (a) Temperature dependence of the mean persistence time. (b) The fitting shows that J^2 is inversely proportional to the dimension.

probe particles do not interact with the background liquids and attempt to move to neighbor lattice in every 1 Monte-Carlo sweep. To satisfy the detailed-balance, the particles can only move from the excitation to the excitation. The diffusion constants are determined from the mean-square displacements of the probe particles, $D = \lim_{t\to\infty}\langle[\Delta\mathbf{x}(\mathbf{t})]^2\rangle/2dt$, where $\Delta\mathbf{x}(t) = \mathbf{x}(t) - \mathbf{x}(0)$. The diffusion of the probe particles is getting faster and getting closer to the Arrhenius behavior as the dimension is increased, Fig.3.2(a). Similar to the fitting of $\ln(\tau_{\rm per})$ to quadratic function, we assume that

$$\ln(D/D_0) = -K^2(1/T - 1/T_0')^2. \tag{3.4}$$

Here, D_0, K and T_0' are fitting parameters. Fig.3.2(b) shows K^2 and d have the relation, $K^2 \sim A/d + B$. The fitting suggests the existence of a time scale that can be a characteristic time for the diffusion of the probe particles, $\tau_{\rm diffusion} \sim 1/D$.

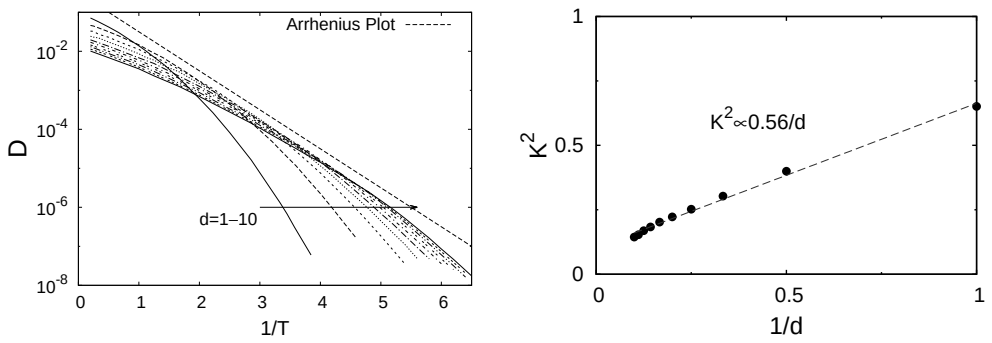

(a) (b)

Figure 3.2: (a) Temperature dependence of the diffusion constants is shown. As the dimension is increased, super-Arrhenius behavior is getting weaker. (b) Diffusion constants of each dimension is fitted to the equation, $\ln(D/D_0) = -K^2(1/T - 1/T_0')^2$. The fitting shows that K^2 is inversely proportional to the dimension similar to the case of the mean persistence time.

Although the mean persistence times and the diffusion constants both show super-Arrhenius behavior, the fractional power law relations hold for each dimension. The power law relations of the mean persistence time and the diffusion constants are shown in Fig.3.3. The value of ω is very sensitive to the power law fitting. To minimize the error and to investigate the systems at the low temperature condition, the data points which have the mean persistence time longer than 10^4 MC sweeps are used. The error bar is defined as the half of the difference between the maximum exponent and the minimum exponent calculated using more than 5 data points.

Obtained exponent ω is shown in Fig.3.4. The decreasing aspect of the exponent is different from the previous study of hard sphere system. In the study of Charbonneau et al., ω decreases linearly up to $d = 8$ showing that $d_u = 8$ [54]. In our study, however, the exponent decreases non-linearly and the

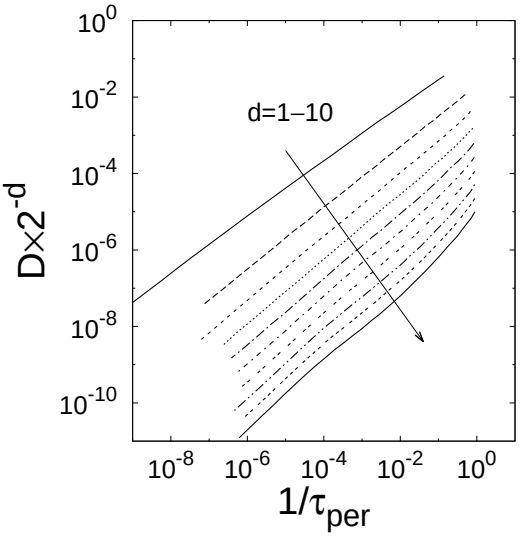

Figure 3.3: The power law relation between $\tau_{\rm per}$ and the diffusion constant, $D \sim \tau^{-1+\omega}$, are shown. Data points which have $\tau_{\rm per}$ longer than 10^4 MC steps are used for the power-law fitting.

exponents are still far from zero in $d > 8$.

Based on the assumption that equation 4 holds, the exponent ω has the form, $\omega(d) = (A'/d + B')/(C'/d + D')$. Fig.3.4 shows the fitting of the data. The fitting agrees well and our assumption on the diffusion constants holds up to $d = 10$. This decreasing behavior strongly supports that the upper critical dimension of the East model is infinite. The result is consistent with the estimation of the previous work.[50] Because the hierarchical kinetic rules that control the dynamics of 1-dimensional East model is still preserved in the higher dimensions, the mean-field like environments are not found in finite dimensions. Note that the degree of heterogeneity is decreasing as the dimension is increased, even if the dynamic heterogeneity remains in the higher dimensions. The evidence of decreasing dynamic heterogeneity can be found through the

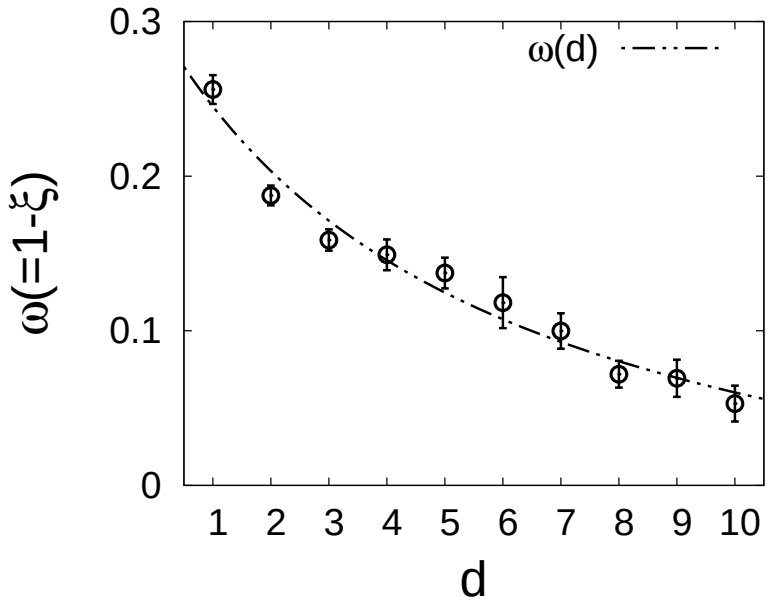

Figure 3.4: The power law exponents obtained using data points in Fig.3.3. ω decreases non-linearly as the dimension is increased. Based on the result, the upper critical dimension, d_u, is not found up to $d = 10$. This result is distinctive from the result of the hard sphere system which shows the linear decrease and $d_u = 8$. We suggest the fitting form $\omega(d) = (A'/d + B')/(C'/d + D')$. The fitted graph shows a good agreement with the data points. The result shows that the exponent ω decreases slowly to 1 and supports that d_u is infinite in our model system.

analysis of the dynamic physical properties like a time dependent four-point time correlation function.[34]

In this paragraph, we show the error analysis schemes that is used for the error bars in Fig.3.4. Calculation of the error using nonlinear least-squares algorithm may underestimate the size of error bars. In this study, we defined new error, $e_\Delta = (\omega_{\max} - \omega_{\min})/2$. $\omega_{\max}$ and $\omega_{\min}$ is the maximum and minimum power law exponents among the various sets of data points at certain dimension. We chose the data sets having more than 5 data points. For example, when the number of data is 8, there are 93 sets of data having more than 5 data points. We performed nonlinear least-squares fitting for all sets to obtain $\omega_{\max}$ and $\omega_{\min}$. Fig.3.5(a) shows the comparison between e_Δ and the error bar obtained by nonlinear least-squares algorithm, e_{NLS}. The error bar defined in our study is larger but more reasonable, because it covers wide range of uncertainty caused by computational results.

One more important factor for determining the power law exponent is fitting range. At high temperature, the power law relation is not perfectly valid especially in high dimensions, Fig.3.3. In this study, we used the data points which have the mean persistence time longer than 10^4 MC sweeps so that the system shows the power law relation between D and τ_{per}. In Fig.3.5(b), the power law exponents are shown with the different minimum range, $r_{\min}$, of the mean persistence time. $r_{\min}$ affects the exponents in high dimensions. Considering the accuracy of the fitting and the number of data points, we chose $r_{\min} = 10^4$.

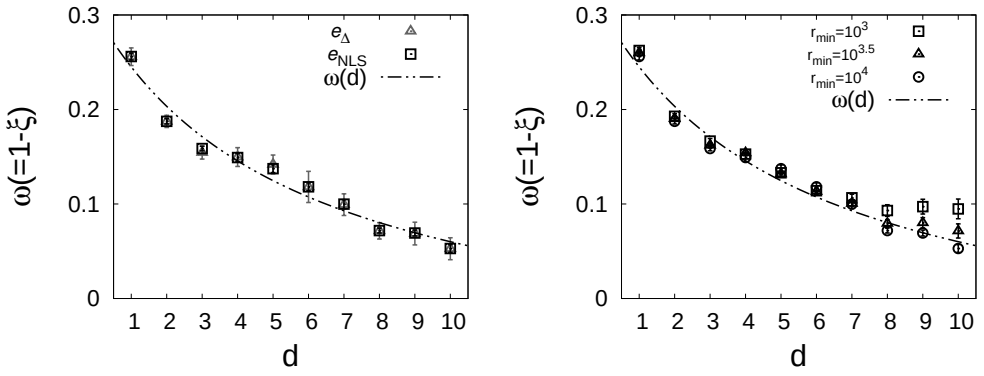

(a) (b)

Figure 3.5: (a) The comparison between differently defined error bars. (b) The power law exponent, ω, changes as the fitting range is changed.

3.3.2 Decoupling of the mean exchange time and the mean persistence time

The decoupling of the mean exchange time and the persistence time is highly connected to the dynamic heterogeneity.[7,27,57] In our study, the exchange time is defined as a time interval between nearest flips at same lattce site.[26] In normal liquid, or in high temperature, there are poor correlations between the exchange events. The distribution of the exchange time will show exponential decay and the distributions of the exchange time and the persistence time would be identical. At low temperature, the distribution of the exchange time is non-Poisson distribution which causes the decoupling of the exchange time and persistence time.

Dimensional comparison of the time scales is shown in Fig.3.6. As expected from the previous study, the mean exchange time is inversely proportional to the dimension at low temperature, $\tau_{\rm exc} = 1/2dc^2$.[49] This relation is derived

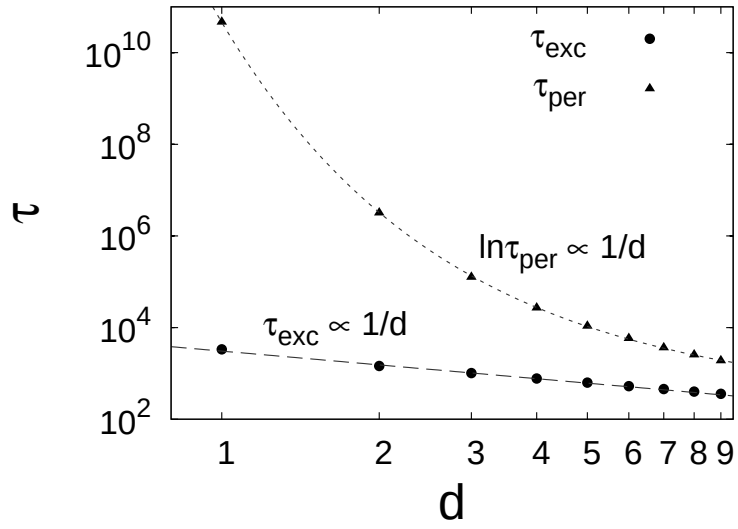

Figure 3.6: Decoupling of the mean exchange time, $\tau_{\rm exc}$, and the mean persistence time, $\tau_{\rm per}$, at $T = 0.23$. At low temperatures, the mean exchange time is inversely proportional to the dimension, $\tau_{\rm exc} = 1/2dc^2$. The fitting of the $\tau_{\rm per}$ shows that $\ln \tau_{\rm per}(d;T) \sim 1/d$ which is inferred from eqaution 3. The decoupling of the time scales is getting weaker as the dimension is increased.

from flip rates of the lattice sites. On the other hand, the dependence of the mean persistence time on dimension shows $\ln \tau_{\rm per} \sim 1/d$, which is a result of the equation 3. The degree of the decoupling is getting smaller as the dimension is increased. However, there are still significant differences in higher dimensions and the dynamic heterogeneity remains.

3.3.3 Charateristic time scale for diffusion of probe particles

In the Fredrickson-Andersen (FA) model, the translational diffusion constant is inversely proportional to the mean exchange time.[26] For the East model, however, the representing time scale for the abnormal behavior of the diffusion

constants is not discovered. To understand the precise mechanism of the diffusion motion, we investigate the time scales that are related to the diffusive behavior of the East model. So we can infer which process is important for the diffusion of the probe molecules. In this study, the mean exchange time of the enduring kinks and the mean waiting times between the neighboring kinks are considered. Here, the kink means the flipping of certain lattice site. These time scales are suggested in the study of Elmatad et al..[58]

The enduring kink represents change of the excitation that persists for a certain period of time. Fast blinking motion of the excitation, which would not have a heavy effect on diffusion, is coarse-grained out in the enduring kink. When the interval between the nearest kink is shorter than the mean exchange time, we call it fast kink. The precise definition of the enduring kink can be found in the previous study.[58] We calculate the mean exchange time of the enduring kinks, $\tau_{\rm exc}^{\rm end}$. There is power law relation between the diffusion constants and $\tau_{\rm exc}^{\rm end}$, $D \sim \tau^{-\delta}$. For $d = 1$, the diffusion constant is inversely proportional to $\tau_{\rm exc}^{\rm end}$, Fig.3.7. However, as the dimension is increased, the exponent δ decreases and the correlation between the diffusion and $\tau_{\rm exc}^{\rm end}$ is getting weaker.

Further, the waiting time between neighboring kinks, $t_{\rm w}$, is defined as follows.[58]

$$t_{\rm w}^{\rm all} = \min\left\{\, t \,|\mathbf{x}_j \in \mathbf{x}_i + \delta\widehat{\mathbf{u}}_l, t \geq \delta t, |\kappa_{\mathbf{x}_i}(0)\kappa_{\mathbf{x}_j}(t)| = 1\right\}, \tag{3.5}$$

$$t_{\rm w}^{\rm short} = \min\left\{\, t \,|\mathbf{x}_j \in {\rm nbrs}(\mathbf{x}_i), t \geq \delta t, |\kappa_{\mathbf{x}_i}(0)\kappa_{\mathbf{x}_j}(t)| = 1\right\}, \tag{3.6}$$

where, $\kappa_{\mathbf{x}_i}(t) = n_{\mathbf{x}_i}(t) - n_{\mathbf{x}_i}(t - \delta t)$. $\tau_{\rm w}^{\rm all} = \left\langle t_{\rm w}^{\rm all} \right\rangle$ is the averaged time interval between the certain kink and the kinks at the neighbor sites. Among $2d$ time

values for the certain kink, shortest time value is averaged to give $\tau_{\mathrm{w}}^{\mathrm{short}} = \left\langle t_{\mathrm{w}}^{\mathrm{short}} \right\rangle$. Because the particle displacements are highly dependent on the change of its neighbor, $\tau_{\mathrm{w}}^{\mathrm{all}}$ or $\tau_{\mathrm{w}}^{\mathrm{short}}$ would be related to the diffusion of the probe particles. These time values also show the power law relation with the diffusion constant, $D \sim \tau^{-\delta}$. The exponents are shown in Fig.3.7. At low dimensions such as $d = 1$, the fitted exponent is far from 1. As the dimension is increased, the exponents are getting close to 1. $\tau_{\mathrm{w}}^{\mathrm{all}}$ shows enhanced correlation with the diffusion constant compare to τ_{per}. But there is still missing correlation even in $d = 10$. For the $\tau_{\mathrm{w}}^{\mathrm{short}}$, the exponent decreases dramatically to 1 as the dimension is increased. Considering the error bar, the exponent is close to 1 in $d \geq 7$. Relatively large error bar is due to a poor power law fitting quality compared to other time scales. The result supports that the fastest change of the environment of certain kink is important to the movement of the probe particle especailly in high dimensions. On the other hand, the inaccuracy in low dimensions may come from the existence of sub-diffusive behavior of the probe particles. Unlike in the FA model, the probe particles experience sub-diffusive behavior in the East model. In consequence, the information of the nearest neighbors are not enough to describe the behavior of the probe particles at long times. As the dimension is increased, sub-diffusive regime shrinks and the mean field effect is getting strong.

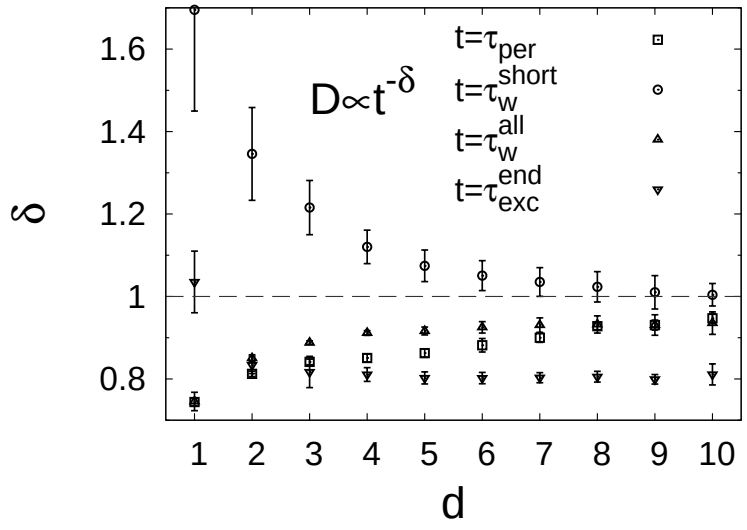

Figure 3.7: The power law exponents, δ, between the diffusion constant, D, and various time scales. $1/\tau_{\rm exc}^{\rm end}$ shows close relation in $d = 1$. As the dimension is increased, the exponent is decreasing. $\tau_{\rm w}^{\rm all}$ and $\tau_{\rm w}^{\rm short}$ are calculated using the Eq.3.5 and 3.6. In high dimensions, $1/\tau_{\rm w}^{\rm short}$ is highly correlated with D.

3.3.4 Persistence function

We define the site dependent persistence function, $P_i(t)$, and the mean persistence function,

$$P(t) = \left\langle \frac{1}{N} \sum_{i=1}^{N} P_i(t) \right\rangle, \tag{3.7}$$

in order to quantify the correlation of supercooled liquids in time scales. If the mobility of the certain site changes at time t, the value of the site dependent persistence function is converted from 1 to 0. The mean persistence function is the averaged value over the site and over the ensembles. This function can be thought as the analogue of the self-intermediate scattering function, $F_s(k, t)$, with large wavevector, k.[50,59]

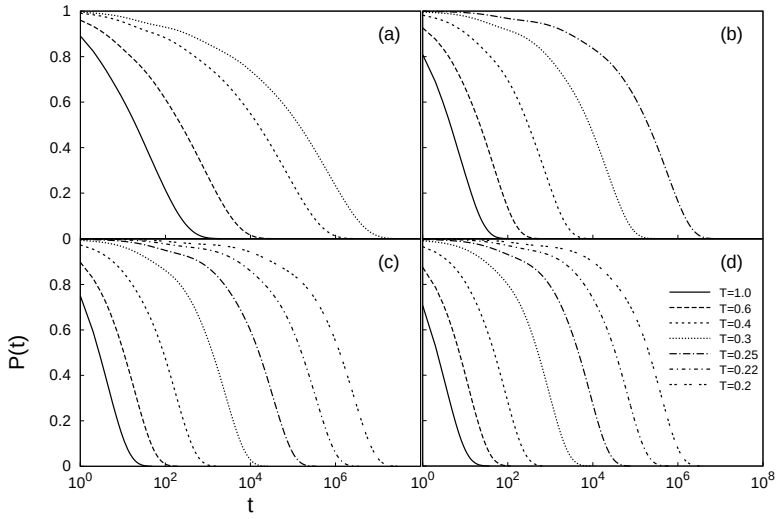

Figure 3.8: Mean persistence function of the East model systems, (a) $d = 1$, (b) $d = 2$, (c) $d = 3$, and (d) $d = 4$. The functions show non-exponential decay as the temperature and the dimension are lowered.

Fig.3.8 shows the time evolution of the mean persistence function over the four different dimensions at variety temperatures. As expected, the mean persistence time, $\langle t_{pers} \rangle$, which is integrated value of the mean persistence function, is large at low temperatures at fixed dimension. Further, it is noticeable that the function has non-exponential shape at long time scales. This non-exponential decay is found in the supercooled liquids and it is possibly caused by the heterogeneity of the supercooled liquids. From the shape of the non-exponential decay, one can estimate that the heterogeneity of the system increases as the temperature is decreased and as the dimension is decreased. It is trivial that the dynamics of the system at low temperature are more affected by the heterogeneity since the collective behavior increases near the glass transition temperature.

Now, we turn our concern on the dimensional dependence of the mean persistence function. At same temperature, fast decay of mean persistence function is observed in high dimensional system because of the enhanced relaxation through the increased number of neighbors. To see the effect of spatial dimension to the heterogeneous dynamics, it is reasonable to compare the heterogeneity of the model system with fixed relaxation times for various dimensions. We choose four different temperatures that make the each system of various dimension to have same mean persistence time of 10^4. The reduce temperatures are 0.476, 0.314, 0.269, and 0.245 from one dimensional system to four dimensional system, respectively.

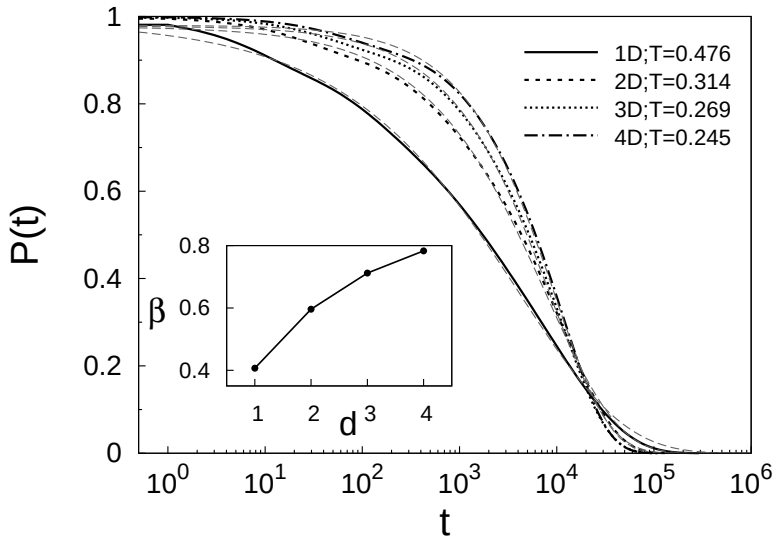

Figure 3.9: Comparison of the mean persistence functions of various systems which have same mean persistence time of 10^4. The functions are fitted to the stretched exponential functions, $e^{-(t/\tau)^\beta}$, to reveal the exponents 0.407, 0.596, 0.712, and 0.783 for $d = 1$ to $d = 4$ system, respectively.

In the Fig.3.9, four different mean persistence function and fitted function

with stretched exponential function, $e^{-(t/\tau)^{\beta}}$, are plotted. Fitting parameters, β, are calculated to give 0.407, 0.596, 0.712, and 0.783 for $d = 1$ to $d = 4$ systems. It is notable that the exponent beta is increasing as the dimension increases. The facilitation causes the systems in low dimensions to make clusters of excitations which are showing faster or slower dynamics than averaged value. Because the clusters have different time scale of relaxations, mean persistence functions of low dimensional system show highly stretched exponential shape. Although the systems have same relaxation time, the local dynamics of the excitations in the high dimensions do not show strong dependence to the nearest neighbors because of increased number of ways to be relaxed. As a result, the time scale of the local dynamics in high dimensions become similar to mean relaxation time. The mean persistence function with beta exponent near the unity is the evidence that high dimensional East model has more homogeneous than low dimensional systems.

In the previous paragraph, we discussed the heterogeneous dynamics of East models in several dimensions using the mean persistence functions. However, it is not rigorous enough because the stretched exponential functions may be shown in the homogeneous systems. The distributions of the persistence time, t_{pers}, are helpful to analyze the heterogeneous dynamics of the system, Fig.3.10. Four different systems have same mean persistence time of 10^4. There are significant difference among the distributions of the persistence times. There is a peak at the value of 10^4 for all systems, but width of the distribution is clearly wide for low dimensional systems. Moreover, there is a long tail at the long times which means time scales for the relaxation are so heterogeneous at low dimensions.

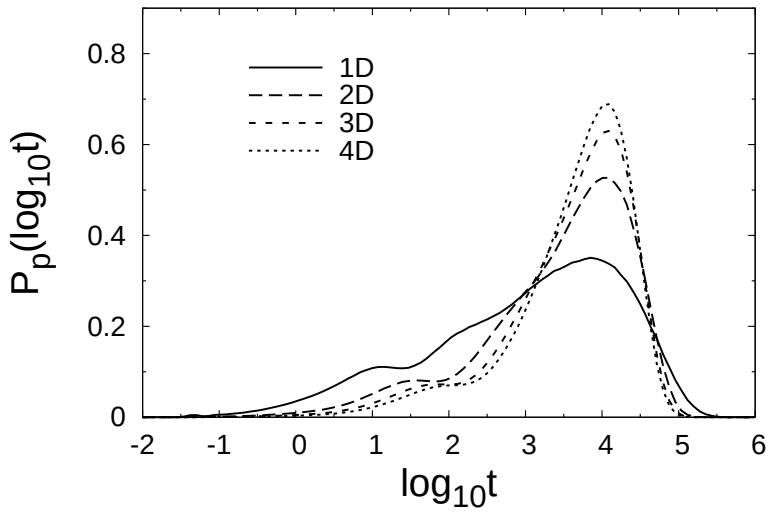

Figure 3.10: The distributions of the persistence time, t_{pers}. The temperatures of the systems are same with the temperatures used in Fig.3.9.

3.3.5 Dynamic susceptibility

We define dynamic susceptibility,

$$\chi(t) = \frac{N}{f(t)}\Big[\langle p^2(t)\rangle - \langle p(t)\rangle^2\Big], \tag{3.8}$$

which quantifies fluctuation of persistence function,

$$p(t) = \frac{1}{N}\sum_{i=1}^{N} P_i(t). \tag{3.9}$$

The function $f(t) = P(t) - P^2(t)$ is inserted to satisfy the normalization condition which is related to the spatial correlator and structure factor. The precise explanation will be mentioned in the next section. The dynamic susceptibility

is known to be an index of the dynamic heterogeneity of the system and can be used to compare the heterogeneity of the system at different conditions.[34,60] From equation 12, it is obvious that the dynamic susceptibility has large value when the fluctuation of the persistence function is huge. Fig.3.11 shows the

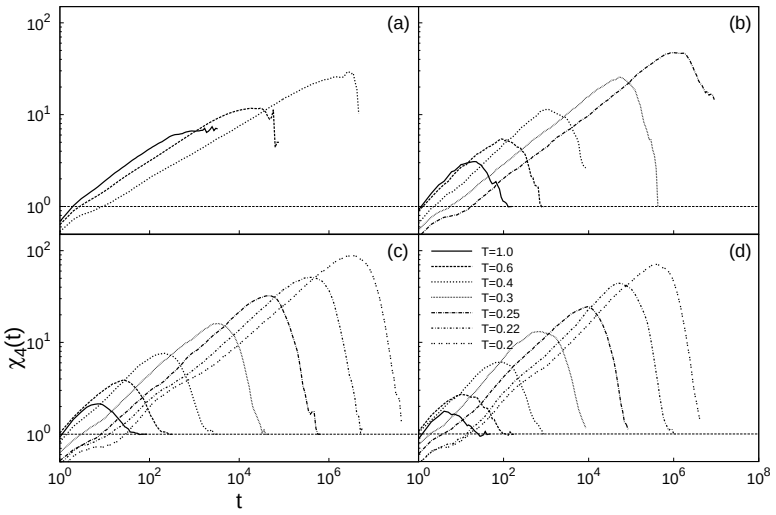

Figure 3.11: Dynamic susceptibility is calculated at various temperatures which is defined in Eq.3.8, (a) $d = 1$, (b) $d = 2$, (c) $d = 3$, and (d) $d = 4$.

time dependent dynamics susceptibilities at different dimensions and different temperatures. As expected, the location of the peak of the function is increasing and the height of the peak is also increasing when the temperature of the system is lowered. It is noteworthy that the positions of the peaks are proportional to the relaxation times for all dimensions. The dynamics are maximally correlated when the time is comparable to relaxation time of the system.

Further, the dynamic susceptibility satisfies following scaling law via the

concentration of the excitation, c,

$$\chi(\tau) \propto c^{-\gamma}, \tag{3.10}$$

where τ is the relaxation time and γ is the scaling exponent. For East models, we find that γ is equal to unity for all dimensions.

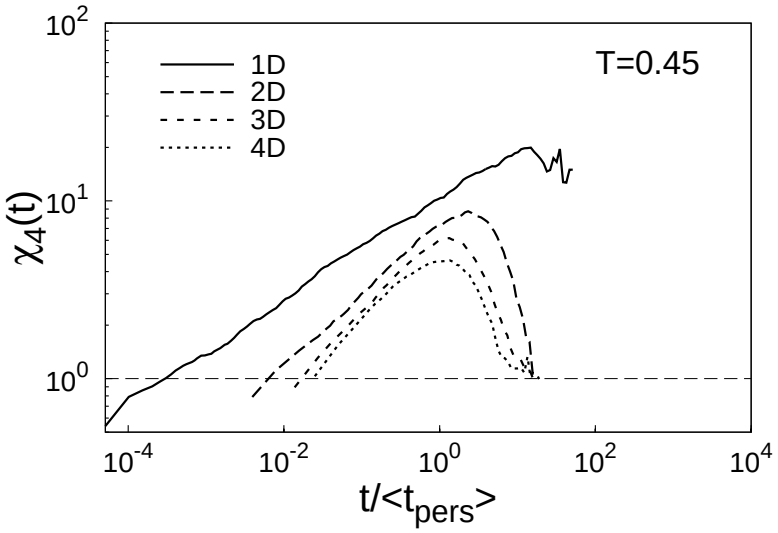

Figure 3.12: Dynamic susceptibilities scaled with the mean persistence time at $T = 0.45$.

To compare the dynamic heterogeneity of the systems in various dimensions, the time axis of the dynamic susceptibility is scaled with the mean persistence time of the each systems at fixed temperature, T=0.450, Fig.3.12. The results show that the height and the width of the peak is decreasing as the dimension increases. From the behavior of scaled functions, it is certain that collective motion of the spins are weak and the life time of mobile (immobile) clusters are narrowly distributed at high dimensions. This fact certifies our argument that

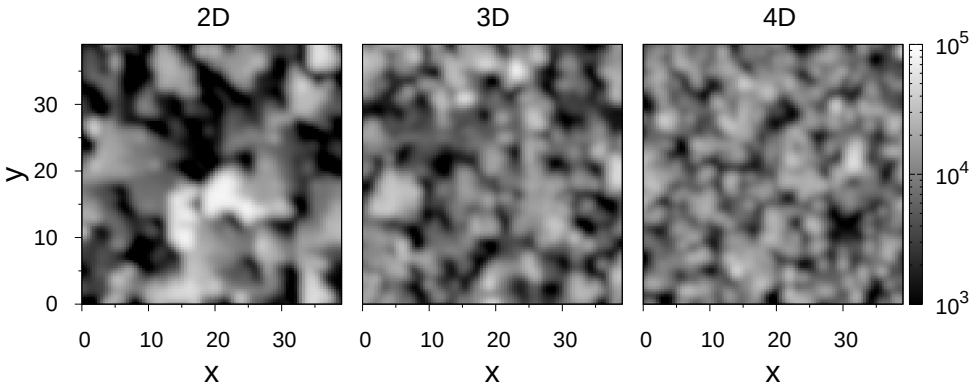

Figure 3.13: Two dimensional cross sectional view of the persistence times. The bright part represents the slow clusters. The temperatures of the system is same with the temperatures used in Fig.3.9 and Fig.3.10. The spins are heterogeneously distributed as the dimension is decreasing.

high dimensional East models are less heterogeneous.

3.3.6 Length scale analysis

In the previous section, we discussed behaviors of the dynamic heterogeneity in time scales. Indirect and direct evidences are found that number of the nearest neighbors are important parameter for the heterogeneity of the East model systems. Because the dynamics are heterogeneous not only in time scale but also in length scale, the spatial functions can be used to quantify the heterogeneous dynamics.[34] Following section introduces length scale analysis for higher dimensional generalizations of East models. Fig.3.13 shows the two dimensional cross sectional view of the persistence times in $d = 2$ to $d = 4$ systems. The temperatures of the systems are set to have same relaxation times which are 10^4 Monte Carlo steps. The bright part represents the spins which are dynamically

slow, while dark area represents the fast relaxations. In the two dimension system, the clusters of the spins are clearly separated in the sense of fast and slow clusters. In four dimension system, however, the fast or slow spins are more homogeneously distributed in time and space. From the results, it is obvious that high dimensional East model has spatially more uniform distribution. In the following subsections, quantitative analysis of length scale variation due to the dimension of the systems will be done using spatial correlators and structure factors.

3.3.7 Spatial correlator and structure factor

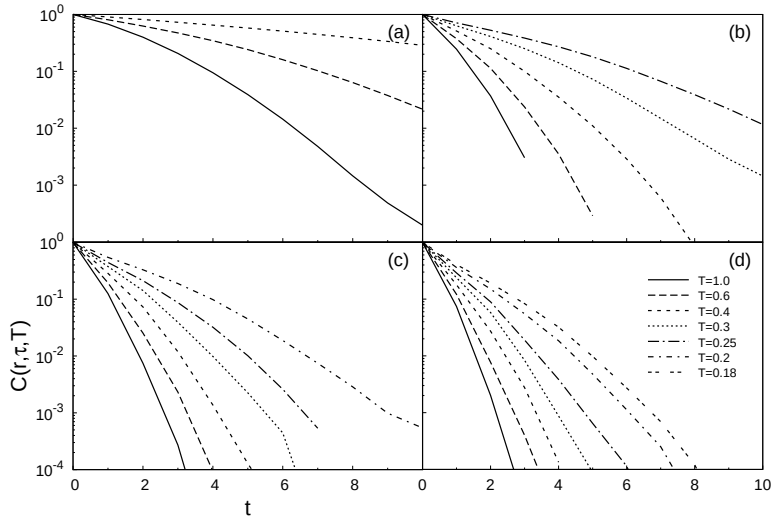

Figure 3.14: Spatial correlators of the East model is shown. As the dimension is increasing, the correlation lengths of the East model systems are decreased.

S. Whitelam et al. introduced spatial correlator,[51,61]

$$C(r,t,T) = \frac{1}{Nf(t)} \sum_{i=1}^{N} \sum_{j=1}^{N} [\langle P_i(t) P_j(t) \delta(|\mathbf{r}_i - \mathbf{r}_j| - r) \rangle - P^2(t)], \tag{3.11}$$

to investigate correlations of local dynamics in length scale. The function $f(t) = P(t) - P^2(t)$ enables the spatial correlator to be unity when $r = 0$. The spatial correlator are four point correlation function that effectively reveals the relations between two spatially separated sites. If the system is homogeneous, the spatial correlators have to show exponential decay. Fig.3.14 plots the spatial correltors in various temperatures and dimensions at $t = \tau(T)$ where the dynamic heterogeneity of the system is maximum. Speaking qualitatively, the correlations between two sites are increasing as the temperature is decreased. For all dimensions and temperatures, the shapes of the function show decay of the correlation faster than exponential which suggests spatially heterogeneous dynamics.

The correlation length, ξ, can be obtained from fitting the spatial correlator with stretched exponential functions, $e^{-(r/\xi)^\beta}$. It is known that the correlation lengths satisfy following scaling law,

$$\xi \propto c^{-\nu}. \tag{3.12}$$

The TABLE 3.1 lists the value of the scaling exponent ν for each dimensions. Note that ν decreases abruptly as the dimension increases. As a result, one can say that the correlation dependence on the concentration of the defect is weak at high dimensions.

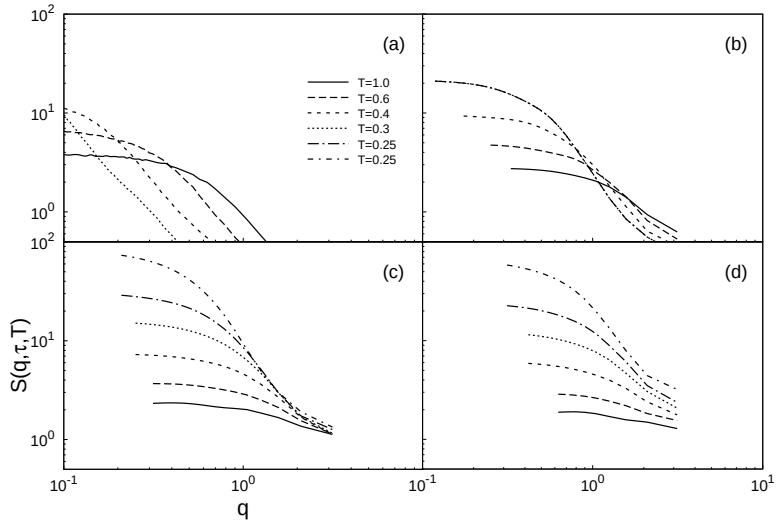

Figure 3.15: Structure factors of the East model in various dimensions.

Further, we define the structure factor,

$$S(q,t,T) = \frac{1}{Nf(t)} \sum_{k=1}^{N} \sum_{l=1}^{N} [\langle P_k(t) P_l(t) \rangle - P^2(t)] e^{iq(\mathbf{r}_k - \mathbf{r}_l)}, \tag{3.13}$$

which is fourier transform of the spatial correlator. It is obvious that if q is in the limit to zero, the structure factor become same as the dynamics susceptibility which is defined in eqaution 10. In Fig.3.15, we show the structure factors at the fixed times of relaxation time.

It is suggested that the functional form of the structure factor is $S(q,\tau,T) \sim \chi(\tau,T)\mathbf{S}(q\xi')$, where $\mathbf{S}(x) = 1/(1+x^{2-\eta})$. We determine $\xi'(T)$ by fitting $S(q,\tau,T)$. The scaling exponent ν' is reported in TABLE 3.1.

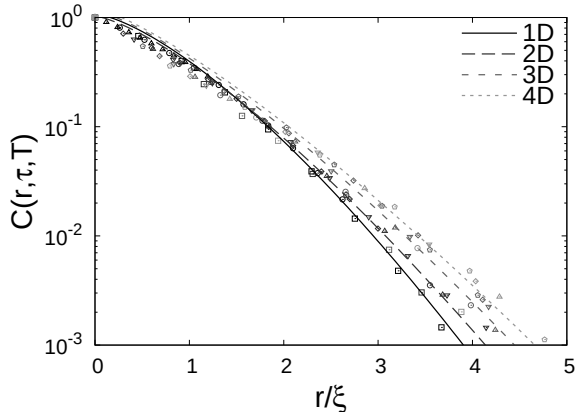

(a)

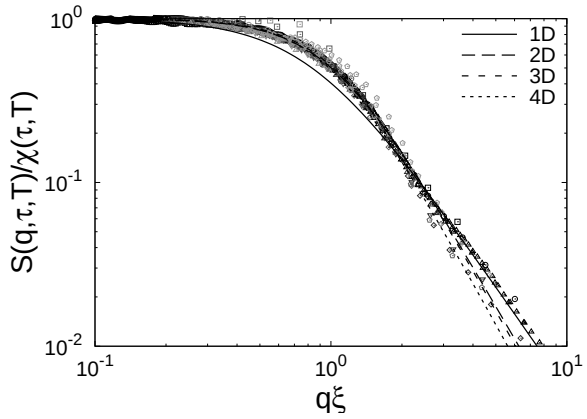

(b)

Figure 3.16: Using Eq.3.14 and Eq.3.15, spatial correlator and structure factor are rescaled. (a) When the spatial correlator is scaled with proper correlation lengths, every data in the same dimension collapses into single stretched exponential function. The scaling exponents, β, are 1.43, 1.36, 1.31, and 1.27 for $d = 1$ to $d = 4$ dimensional systems. (b) The structure factor is scaled with proper correlation lengths to give unique functional form of $1/(1 + (q\xi')^{2-\eta})$. The scaling exponents, η, are -0.09, -0.51, -0.58, and -0.64 for $d = 1$ to $d = 4$ dimensional system, respectively.

3.3.8 Scaling analysis

It is found that spatial correlator and structure factor, which are shown in previous section, satisfy following scaling laws,

$$C(r,\tau,T) \sim \mathbf{C}(\frac{r}{\xi},\tau), \tag{3.14}$$

$$S(q,\tau,T) \sim \chi(\tau,T)\mathbf{S}(q\xi'), \tag{3.15}$$

where ξ is the correlation length obtained using spatial correlator and ξ' is another correlation length obtained using structure factor. This scaling laws state that the length and structural behaviors are same when the correlations are scaled with correlation lengths even if the temperatures of the systems are different. However, the functional form of the **C** and **S** may be different when the dimension is changed. In this sense, we analyze the functional form of the scaled function for various dimensional systems.

Fig.3.16 shows the scaled form of the spatial correlator and structure factor. For the spatial correlator, we find agreeable collapse of the data points in each dimensional systems. However, each system has different shape depend on

	ν	ν'	β	η
$d=1$	1.063 ± 0.007	1.06 ± 0.02	1.43 ± 0.02	-0.09 ± 0.04
$d=2$	0.50 ± 0.03	0.57 ± 0.02	1.36 ± 0.02	-0.51 ± 0.02
$d=3$	0.30 ± 0.01	0.40 ± 0.02	1.31 ± 0.02	-0.58 ± 0.06
$d=4$	0.24 ± 0.02	0.34 ± 0.02	1.27 ± 0.04	-0.64 ± 0.09
	$\xi \propto c^{-\nu}$	$\xi' \propto c^{-\nu'}$	$\mathbf{C}(\frac{r}{\xi},\tau) \propto exp(-(r/\xi))^{\beta}$	$\mathbf{S}(q\xi') \propto 1/(1+(q\xi')^{2-\eta})$

Table 3.1: Various scaling exponents and corresponding equations are shown.

dimensionality of the system. When scaled correlator is fitted to the stretched exponential function, the system gives different β exponents which are 1.43, 1.36, 1.31 and 1.27 for $d = 1$ to $d = 4$ dimensional systems. It is quite interesting that the exponent shrinks to unity as the dimension of the system is increased, meaning that the correlation of the local spins is restricted at low dimensional systems. The structure factor also gives collapsed form when we plot $S(q, \tau, T)/\chi(\tau, T)$ with $q\xi'$ on the x axis. The fitting parameter, η, is calculated to give -0.09, -0.51, -0.58, and -0.64 for $d = 1$ to $d = 4$ dimensional systems. Because of insufficient data, the scaling exponents might be inaccurate to give precise explanation of fragility. However, aspect of varying exponents are consistent to our previous simulation results. From the variance of the exponents, one can possibly interpret that boundary of the spin cluster is more smooth when the dimension is high. In this sense, both the results of the scaling analysis show that clustering of the local spins are found in low dimensional systems. For the future studies, noble definition of the cluster size may give important insight to the spatial behavior of the dynamic heterogeneity.

3.4 Conclusion

In conclusion, our simulation results strongly support that the upper critical dimension of the higher dimensional generalization of 1-dimensional East model is infinite. This result is expected from the previous studies, based on the asymmetric and hierarchical dynamic rules of the model system. Moreover, the upper critical dimension and the facilitation function of KCMs could be connected via the hierarchical dynamics. For the FA model which does not show directional

dependence of the dynamic rule, the upper critical dimension is found to be finite.[61,62] Considering that the FA and the East models are the two extreme cases, we suggest that the study on the relation between hierarchical dynamics and spatial dimension would be worth.

Furthermore, mean exchange time of the enduring kinks, $\tau_{\mathrm{exc}}^{\mathrm{end}}$, the mean waiting times between neighboring kinks, $\tau_{\mathrm{w}}^{\mathrm{all}}$, and the shortest waiting times between neighboring kinks, $\tau_{\mathrm{w}}^{\mathrm{short}}$, are calculated. The exponents are obtained by the power law fitting. The results suggest that $\tau_{\mathrm{w}}^{\mathrm{short}}$ can be the characteristic time scales for the diffusion of the probe particles in high dimensions. From the result, we find that the movement of the probe particle is highly dependent on the fastest change of the environment.

The dynamic heterogeneity observed in the model system is getting weaker as the dimension is increased. Increased number of the neighbor makes the environment less heterogeneous and the fluctuation of the physical properties are reduced. This phenomenon was also found in the previous studies using molecular dynamics simulations.[63,64] In our simulation, we suggested that the dynamics of the high dimensional East model are less heterogeneous. To prove the arguments, we show the evidences for the reduced heterogeneity. First, the decoupling of the mean exchange time and the mean persistence time is shown. As the dimension is increased, the decoupling is decreased. Moreover, the time scale analysis shows that direct measure of the dynamic heterogeneity, dynamic susceptibility, reveals higher dimensional East models are less heterogeneous. The length scale analysis and associated scaling analysis also state that the lower dimensional East models are spatially more heterogeneous. It is noteworthy that the East model which has extremely strong directional facilitation is

also getting less heterogeneous in high dimensions.

Chapter 4

Dynamic Heterogeneity in Crossover Spin Facilitated Model of Supercooled Liquid and Fractional Stokes-Einstein Relation

4.1 Introduction

Supercooled liquid is a metastable state of matter that appears below the melting temperature of liquid.[1,2,5,11,35] One of the intriguing features of the supercooled liquid is rapidly growing relaxation times at low temperatures. Using the temperature dependent behavior of the relaxation time, they can be classified into two different cases. Both the viscosity and relaxation times of the strong liquids show Arrhenius behavior, while those of the fragile liquids show super-Arrhenius behavior.[1,5,11] The Arrhenius behavior shows that the effective energy barrier is constant under the temperature variation. In the fragile liquids, however, the effective energy barrier increases as the temperature decreases. Many theoretical and numerical studies indicate that the energy barrier of fragile liquids is inversely proportional to the temperature,

$\Delta E \sim A/T$,[42,48,52] which yields the log of the relaxation time that is inversely proportional to the square of temperature, $\tau \sim e^{A/T^2}$.

Various models have been proposed to explain and to analyze the properties of the supercooled liquids. Among these models, kinetically constrained models (KCMs) are particularly important and have attracted much scientific interest because it can explain the dynamic properties of supercooled liquids despite its simplicity.[26,49,52,65,66,66,67] KCMs are lattice models which are designed based on the dynamical facilitation mechanisms, where the thermodynamic interactions are suppressed. Each lattice site represents spatially coarse-grained liquids, which is assumed to have length scale larger than the interaction range of molecules. Only with simple kinetic constraints in the absence of complicated static interactions, KCMs have been recognized as useful theoretical models that are able to describe the distinctive properties of the supercooled liquids.

The fragile-to-strong crossover behavior has been experimentally observed in confined waters and many glass forming liquids.[68–72] In many of these studies, it has been considered that the local structure change causes the fragile-to-strong crossover. To model the crossover behavior, many different theoretical crossover models have been proposed using KCMs.[52,65–67] Among the models, Buhot et al. used a combination rule of symmetric and asymmetric facilitations to realize crossover behavior based on the Frederickson-Andersen (FA) model and the East model.[52,65] In their study, the crossover temperature depends on the asymmetric parameter which controls the extent of asymmetricity.

In this study, we use a similar model system as used in Ref. 65, and analyze the crossover behavior of the relaxation time, the diffusion constant and the dynamic length scale. We also study the heterogeneous dynamics found in

the crossover models which is an important dynamic property of supercooled liquid systems. Investigating the relation between the relaxation time and the diffusion constant, we find the fractional Stokes-Einstein relation in this model.

The contents in this chapter are organized as follows: In Section 4.2, we introduce the crossover model system. In Section 4.3, various physical quantities showing crossover behavior are calculated. The breakdown of Stokes-Einstein relation and the power behavior of the dynamic length scale between the relaxation time are also demonstrated. Finally, concluding remarks follow in Section 4.4.

4.2 Theory and computational method

Theories based on kinetically constrained models grant a privileged role to dynamics in explaining most properties of supercooled liquids, without invoking explanations based on structural properties.[73] One family of the models in this field is spin facilitated model, first proposed by Frederickson and Andersen.[40] In this model, the liquid is described as a lattice of spins that can either take value of 1 or 0. We choose 1 for the active region and 0 for the inactive region. Spins that satisfy a certain constraint in the neighboring configuration can undergo flipping transition under the condition of detailed balance. The simplest version requires only one adjacent active spin. This model, called FA model, has inspired many variations of spin facilitated models. One variation, called the East model,[41] incorporates directional facilitation; a spin can flip only if there is an adjacent active spin to a pre-specified direction, say, to the East direction. The FA model is a well known model for describing strong liq-

uids and the East model shows the properties of fragile liquids in terms of the temperature dependence of the relaxation times.[26,49]

We use an one-dimensional crossover model that interpolates between the FA-like model and the East model according to the asymmetry parameter, $0 \leq b \leq 1/2$, which was proposed by Buhot et al.[65] The equilibrium Hamiltonian of the system is trivial; if n_i stands for the i-th spin, $H = \sum_{i=0}^{N-1} n_i$ ($n_i = 1, 0$). The equilibrium concentration c of active spins is

$$c = \frac{e^{-1/T}}{1 + e^{-1/T}}. \tag{4.1}$$

For convenience, the Boltzmann constant is taken to be unity. In our calculation, the system size is set to contain 100 active spins. The probability P_i for the i-th spin to flip is given by

$$P_i = (bn_{i+1} + (1-b)n_{i-1})\min\left\{1, \exp\left(-\frac{\Delta H}{T}\right)\right\}. \tag{4.2}$$

Note that the $b = 0$ case coincides with the East model, while the $b = 1/2$ case is symmetric like the genuine FA model. There is a subtle difference between the $b = 1/2$ case and the FA model, which differs by factor of 2 in the relaxation time in the low temperature limit. Therefore, from now on, we will use labels FA and East in place of $b = 1/2$ and $b = 0$, respectively. To calculate temporal evolution of the system, a simple version of continuous-time Monte Carlo method, called the n-fold way method is used.[55]

4.3 Results and discussion

4.3.1 Dynamic heterogeneity and the breakdown of Stokes-Einstein relation

An important dynamic property of supercooled liquid is dynamic heterogeneity.[57,73–75] In supercooled liquids, particles with similar mobilities cluster together, giving rise to a mosaic of microscopic regions with different dynamics. This spatio-temporal correlation is dubbed dynamic heterogeneity. Common manifestations of dynamic heterogeneity are stretched exponential decay of correlation functions and the decoupling of the diffusion constant and structural relaxation.[34,76] At low temperatures, local regions where structural relaxations are fast make dominant contribution to the diffusion constant, while local regions where structural relaxations are slow and have long relaxation time determine the relaxation times of the whole system. As a result, the Stokes-Einstein relation, $D\tau \sim$ const, satisfied in normal liquids, does not hold in the supercooled regime.

Dynamic heterogeneities of either strong or fragile liquids have been studied thoroughly using computational models. In contrast, dynamic heterogeneities of systems showing the fragile-to-strong transition have been investigated to much less degree in terms of the variety in models and observables.[52,65,66] In this work, we investigate physical properties closely connected to dynamic heterogeneities of the fragile-to-strong crossover model. In the following paragraph, results of the relaxation time and the diffusion constant will be shown. Then, the fractional Stokes-Einstein relation and corresponding power law exponent will be presented.

First, we use the mean persistence time, $\tau_{\rm pers}$, as the relaxation time of the system. The persistence time of the i-th spin is defined as the time interval between the beginning of the simulation and the first flip of that spin.[26] The mean persistence time is calculated by averaging over the whole systems and 10,000 independent trajectories.

$\tau_{\rm pers}$ of the crossover model is plotted against temperature in Fig.4.1(a). The $b = 0$ model reproduces fragile behavior and the behavior of $b = 1/2$ model is same as that of the true FA model, which is $\tau_{\rm pers} \sim c^{-3}$.[26] Intermediate models with b between 0 and 1/2 show super-Arrhenius behavior in high temperature regime, but below a certain crossover temperature, T_c, their relaxation times follow the Arrhenius law. Fig.4.1(b) shows this in clear fashion by plotting effective energy barrier of relaxation,[65]

$$\Delta E = \frac{{\rm d}\ln\tau_{\rm pers}}{{\rm d}(1/T)}. \tag{4.3}$$

These are in accordance with the results obtained by Buhot et al.,[65] in spite of different definition of the relaxation time.

If the relaxation mechanism of the intermediate model is additive with respect to the symmetric and asymmetric processes, then the relaxation time of the intermediate models can be expressed in the following way.

$$\frac{1}{\tau_{\rm pers}} \approx \frac{4b(1-b)}{\tau_{\rm sym}} + \frac{1-2b}{\tau_{\rm asym}}, \qquad (0 \le b \le 1/2) \tag{4.4}$$

where $\tau_{\rm sym}$ is the relaxation time of the symmetric model (FA model) and $\tau_{\rm asym}$ is the relaxation time of the asymmetric model (East model). In our model system, we use the constraint that satisfies Eq.(4.2). Considering the

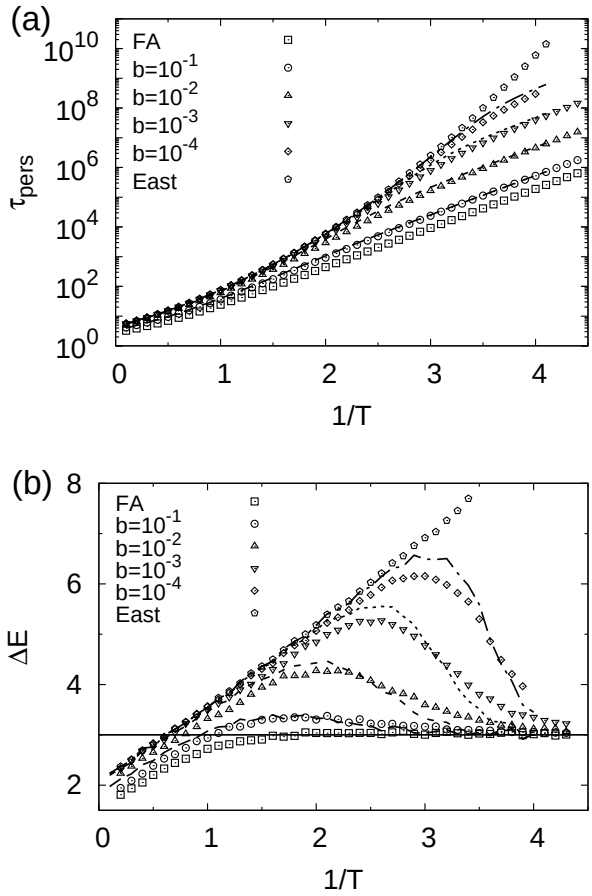

Figure 4.1: (a) The mean persistence times of the models with various values of the asymmetric parameter b. The black curves are the values calculated using Eq.4.4. The crossover behavior is observed in the models with $b = 10^{-1}, 10^{-2}, 10^{-3}, 10^{-4}$. (b) Effective energy barrier of the relaxation process. For the $b = 0$ model, the energy barrier is constant at sufficiently low temperatures, $\tau \sim c^{-3} \sim e^{3/T}$. Energy barrier of the East model is inversely proportional to the temperature. Other crossover models show a peak which could be used for defining crossover temperature, T_c. Note that the derivatives of $\tau_{\rm pers}$ obtained using Eq.4.4 well describe each system.

probability of flipping through the symmetric process, temperature dependent rate of symmetric process would be $\Gamma_{\rm sym} \propto b(1-b)/\tau_{\rm sym}$ where $\tau_{\rm sym}$ is the temperature dependent relaxation time of symmetric model (FA model). A product of probabilities of a flipping neighboring site ($be^{-1/T}$ or $(1-b)e^{-1/T}$ for neighboring site of left or right, respectively) and then flipping itself ($(1-b)$ or b) is used to derive the equation. For the asymmetric process, we can rearrange Eq.(4.2) to find the portion of asymmetric process: $P_i = (b(n_{i-1}+n_{i+1}) + (1-2b)n_{i-1})\min\left\{1, \exp\left(-\frac{\Delta H}{T}\right)\right\}$. In this way, we estimated that additional portion which comes from the asymmetric process would be proportional to $1-2b$. The mean persistence time of the crossover model can be written in the following form:${\tau_{\rm pers}}^{-1} = \Gamma_{\rm total} = \Gamma_{\rm sym} + \Gamma_{\rm asym} \approx 4b(1-b){\tau_{\rm sym}}^{-1} + (1-2b){\tau_{\rm asym}}^{-1}, \quad (0 \le b \le 1/2)$. The coefficient 4 in the numerator is adopted to reproduce the condition, $\tau_{\rm pers}(b=1/2) = \tau_{\rm sym}$. A similar equation has been proposed and used in Ref. 65. The overall agreement between Eq.4.4 and simulation results is excellent as shown in Fig.4.1.

Second, the diffusion constant is calculated by inserting the probe particles in the model and tracking the displacements of the probe particles.[26] The probe does not interact with the background liquids or other probes. The probe makes an attempt to move to neighbor lattice sites in every 1 MCS. The diffusion constant is defined as in the following equation,

$$D = \lim_{t\to\infty} \frac{\langle[\Delta\mathbf{r}(t)]^2\rangle}{2t}, \tag{4.5}$$

where $\Delta\mathbf{r}(t) = \mathbf{r}(t) - \mathbf{r}(0)$ and the bracket is the average of the term inside over different probes and trajectories. The square of the displacement is averaged

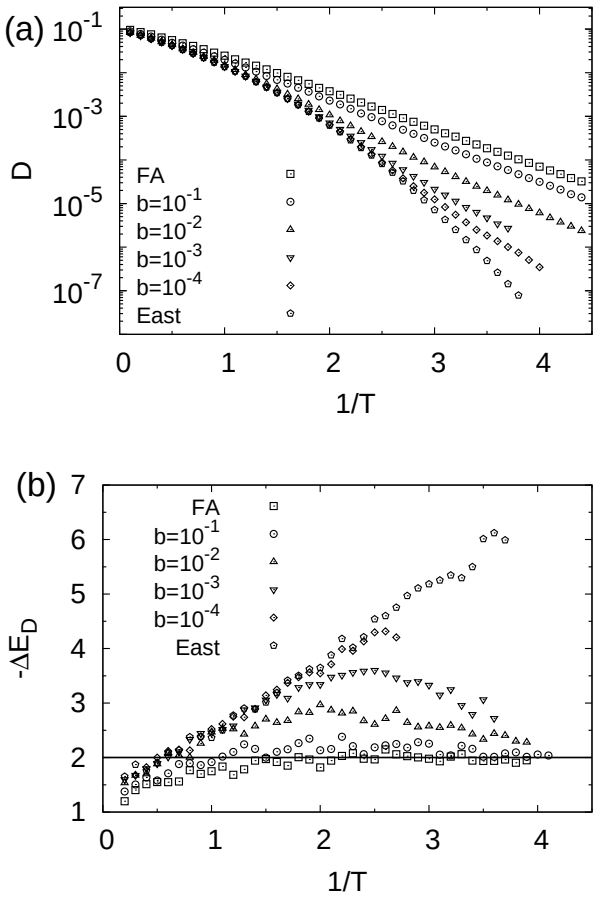

Figure 4.2: (a) The diffusion constant also shows fragile-to-strong crossover behavior. However, the crossover behavior is much slower compared to the mean persistence time (Fig.4.1(a)). (b) Effective energy barrier of the diffusion process. For the $b = 0$ model, the energy barrier is constant at sufficiently low temperatures, $D \sim c^2 \sim e^{-2/T}$.

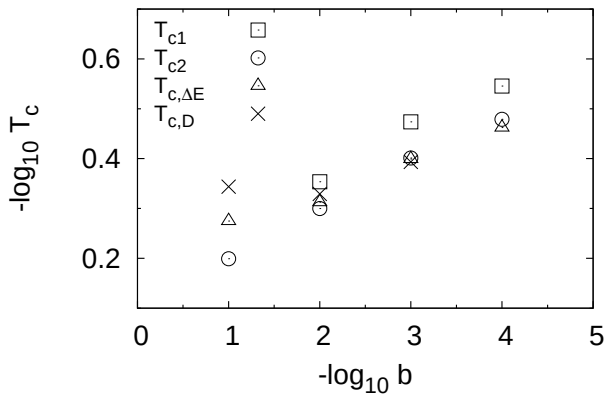

Figure 4.3: The crossover temperatures with different definitions. T_{c1} is obtained using the definition in Ref. 65. T_{c2} is the temperature of inflection point in the Eq.4.4. $T_{c,\Delta E}$ is the position of the peak in the Fig.4.1(b). $T_{c,D}$ is defined in the same way as $T_{c,\Delta E}$ using data of Fig.4.2.

about 10 probes and 2,400 independent trajectories. Simulation time of $10^4 \sim 10^8$ MCS is sufficient for our temperature range. The dynamic crossover of the diffusion constant that is similar to that of the relaxation time could be observed (Fig.4.2). However, the convergence to the FA-like behavior[26] of $D \sim c^{-2}$ is slower than the case of the mean persistence time and the simple analytical model like Eq.4.4 is not found for the diffusion constant. Note that this crossover in the diffusion constant also happens in triangular lattice gas model.[66]

To account for the crossover temperature, different definitions are formulated and compared with each other. One possible definition utilized in Ref. 65 is the temperature at which the rate of the symmetric process and asymmetric processes are equal, T_{c1}. Another possible choice is the temperature at the inflection point, and such temperatures on our analytic curve based on Eq.4.4,

T_{c2}, and numerically obtained curve on $\tau_{\rm pers}$ and diffusion constant are denoted respectively as $T_{c,\Delta E}$ and $T_{c,D}$. As the asymmetric parameter decreases, the crossover becomes more apparent and different definitions tend to agree with each other, with the exception of the T_{c1} (Fig.4.3).

Using the mean persistence time and the diffusion constant, the breakdown of Stokes-Einstein relation is investigated as shown in Fig.4.4(a). At high temperatures, $D\tau_{\rm pers}$ is nearly constant. However, as the temperature decreases, $D\tau_{\rm pers}$ increases abruptly in all models. Furthermore, the fragile-to-strong dynamic crossover is visible. This result is consistent with that obtained from triangular lattice gas.[66]

When the diffusion constant is plotted against the relaxation time (Fig.4.4(b)), they seem to be related by fractional exponent, $D \sim \tau_{\rm pers}^{-\xi}$, for all models. Note that the log-log plot does not show a clear crossover behavior in the crossover models. The power law exponent, ξ, does not change under the range, while it has the value between that of the FA model ($\sim$0.67) and the East model ($\sim$0.73).[26] We expect that simulations in higher dimension where the difference between the exponent of the FA model and the exponent of the East model is larger[65] would reveal the transition appearing at a single crossover temperature. Note that, in higher dimensions, the FA model which has a finite upper critical dimenion recovers Stokes-Einstein relation,[61,62] while the East model is expected to exhibit the exponent lower than 1.[26,50] In Fig.4.4(c), the average exponents are shown. The exponents smoothly change from the value of the FA model to the value of the East model.

In some cases, the condition that $D\tau/T$ is constant over temperature change is used for the Stokes-Einstein relation.[77,78] We also show the temperature

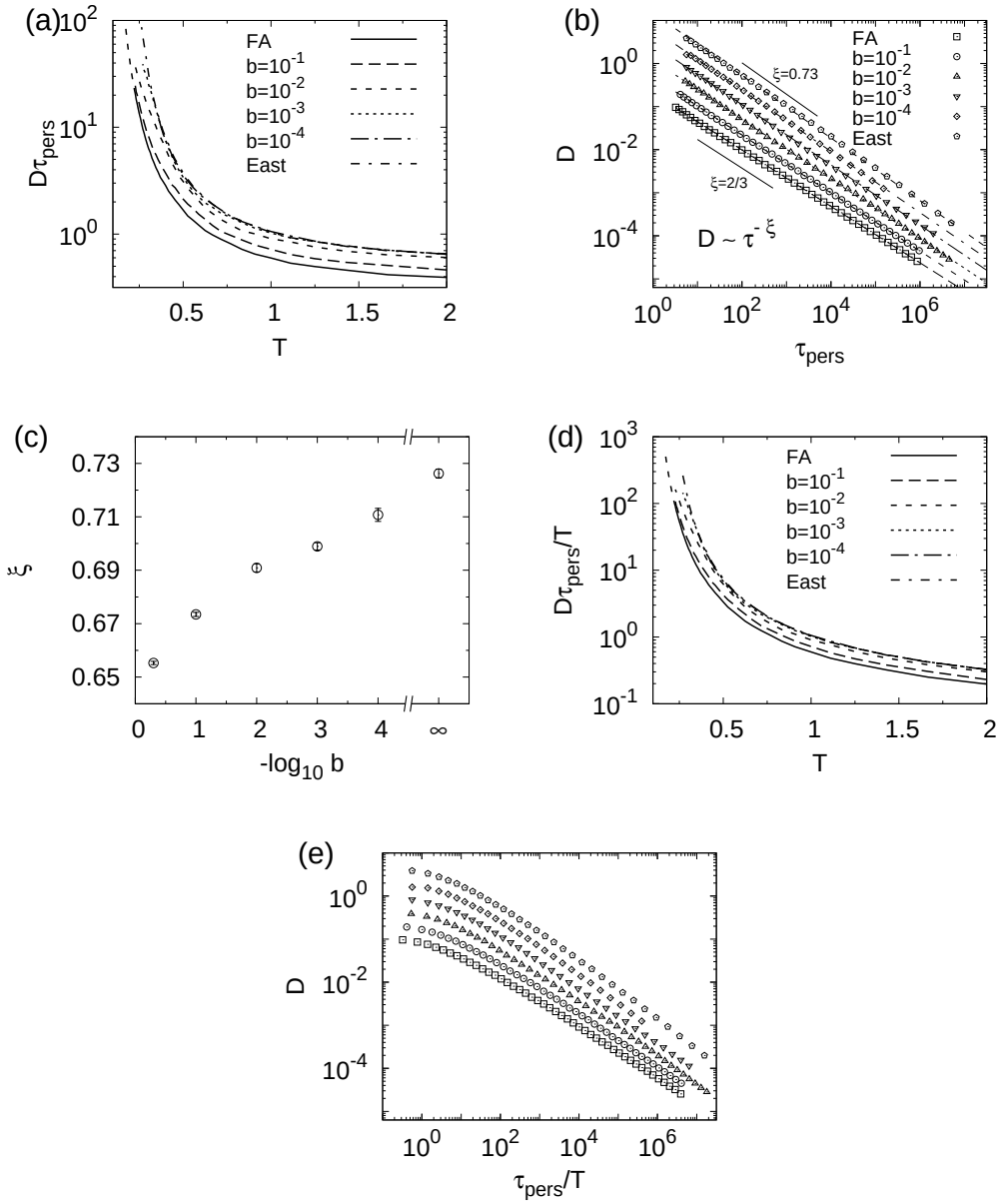

Figure 4.4: (a) Breakdown of the Stokes-Einstein relation and fragile-to-strong dynamic crossover. (b) The fractional Stokes-Einstein relation, $D \sim \tau^{-\xi}$. The data other than those belonging to the FA($b = 1/2$) model were offset by factors of $10^{1/6}$ for clear comparison. (c) The increase of the fractional Stokes-Einstein exponent by the increase in asymmetry. The East model's value is also marked on the right end. (d) Temperature dependence of $D\tau_{\mathrm{pers}}/T$. As the temperature decreases, $D\tau_{\mathrm{pers}}/T$ increases abruptly. (e) Log-log plot of D versus τ_{pers}/T. As the temperature decreases, the power law is recovered.

dependence of $D\tau_{\rm pers}/T$ in Fig.4.4(d), which shows similar result as Fig.4.4(a). When D is scaled with $\tau_{\rm pers}/T$, the power law relation does not hold as strongly as in the $D\tau_{\rm pers}$ case at high temperatures as shown in Fig.4.4(e). As the temperature decreases, however, D and $\tau_{\rm pers}/T$ show power law behavior similar to Fig.4.4(b). In the asymptotic limit that the temperature is low enough, the power exponent would be eventually the same as one obtained in Fig.4.4(b), because $\log\tau_{\rm pers}$ increases much faster than $\log T$.

4.3.2 Dynamic correlation lengths

The mobility of the spin is estimated by the persistence function $\pi_i(t)$ that is 1 if spin i has never flipped, or 0 if spin i has flipped at least once. The four-point correlation function $C(r,t)$ defined from the persistence function contains the information on the length and time scale of the dynamic heterogeneity:

$$C(r,t) = \frac{\langle \frac{1}{N}\sum_{i=0}^{N-1}\pi_i(t)\pi_{i+r}(t)\rangle - \langle \frac{1}{N}\sum_{i=0}^{N-1}\pi_i(t)\rangle^2}{\langle \frac{1}{N}\sum_{i=0}^{N-1}\pi_i(t)\rangle - \langle \frac{1}{N}\sum_{i=0}^{N-1}\pi_i(t)\rangle^2}. \tag{4.6}$$

The terms in the bracket are averaged over 100,000 independent trajectories. As the time scale of the maximal dynamic heterogeneity is comparable to the relaxation time of the system,[51,61] the time is fixed to be $\tau_{\rm pers}$ of the system. In order to prove spatial aspects of dynamic heterogeneity in the crossover model, dynamic length scale is calculated (Fig.4.5(a)). The dynamic correlation length, ζ, which is defined as the distance that $C(r,\tau_{\rm pers})$ falls to $1/e$, is chosen as the dynamic length scale.

Unlike $\tau_{\rm pers}$ or diffusion constant, the dynamic correlation length turns out to be a robust quantity that depends on the asymmetry parameter lit-

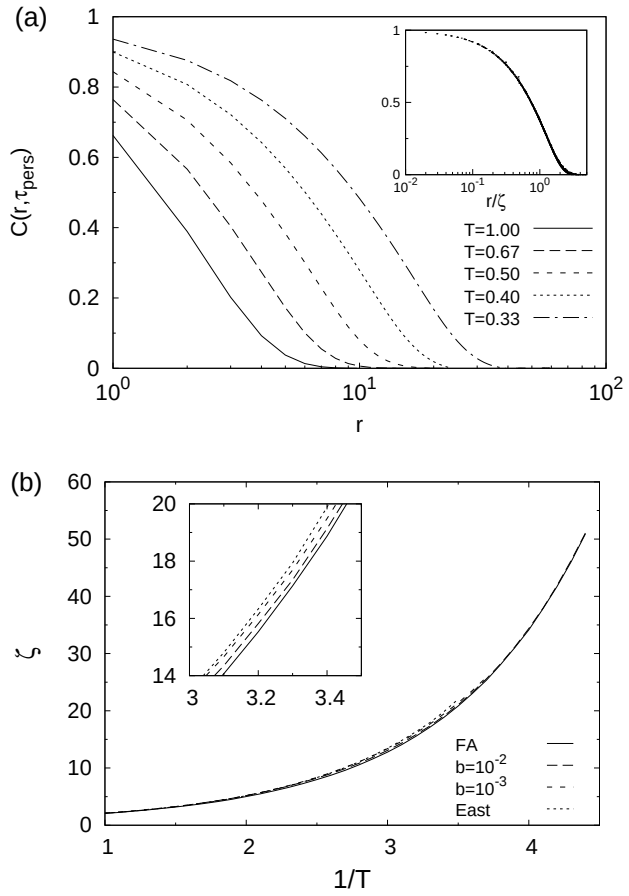

Figure 4.5: (a) Correlation function calculated with parameter b=0.01. Inset shows the collapse of different sets of parameters into a single curve. (b) Dynamic correlation length is increasing as the temperature decreases. Inset is the magnification of data to see clear crossover behavior.

tle (Fig.4.5(b)). Nonetheless, there is a non-trivial difference between the two extreme cases - ζ_{East} is consistently larger than ζ_{FA} - and the intermediate models are in between.

In related studies,[51,61,79,80] the dynamic length scale was defined as the scaling factor for the correlation function $C(r,t)$ or its Fourier transform $S(k,t)$. In Fig.4.5(a), it is demonstrated that our dynamic length scale can also act as a scaling factor and thus the two definitions are in agreement with each other. This also means that a different choice of the cutoff value for the correlation function would not affect our conclusion.

The crossover from the $b = 1/2$ model behavior to the $b = 0$ model behavior with respect to temperature is studied (Fig.4.6(a)). When the temperature is low enough ($T \leq 0.35$) $\zeta_{\mathrm{East}} - \zeta_{\mathrm{FA}}$ is much larger than statistical fluctuation, so smooth and approximately linear transition is obtained. The onset temperature of such crossover is similar to the crossover temperature obtained from τ_{pers} and diffusion constant.

Intuition tells us that when temperature is sufficiently low, the active spins are sparse and each spin will be visited by a single active spin on average during the relaxation time, and therefore $\zeta \sim c^{-1}$. Combined with the FA models' scaling law $\tau_{\mathrm{pers}} \sim c^{-3}$,[26] it is expected that the $b = 1/2$ model will show scaling behavior of $\zeta \sim \tau_{\mathrm{pers}}^{\nu}$ with $\nu = 1/3$ in low temperature, which is confirmed by our calculation as shown in Fig.4.6(b). The fragile-to-strong crossover is apparent in the intermediate models. The crossover temperatures would be those of τ_{pers}, as the change in τ_{pers} over the temperature is much more significant than the change in the dynamic correlation length over the same range.

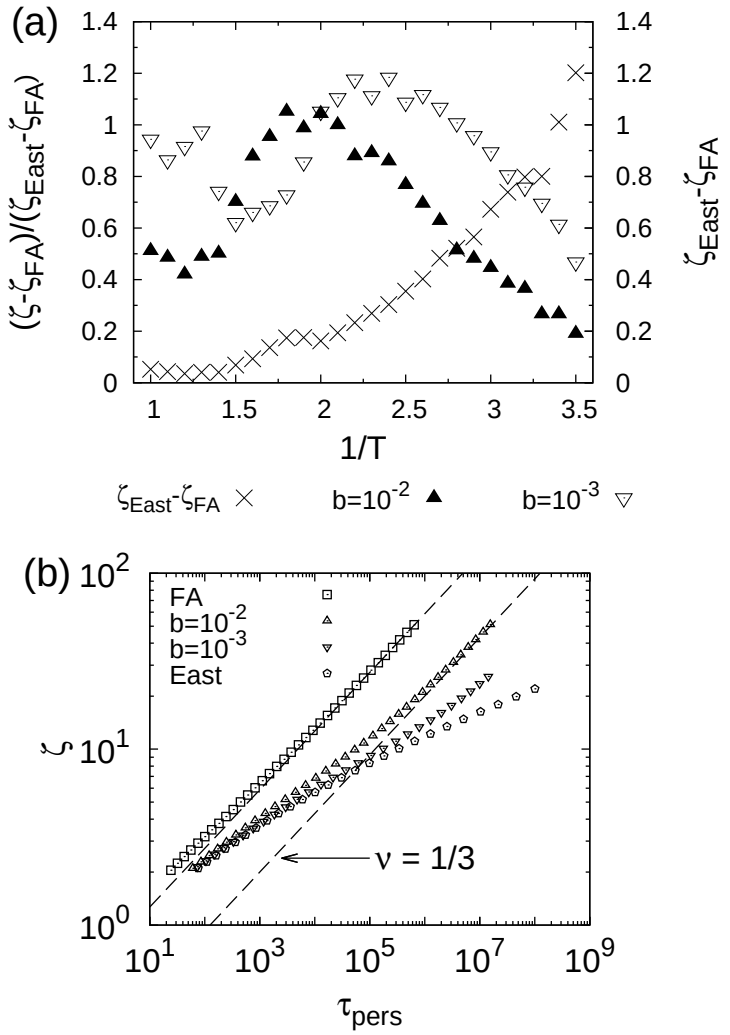

Figure 4.6: (a) Crossover of dynamic length scale from the FA model to the East model. (b) The relation between the dynamic correlation length and $\tau_{\rm pers}$.

4.4 Conclusion

Evidence of dynamic heterogeneity in a theoretical model that shows the fragile-to-strong transition is investigated. As the temperature decreases, functions related to dynamic heterogeneity make smooth fragile-to-strong crossover around a certain crossover temperature. The dynamic properties such as the mean persistence time and the diffusion constant clearly show the crossover behavior. The onset temperature of the transition is given as the function of asymmetry parameter, practically independent of the observable. It monotonously decreases as the asymmetry of the kinetic constraint increases. These observations are consistent with the entropic barrier mechanism proposed by Buhot et al.,[65] although our data shows that there is a room for improvement for better predictions around the crossover temperature.

Using the relaxation time defined as the mean persistence time and the diffusion constant, the fractional Stokes-Einstein relation is investigated. One interesting feature is that there is no crossover behavior for the power law relations. When the asymmetry parameter b is fixed, the power law exponent is constant under the temperature change. Above and beneath the transition temperature, the exponents are same in the range of error. As expected, however, we find smooth transition of the exponents from 0.67 to 0.73 as the b is reduced. We note that there has been a recent debate on the nature of Stokes-Einstein breakdown in kinetically constrained models.[53,81]

The dynamic length scale extracted from the spatial correlator $C(r,t)$ is also studied. The correlation length experiences crossover from the value of the FA model to that of the East model. Similar to the behavior in the triangular

lattice gas (TLG) model system,[66] the correlation length shows clear crossover with the relaxation time and recovers the power relation, $\zeta \sim \tau_{\rm pers}^{1/3}$. Note that, in our study, the dynamic length scale is much less sensitive to asymmetry of the kinetic constraint than the transport properties such as the relaxation time and the diffusion constant.

The dynamic crossover has been explained as the consequence of the competition between entropy barrier of symmetric mechanism and energy barrier of asymmetric mechanism.[65] That the crossover temperatures of different physical quantities are the same function of asymmetry parameter seems to validate this explanation, although during the discussion on Eq.4.4, this picture seems to be in need of a refinement around the crossover temperature where the symmetric process and asymmetric process occur in similar rate.

Finally, we would like to mention that fragile-to-strong crossover seen in our calculation has been experimentally observed in various glass-forming liquids and supercooled waters in confined state.[68–72] The authors of these papers conjectured that there is a liquid-liquid phase transition occurring at the point of crossover. Furthermore, the fragile-to-strong crossover behavior has its origin to local structure change such as change of hydrogen bonding environments. In our crossover model, however, the detailed information of local structure is coarse-grained out and the structure change is not considered as a critical origin of a crossover behavior. In place of invoking local structure change, we use kinetic constraint and the asymmetric parameter to realize the crossover behavior. Further scrutinies would seem necessary to reveal the microscopic mechanisms involved in the liquid-liquid transition.

Chapter 5

Heterogeneous Dynamics and its Length Scale in Simple Ionic Liquid Models: A Computational Study

5.1 Introduction

Room-temperature ionic liquids (RTILs) have attracted great attention because of their uncommon physical properties and various applications for non-toxic solvent.[82–84] Widely known features of RTILs are their thermal stability, high polarity, high viscosity, very low vapor pressure, and low combustibility. Usually, RTILs are composed of bulky, asymmetric cations and small, symmetric anions. Due to their considerable size difference, RTILs exist in a liquid phase near the room temperature in spite of having strong Coulomb interactions. One of the intriguing feature of RTILs is their heterogeneous dynamics which could be found in the supercooled liquids. As reported by theoretical[27,32,33] and experimental studies,[4] RTILs have non-exponential decay of correlation functions, which could be regarded as an evidence of heterogeneous dynamics.

Computer simulation study also has found the glassy dynamics of RTILs via the breakdown of the Stokes-Einstein relation and decoupling of exchange and persistence events of defined excitations.[27]

The heterogeneous dynamics found in RTILs are originally found in the supercooled liquids. When the liquids are cooled down rapidly, they exist in a supercooled liquids rather than forming a crystal structure. The viscosity and the structural relaxation time are growing dramatically as the temperature of the system is lowered. The complete understanding of physical phenomena and theoretical explanations are still missing. Among the distinctive behaviors of the supercooled liquids, the correlations between the local density fluctuations are found to play an important role in the slowing down of system. This phenomenon, typically called dynamic heterogeneity, has been investigated through diverse theoretical[8,20,22,25,26,34,49,50,60,85–89] and experimental studies.[21,90–93]

In the previous theoretical and computational studies, the time scale and the length scale of the dynamic heterogeneity have been obtained using the four-point density correlation functions[20,24,34,60,87,88,94–99] , which has its origin in the study of spin glasses.[100] A four-point correlation is defined as

$$\begin{aligned} g_4(\mathbf{r},t) = &\langle \delta\rho(0,0)\delta\rho(0,t)\delta\rho(\mathbf{r},0)\delta\rho(\mathbf{r},t)\rangle \\ &-\langle \delta\rho(0,0)\delta\rho(0,t)\rangle\langle \delta\rho(\mathbf{r},0)\delta\rho(\mathbf{r},t)\rangle, \end{aligned} \tag{5.1}$$

where $\delta\rho(\mathbf{r},t)$ is the deviation of the local density at the position $\mathbf{r}$ and at time t. $g_4(\mathbf{r},t)$ measures the correlation of relaxation of the density fluctuation between the two points separated by $\mathbf{r}$. The dynamic susceptibility and the dynamic structure factor can be derived from this function, by integrating and by performing Fourier transform, respectively. Obtained functions can be ex-

pressed in the form of Eq.5.5 and Eq.5.10. We use the dynamic susceptibility as a index of the quantification of the dynamic heterogeneity and define the time value that makes the dynamic susceptibility maximum as a lifetime of the dynamic heterogeneity. The dynamic structure factor is also calculated to extract the dynamic length scale, $\xi_4(t)$, which could be interpreted as a length scale of dynamically correlated regions. With these schemes, we find the characteristic time scale and the length scale of dynamic heterogeneity in the ionic liquid model systems.

There have been several computational studies on the description of the heterogeneous dynamics in the ionic liquid systems. However, the length scale of the dynamic heterogeneity has not been investigated thoroughly because of the difficulties on performing massive simulation with complex structures and long range interactions. To overcome this difficulty and to enhance computational efficiency, various levels of coarse-grained models have been proposed.[27,32,33,101,102] Among these models, we use simple models of RTILs introduced by a previous study.[101] In the model, cations are composed of two rigidly linked particles and anions are represented with single particle. We put the variation on the distributions of positive charge on the cations by making them symmetric or asymmetric. Detailed model description will be followed in the next section.

The contents in this chapter are organized as follows: In Section 5.2, we introduce ionic liquid models and shortly describe the simulation methods. In Section 5.3, the evidences of heterogeneous dynamics in the ionic liquid models are shown using displacement distributions and the decoupling of the mean exchange time and the mean persistence time. Furthermore, the dynamic length

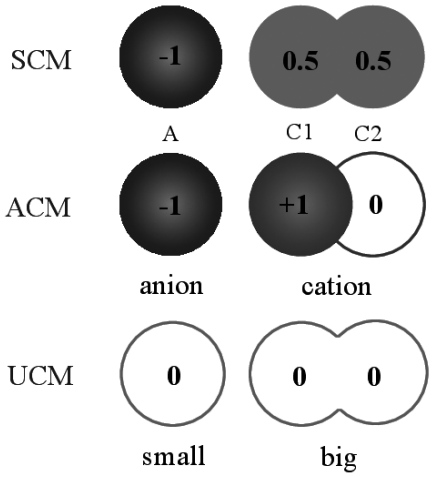

Figure 5.1: Schematic representation of the three models. SCM (top) and ACM (middle) represent symmetrically charged and asymmetrically charged model of ionic liquid, respectively. While the anions of both model have the charge of $-1.0e$, the cations have different charge distribution: the positive charge is equally distributed for SCM cation particles ($+0.5e$ for C1 and C2), the charge is separated for ACM cation particles ($+1.0e$ for C1 and zero for C2). UCM (bottom) denotes the uncharged model as a comparison group without charge on every particles.

scale obtained by calculating four-point correlation functions and related scaling behavior will be illustrated. Finally, the conclusions on this work are shown in the Section 5.4.

5.2 Models

We use simple coarse-grained models to investigate the heterogeneous dynamics of the room-temperature ionic liquid systems. To study the effect of charge distribution on the cation, the symmetrically charged model (SCM) and the asymmetrically charged model (ACM) are used. In addition, the uncharged

model (UCM) is also used as a comparison group. Three model systems have cation which is composed of two particles and anion of single particle, FIG.5.1. All the physical parameters are the same for those models except the charge distribution. SCM has $+0.5e$ on each particle in the cation and $-1.0e$ on the anion, while ACM has $+1.0e$ on C1 particle, zero charge on C2 particle, and also $-1.0e$ for anion. UCM has zero charge for all particles. In some context, we use "big particle" and "small particle" for the cation and the anion in the UCM.

The total potential energy is given by the sum of the pairwise interactions,

$$U_{\text{total}} = \sum_{i,j} \{U_{\text{LJ}}(r_{ij}) + U_{\text{Coulomb}}(r_{ij})\} \tag{5.2}$$

where,

$$U_{\text{LJ}}(r_{ij}) = 4\epsilon_{ij}\left[\left(\frac{\sigma_{ij}}{r_{ij}}\right)^{12} - \left(\frac{\sigma_{ij}}{r_{ij}}\right)^{6} + \frac{1}{4}\right] H(r_{\text{cut}} - r_{ij}), \tag{5.3}$$

and

$$U_{\text{Coulomb}}(r_{ij}) = \frac{1}{4\pi\epsilon_0}\frac{q_i q_j e^2}{r_{ij}}. \tag{5.4}$$

$H(r_{\text{cut}} - r_{ij})$ is the Heaviside step function, where the cutoff distance is set to be $r_{\text{cut}} = 2^{1/6}\sigma_{ij}$. Note that $U_{\text{LJ}}(r_{ij})$ is purely repulsive and it is called the Weeks-Chandler-Andersen (WCA) potential.[103] In all of three models, $\epsilon_{ij} = \epsilon = 2\text{kJ/mol}$ and $\sigma_{ij} = \sigma = 0.5\text{nm}$ for all i, j pairs. The length of rigid bond between two particles (C1 and C2) in the cation is set to be 0.8σ. The mass of the particles in the cation is $m = 100\text{amu}$ and the mass of the anion is 200amu, so the total mass of the cation and the anion is same. We use the length, energy, and mass scaled by the units of σ, ϵ, and m. The other units

are converted by following relation: unit time, $t_0 = (m\sigma^2/\epsilon)^{1/2} = 5$ps, unit temperature, $T_0 = \epsilon/k_{\mathrm{B}} = 240.5$K, unit charge, $q_0 = (4\pi\epsilon_0\sigma\epsilon)^{1/2} = 0.08484e$, and unit pressure, $P_0 = 262.2$atm. We use 2048 pairs of RTIL molecules in a cubic simulation box of $L = 17.88$, where L is the length of each side. All the system have the reduced number density $\rho^* = \rho\sigma^3 = 0.716$.

We perform molecular dynamics (MD) simulation using GROMACS 4.5 MD package program[104] under NVT ensemble condition with Nosé-Hoover thermostat. Periodic boundary condition is applied to each direction and finite size effect is checked by comparing physical quantities with different system size of 512, 1024, 2048 and 4096 RTIL pairs. For all the systems, ten independent trajectories are used and the length of production run is about 40 times of the α-relaxation time of each system. The details of the molecular dynamics simulation conditions is written in the Ref. 105.

5.3 Results and discussion

5.3.1 Heterogeneous dynamics

Our ionic liquid model systems are expected to have heterogeneous dynamics because of size differences between the cations and the anions. To investigate heterogeneous dynamics in the model systems, we first calculate the displacements of each particles. FIG.5.2 shows the probability of the logarithm of displacements, $P[\log_{10}(\delta r); t]$. The time t is set to be the relaxation time at each temperature, where the relaxation time is defined by the time that the self-intermediate scattering function falls to $1/e$. The precise definition of the relaxation time and the simulation data can be found in the work of Park et al.[105]

$P[\log_{10}(\delta r);t]$ is related with the self-van Hove function, $G_s(\delta r;t)$, through the equation, $P[\log_{10}(\delta r);t] = 4\pi\log(10)\delta r^3 G_s(\delta r;t)$. Since $G_s(\delta r;t)$ is Gaussian function when the particle experiences the Fickian diffusion, $P[\log_{10}(\delta r);t]$ would show single peak. Therefore, the broadening or split of the distribution is a clear evidence for non-Fickian motion and heterogeneous dynamics.

In the FIG. 5.2, the distribution of the cation in SCM is getting broaden as the temperature is lowered. Compared to the anion case, the cation shows clear increment of fast particles. The results that the increasing number of fast cations at low temperature is consistent with the previous study that demonstrates the cation moves faster than the anion.[105] For the ACM, the distribution of the anion is more heterogeneous than the cation. This opposite result comes from the different charge distribution of the cation. Compared to the SCM, the cations in the ACM make irregular structures around the anions because of their asymmetric charge distribution. As a result, it is expected that relatively small anion could have fast movement. In the UCM system, alternative structure of big and small particles are not observed, since there is no charge on the big particles. The cage effect would be suppressed and the distributions of two particles show similar results. The difference of two distributions are not profound but the small particles have higher ratio of fast particles because of lower steric hindrance.

FIG.5.3 and FIG.5.4 show the time dependence of the probability distributions and corresponding the self-van Hove functions in SCM. A single peak at short time evolves into a broad distribution at $t = 1\tau \sim 5\tau$ and becomes a single peak again in the long time limit. From this results, we can infer that the dynamics are most heterogeneous at time around $1\tau \sim 5\tau$. In the ACM and

UCM, similar tendency is found for the calculated distributions. At long time limit, the self-van Hove function is getting close to the Gaussian distribution which is dashed line in the FIG.5.4, $G_s(\delta r;t) = (4\pi Dt)^{-3/2}\exp(-\delta r^2/(4Dt))$, where D is the diffusion coefficient. However, even at $t = 50\tau$, there exists a mismatch at small and large r meaning that the dynamic heterogeneity remains.

To observe the dynamic heterogeneity in a different way, we calculate the excitation of each particle. The excitation is defined as a event that single particle i moves more than d. For example, when particle i moved more than d at time t_1, $|\mathbf{r}_i(t_1) - \mathbf{r}_i(0)| > d$, than the first excitation takes place at $t = t_1$. Further, when particle moved more than d from the $\mathbf{r}_i(t_1)$ after t_2, $|\mathbf{r}_i(t_1+t_2) - \mathbf{r}_i(t_1)| > d$, than the second excitation is at $t = t_1 + t_2$. For the third excitation at $t = t_1 + t_2 + t_3$, same rule is applied, $|\mathbf{r}_i(t_1 + t_2 + t_3) - \mathbf{r}_i(t_1 + t_2)| > d$, and so on. Using the series of the excitations, we can define two time scales which are the persistence time and the exchange time. The persistence time is the time value that the first excitation occurs, so it is the set of all t_1 for every particle and trajectories. Another time scale, the exchange time, is defined by the waiting time between two excitations. It is the set of all $t_2, t_3, ...$ It has been known that the decoupling of two time scales occurs when the system is dynamically heterogeneous.[27,49] Jung et al. first calculated the relationship of two time scales in the kinetically constrained model (KCM) and showed that the dynamic heterogeneity provokes the decoupling of two time scales.[49] Although the definition of the excitation is different from the KCM, the physical meanings are similar in the ionic liquids system and it can be applied to study the heterogeneous dynamics in those systems.

Before analyzing the decoupling of two time scales, we visualize the hetero-

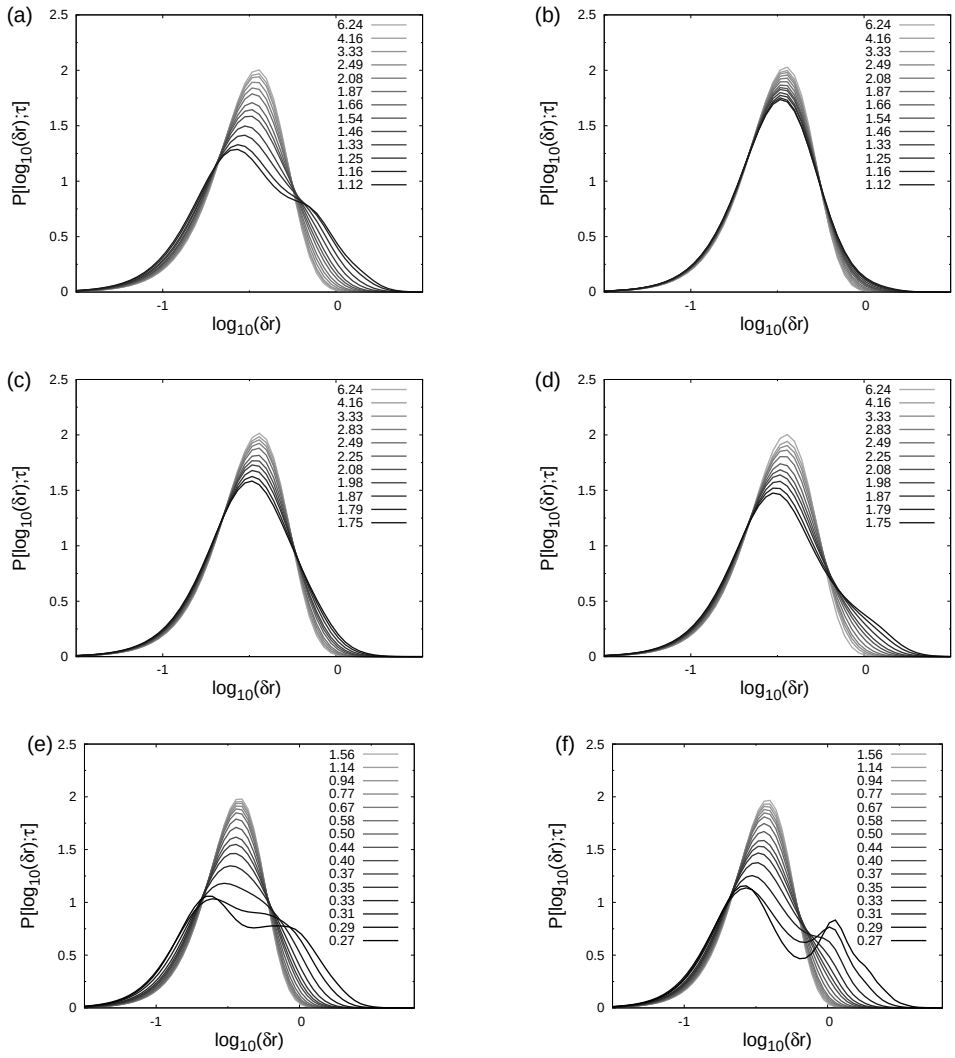

Figure 5.2: Displacement distributions of particles. (a)SCM-cation, (b)SCM-anion, (c)ACM-cation, (d)ACM-anion, (e)UCM-big particle, (f)UCM-small particle. As the temperature is decreased, displacement is getting heterogeneous.

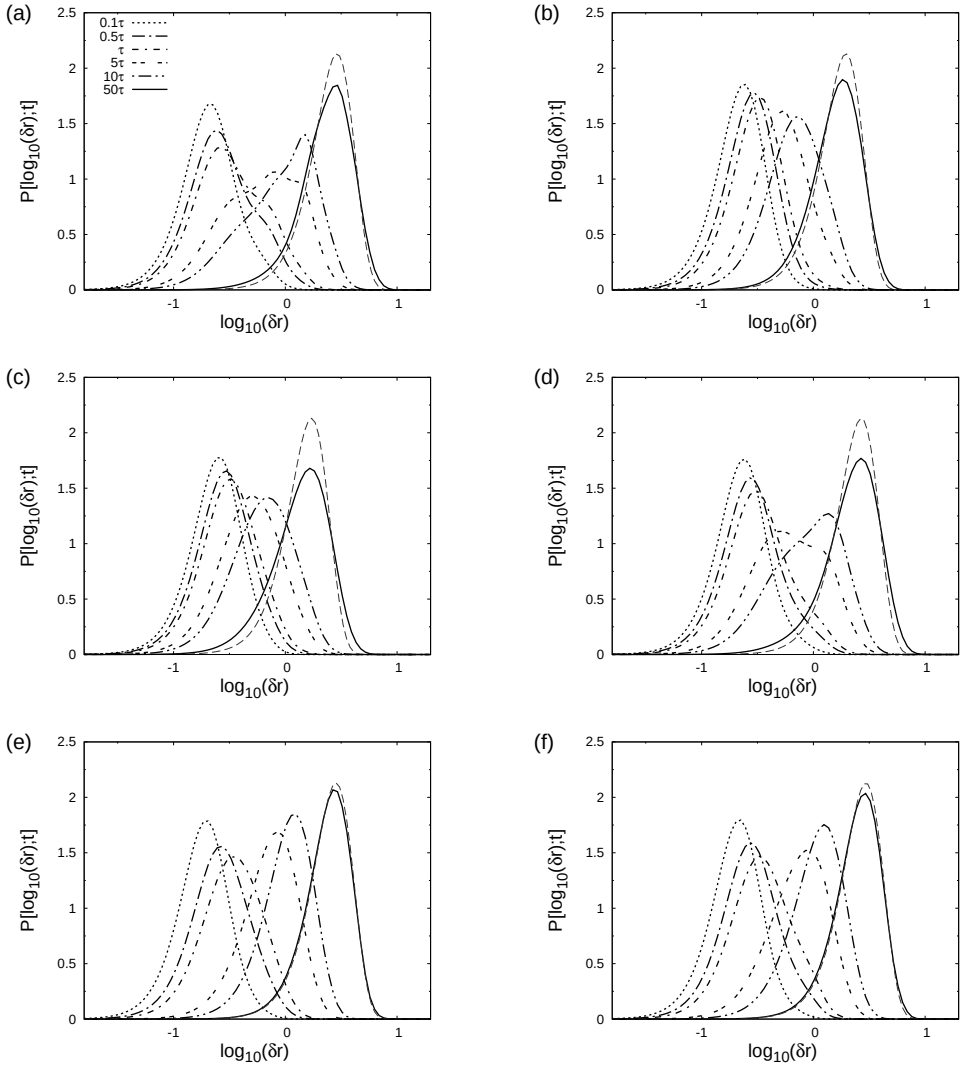

Figure 5.3: Time dependence of the displacement distribution. (a)SCM-cation; T=1.12, (b)SCM-anion; T=1.12, (c)ACM-cation; T=1.75, (d)ACM-anion; T=1.75, (e)UCM-big particle; T=0.35, (f)UCM-small particle; T=0.35. At short time and long time, the distribution has the single peak (dashed line shows Gaussian distribution). The distribution is heterogeneous at the time near the α-relation time.

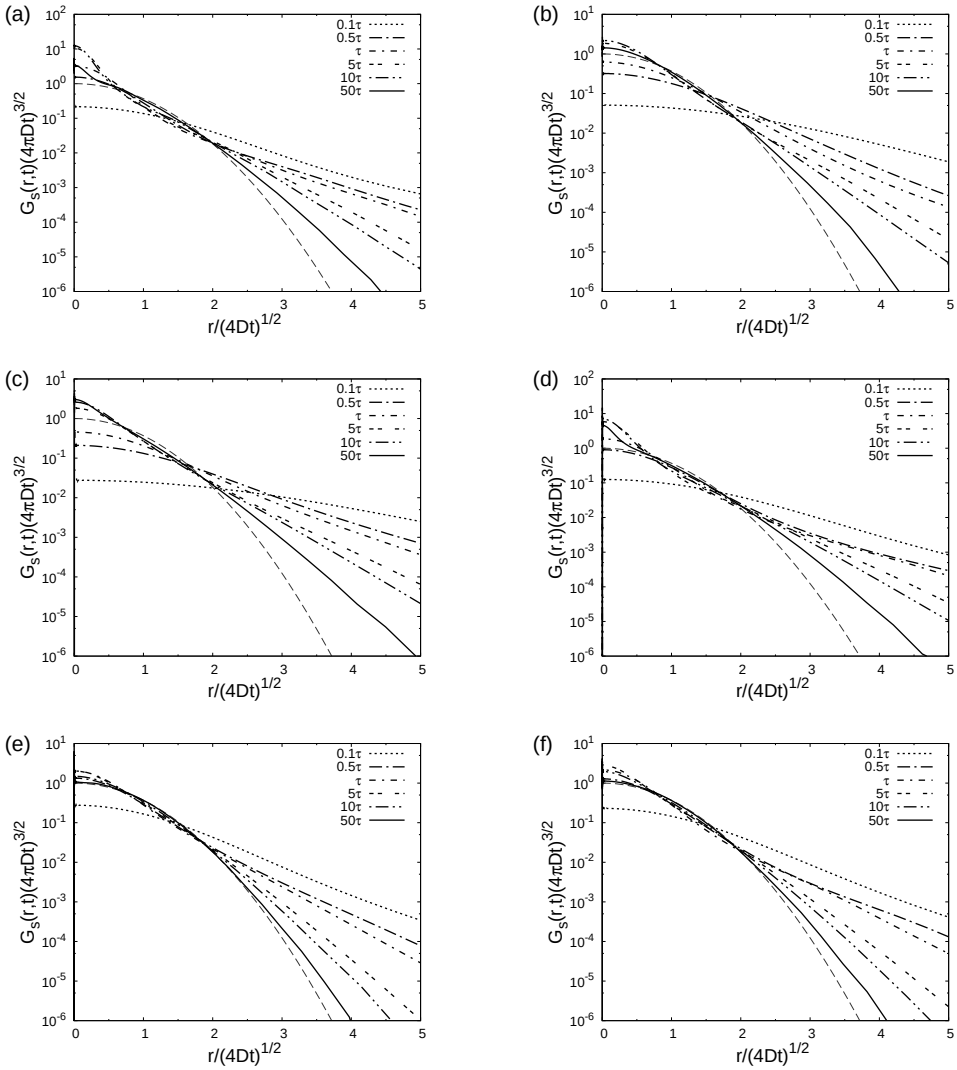

Figure 5.4: Self-van Hove function is getting close to the Gaussian distribution (dashed line). However, there is still mismatch for the fast particles even in the long time limit. (a)SCM-cation; T=1.12, (b)SCM-anion; T=1.12, (c)ACM-cation; T=1.75, (d)ACM-anion; T=1.75, (e)UCM-big particle; T=0.35, (f)UCM-small particle; T=0.35.

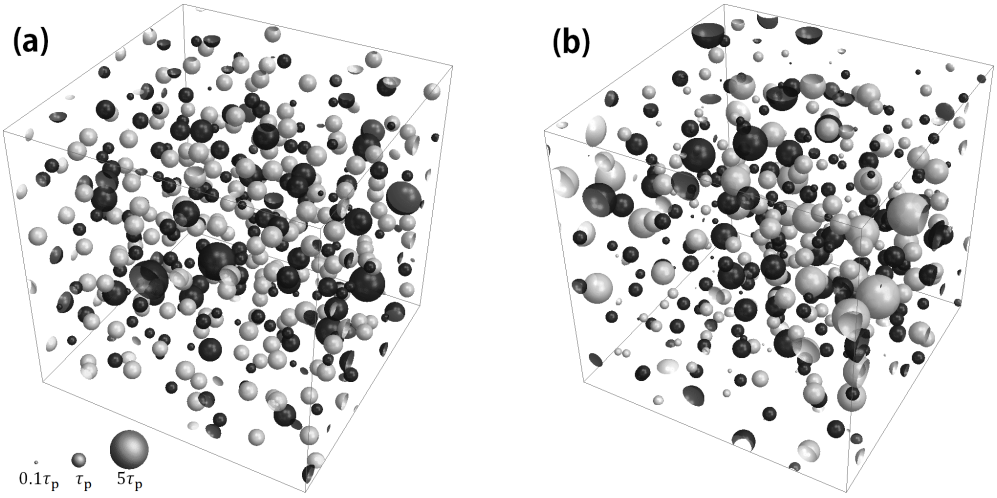

Figure 5.5: Spatial distribution of persistence times of cation (Gray) and anion (Black) at high temperature (T=6.24) (a) and low temperature (T=1.12) (b). The size of the particle is proportional to the log of persistence time of each particle. The comparison of two snapshots clearly shows that persistence time is heterogeneous in time and also in space at low temperature.

geneous dynamics using the persistence time of each particle. Fig. 5.5 shows the spatial distributions of the persistence times. The radius of each particle represents the size of the persistence time in logarithm scale. For the cuf-off distance d, we used $d = 1$ which is comparable to the size of particles. At high temperature, Fig. 5.5(a), the persistence time distribution is relatively homogeneous than the low temperature, Fig. 5.5(b). It can be seen that not only the size of particle is heterogeneous at low temperature but the spatial distribution also shows the heterogeneity. This means that there is correlations between the slow particles and this could be the evidence of growing dynamic length scale.

Now we investigate the decoupling of two time scales and relate this phenom-

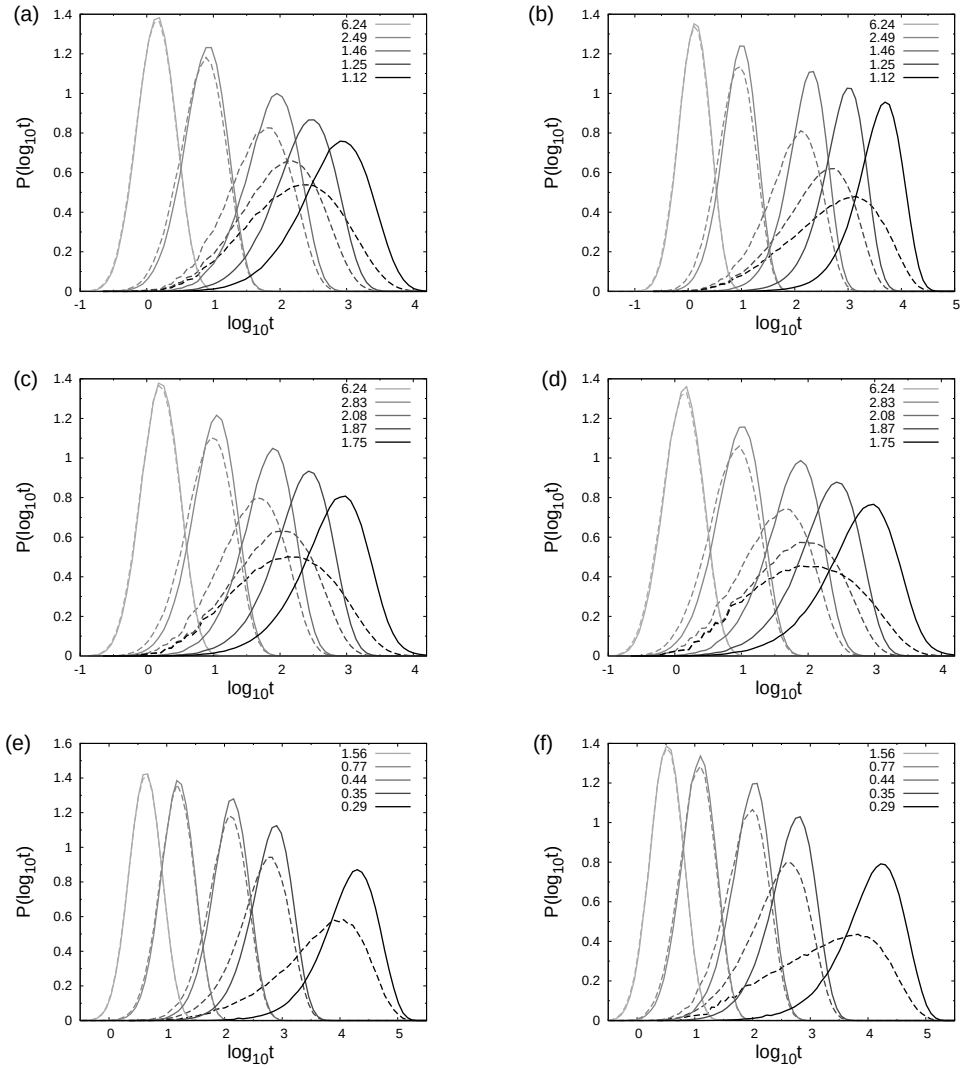

Figure 5.6: Probability distribution of the exchange time and the persistence time. (a)SCM-cation, (b)SCM-anion, (c)ACM-cation, (d)ACM-anion, (e)UCM-big particle (f)UCM-small particle. As the temperature is lowered, the distributions are decoupled.

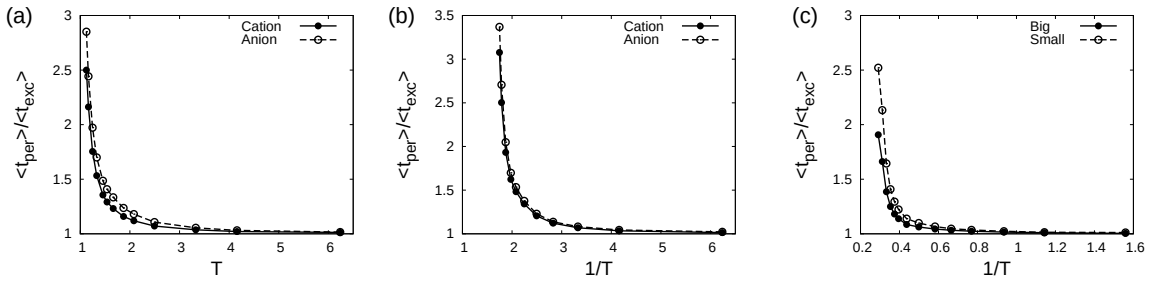

Figure 5.7: The ratio of the mean persistence time and the mean exchange time increases abruptly at low temperatures. (a)SCM, (b)ACM, (c)UCM.

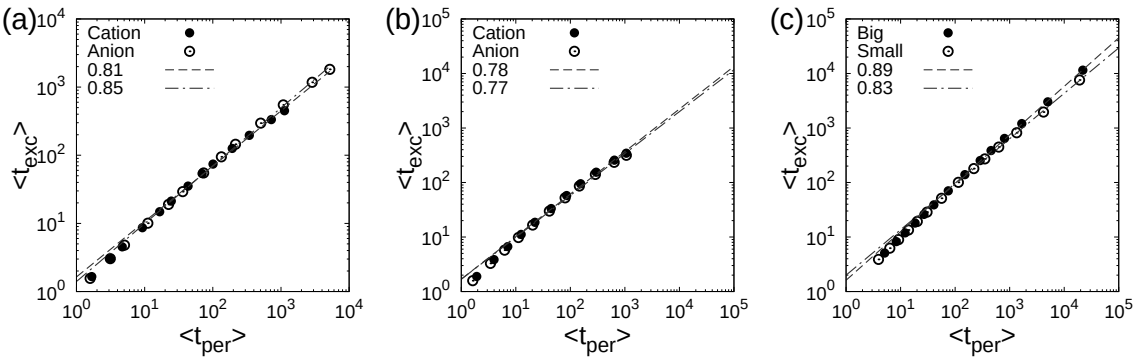

Figure 5.8: The mean persistence time and the mean exchange time show power law relationship. (a)SCM, (b)ACM, (c)UCM.

ena with the breakdown of the Stokes-Einstein relation. When the probability distribution of the exchange time is exponential, the distribution of two time scales would be identical because the persistence time is related with the exchange time though the integral.[49] At high temperature, there would be weak correlations between the excitation events meaning that excitation events are in Possion process. At low temperature, however, the correlations between the excitation would be pronounced and excitation event would experience non-Possion process that results in decoupling of the persistence time and the exchange time distributions, Fig.5.6. We can interpret this phenomenon that the correlations between excitations increased because of the clustering of slow particles.

The mean values of two time scale also show the decoupling. The mean persistence time and the mean exchange time which are defined by the ensemble average of the persistence times , $\tau_p = \langle t_p \rangle$, and the exchange times, $\tau_e = \langle t_e \rangle$, are related to the transport coefficients which are the relaxation time and the diffusion coefficient, respectively.[27] It has been known that the mean persistence time would be proportional to the relaxation time, τ, when d is comparable with $2\pi/q$ where q is the first peak position of the structure factor. Furthermore, the exchange event is governed by the diffusion of particle so that $1/\tau_e$ would have relation between diffusion constant, D, through power law relation. In the ionic liquid system with fragile nature, it has been shown that there is a sublinear relation between $1/\tau_e$ and D, irrespective of d. FIG.5.7 shows the ratio of τ_p and τ_e, which shows similar divergent behavior of $D\tau$ at low temperatures.[105] In addition, there are power law relations, $\tau_e \sim \tau_p^{\nu}$, between two physical time scales as it can be seen in FIG.5.8. The value of

the power law exponents are 0.81(SCM-cation), 0.85(SCM-anion), 0.78(ACM-cation), 0.77(ACM-anion), 0.89(UCM-big particle) and 0.83(UCM-small particle). The exponent of the SCM cation is analogous to that of the coarse-grained ionic liquids system which is 0.80 for cations.[27] Comparing the values of the exponents, we can infer that the fragility of the system increases in the order of UCM, SCM and ACM. All the missing graphs can be found in the supporting information.

In this section, we confirmed that the heterogeneous dynamics found in the supercooled liquids system are also found in our ionic liquids model systems. From the displacement distribution, we find the clue that the mobility of the particles are heterogeneously distributed. However, the correlations between slow or fast particles can not be obtained from this analysis. To observe this correlated behavior, a four-point correlation function will be introduced to calculate dynamic length scale in the next section. It is noteworthy that the distribution of the charge on the cations not only changes the local structure but also affects the fragility of the whole system. From the scaling analysis, we find that the difference between the cation and the anion is smaller compared to the differences between the model systems. So, it is reasonable to concentrate on the differences between the models rather than the particles.

5.3.2 The dynamic susceptibility and the dynamic structure factor

In the previous studies of glassy dynamics, there have been several schemes to define the length scale of the dynamic heterogeneity. Among the various definitions of the length scale, the dynamic length scale defined using the four-

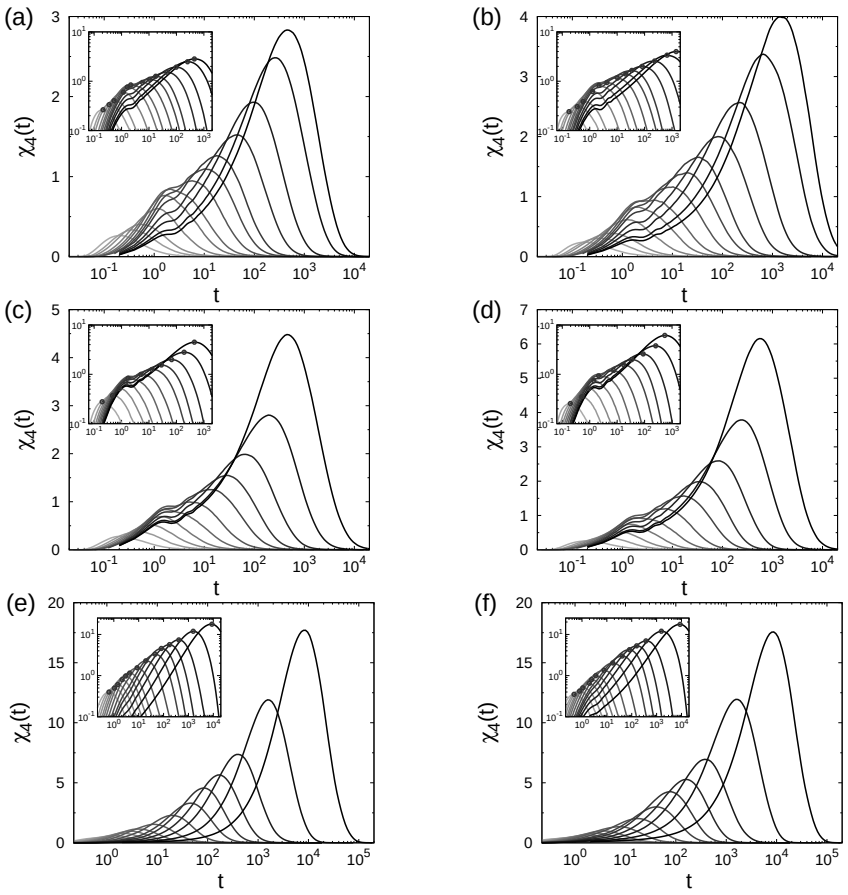

Figure 5.9: Dynamic susceptibility, $\chi_4(t)$, of the cations and the anions in each system calculated using Eq.5.5 at various temperatures. (a)SCM-cation, (b)SCM-anion, (c)ACM-cation, (d)ACM-anion, (e)UCM-big particle, (f)UCM-small particle. From left to right, T= 6.24, 4.16, 3.33, 2.49, 2.08, 1.87, 1.66, 1.54, 1.46, 1.33, 1.25, 1.16 and 1.12 (SCM), T= 6.24, 4.16, 3.33, 2.83, 2.49, 2.25, 2.08, 1.98, 1.87, 1.79 and 1.75 (ACM), T= 1.56, 1.14, 0.94, 0.77, 0.67, 0.58, 0.50, 0.44, 0.40, 0.37, 0.35, 0.33 0.31 and 0.29 (UCM). Log-log plots are also shown (inset). The time value that makes $\chi_4(t)$ maximum is defined as the lifetime of the dynamic heterogeneity, t_4^* (black dots).

point correlation function has been widely used for many systems. We use a conventional framework that has been previously estabilished and applied to analyze the supercooled liquids systems.[20,34,60] The dynamic susceptibility, $\chi_4(t)$, is defined as,

$$\chi_4(t) = \frac{1}{N}[\langle Q(t)^2\rangle - \langle Q(t)\rangle^2], \tag{5.5}$$

$$Q(t) = \sum_{i=1}^{N} w(|\mathbf{r}_i(0) - \mathbf{r}_i(t)|), \tag{5.6}$$

where $w(|\mathbf{r}_i(0) - \mathbf{r}_i(t)|)$ is a overlap function which is 0 when $|\mathbf{r}_i(0) - \mathbf{r}_i(t)| > a$ and 1 when $|\mathbf{r}_i(0) - \mathbf{r}_i(t)| \leq a$. $Q(t)$ counts the number of self overlapping particles using the configurations separated by a time interval t. Thus, $Q(t)/N$ could be regarded as an index how much the system has been relaxed. $Q(t)/N$ decays from 1 to 0 as the time is passed, showing similar functional behavior with the self-intermediate scattering function. Eq. 5.5 tells that $\chi_4(t)$ could be interpreted as a quantification of a fluctuation which $Q(t)$ has. In this study, we choose overlap cutoff $a = 0.3$ which is a conventional value. The α-relaxation time, τ_α, can be defined by the time that makes $Q(\tau_\alpha)/N = 1/e$, FIG.5.17(c). This definition gives analogous value of τ_α with the result of the conventional use of self-intermediate scattering function. Additionally, for the cations, $\chi_4(t)$ calculated using the coordinates of the center of mass and the particle itself did not show distinctive difference for the scaling law. We will use the simulation data obtained by calculations with center of mass for each cation.

FIG.5.9 shows the dynamic susceptibility calculated using the Eq. 5.5 at various temperatures. At fixed temperature, $\chi_4(t)$ increases as the time is passed. $\chi_4(t)$ has a maximum peak at certain time scale, namely $t_4^*(T)$, which

is comparable to the relaxation time, $\tau_\alpha(T)$. We find that t_4^* is proportional to τ_α for all three model systems. This time scale, t_4^*, which shows the maximum value of the dynamic susceptibility, $\chi_4^* = \chi_4(t_4^*)$, is defined as a lifetime of the dynamic heterogeneity. As the time is increased further, $\chi_4(t)$ decreases to zero. The functional form of $\chi_4(t)$ confirms that the dynamic heterogeneity is transient in time. As the y-axis in the inset of the FIG.5.9 is log scale, χ_4^* would show power law relation with t_4^*. Note that the maximum value, χ_4^*, is marked with black dot. We find the power law relations between t_4^* and χ_4^* for all systems. Moreover, the crossover behaviors at short time regime are found for SCM and ACM. The existence of crossover behavior is a unique phenomenon in our model compared to the models of supercooled liquids. This phenomenon is based on the enhanced separation of sub-diffusive regime and diffusive regime for charged model. The details about the crossover behavior will be discussed in the next section.

Alternative definition of the dynamic susceptibility can be used,[95]

$$\tilde{\chi}_4(k,t) = \frac{1}{N}[\langle \tilde{Q}(\mathbf{k},t)^2 \rangle - \langle \tilde{Q}(\mathbf{k},t) \rangle^2], \tag{5.7}$$

$$\tilde{Q}(\mathbf{k},t) = \sum_{l=1}^{N} e^{i\mathbf{k}\cdot(\mathbf{r}_l(t)-\mathbf{r}_l(0))}, \tag{5.8}$$

where $k = |\mathbf{k}|$. Here, k is a wavevector that regulates the length scale of local area and has the similar role of a in the overlap function. Using the Eq.5.7 and

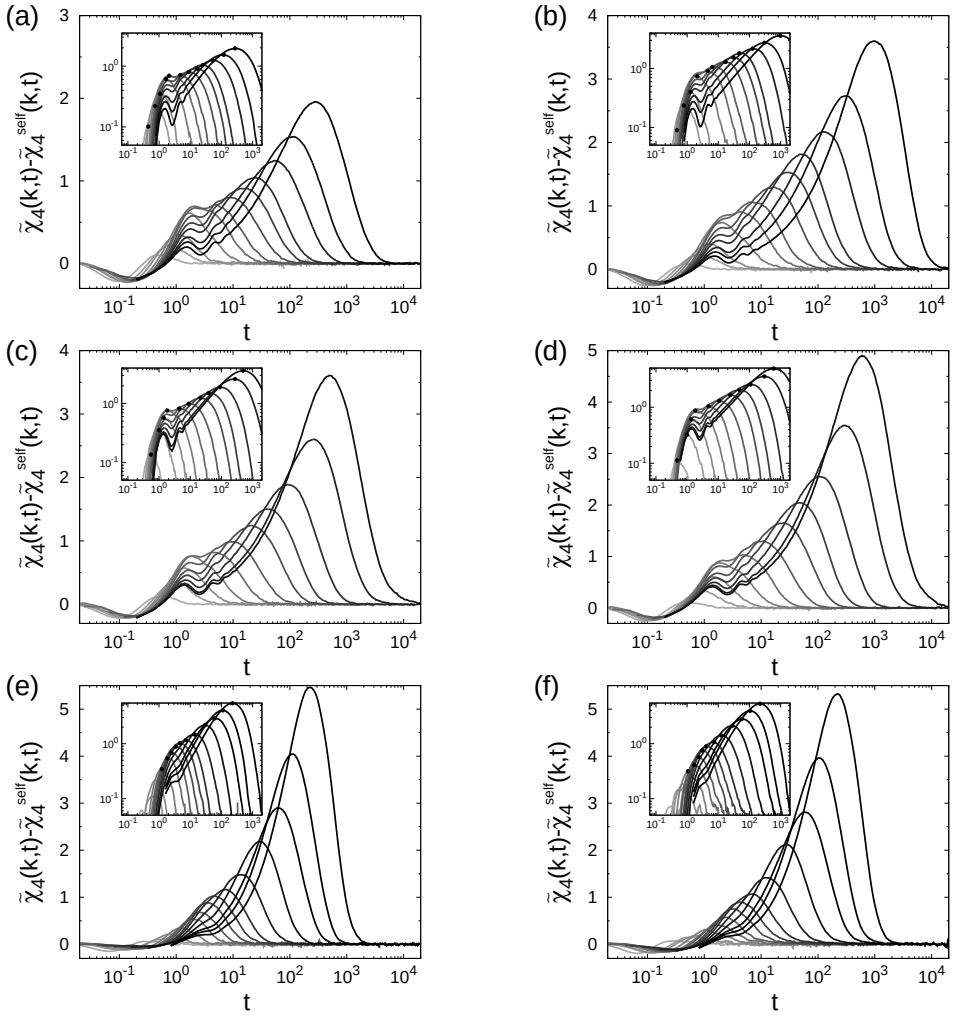

Figure 5.10: The dynamic susceptibility calculated using Eq.5.7. Wavevector k is defined by $k = 2\pi/\lambda_{\max}$, where $\lambda_{\max} = 0.92$ is the shortest peak position of radial distribution function between cation and anion.e Temperatures are same with FIG.5.9. Log-log plot is illustrated in the inset and the maximum points are shown with black dots.

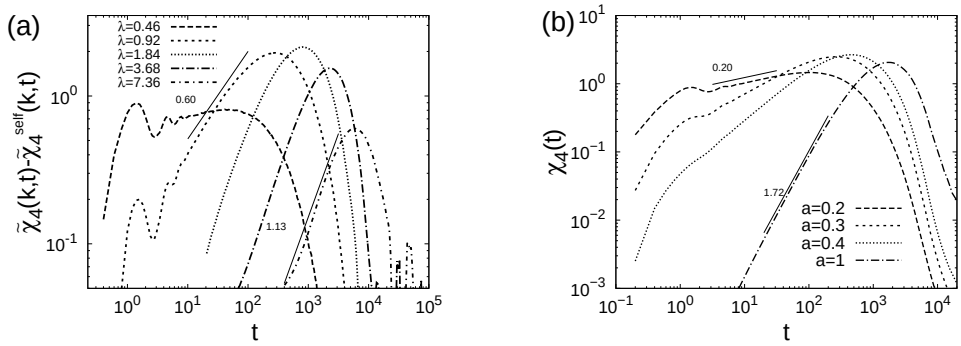

Figure 5.11: (a)Wavevector $k = 2\pi/\lambda$ dependence on $\tilde{\chi}_4(k,t) - \tilde{\chi}_4^{\rm self}(k,t)$. λ is varied from $0.5\lambda_{\rm max}$ to $8\lambda_{\rm max}$. As the k is decreased, the peak appears at longer time. Data is calculated at $T = 1.16$ for cation in SCM. (b)Cutoff length a dependence on $\chi_4(t)$. As the a is increased, the peak appears at longer time. Data is calculated at $T = 1.16$ for cation in SCM.

Eq.5.8, $\tilde{\chi}_4(k,t)$ can be expressed in the form,

$$\tilde{\chi}_4(k,t) = \frac{1}{N}\sum_{j=1}^{N}\sum_{l=1}^{N}\langle\delta\tilde{Q}_j(\mathbf{k},t)\delta\tilde{Q}_l(-\mathbf{k},t)\rangle, \tag{5.9}$$

where $\delta\tilde{Q}_j(\mathbf{k},t) = e^{i\mathbf{k}\cdot(\mathbf{r}_j(t)-\mathbf{r}_j(0))} - \langle e^{i\mathbf{k}\cdot(\mathbf{r}_j(t)-\mathbf{r}_j(0))}\rangle$. In this form, the self part of $\tilde{\chi}_4(k,t)$ can be easily obtained applying $j = l$ condition, $\tilde{\chi}_4^{\rm self}(k,t) = 1 - F_s(k,t)^2$, where $F_s(k,t) = \langle e^{i\mathbf{k}\cdot(\mathbf{r}_j(t)-\mathbf{r}_j(0))}\rangle$ is the self-intermediate scattering function. FIG.5.10 shows the $\tilde{\chi}_4(k,t) - \tilde{\chi}_4^{\rm self}(k,t)$ at various temperatures. The wavevector is defined by $k = 2\pi/\lambda_{\rm max}$, where $\lambda_{\rm max}$ is the shortest peak position of radial distribution function between cation and anion. The overall functional form of $\tilde{\chi}_4(k,t) - \tilde{\chi}_4^{\rm self}(k,t)$ is similar with $\chi_4(t)$, while the peak at short time scale is more pronounced. The crossover behavior for the maximum point of $\tilde{\chi}_4(k,t)$ also can be found in the inset of FIG.5.10. In the study of Chandler et al., the wavevector dependence of the dynamic susceptibility is investigated for

the various supercooled liquid model systems.[95] For our ionic liquid system, similar result is obtained, FIG.5.11(a). Between β-relaxation regime and α-relaxation regime, we find a power law relation $\tilde{\chi}_4(k,t) \sim t^{\mu}$ with an exponent μ. Unlike the prediction of mode-coupling theory (MCT), μ shows the significant dependence on the wavevector. Note that the length scale dependence of the dynamic susceptibility can also be observed by varying the cutoff length, a, of the overlap function, w, FIG.5.11(b)

To obtain the length scale of the dynamic heterogeneity, we calculate the dynamic structure factor with follwing equations,

$$S_4(q,t) = \frac{1}{N}[\rho(\mathbf{q},t)\rho(-\mathbf{q},t)], \tag{5.10}$$

$$\rho(\mathbf{q},t) = \sum_{i=1}^{N} \exp[i\mathbf{q}\cdot\mathbf{r}_i(0)]w(|\mathbf{r}_i(0)-\mathbf{r}_i(t)|), \tag{5.11}$$

where $q = |\mathbf{q}|$. The dynamic correlation length, $\xi_4(t)$, is obtained by fitting the small wavevector regime into the Ornstein-Zernike (OZ) equation,

$$S_4(q,t) = \frac{S_4(q=0,t)}{1+(q\xi_4(t))^2}, \tag{5.12}$$

where, $S_4(0,t)$ and $\xi_4(t)$ are fitting parameters. $S_4(q,t)$ is fitted in the regime of $q \leq 1.5$ which is corresponding to the condition, $4.19 \leq r \leq 17.88$. Obtained correlation length is shown in the FIG.5.12 at various temperature and time. Similar to the dynamic heterogeneity, the correlation length is also transient in time. At first, the correlation length is growing until it reaches the maximum, after that it decreases. The functional form of the correlation length resembles that of $\chi_4(t)$, however, the time values that the peaks occur are not identi-

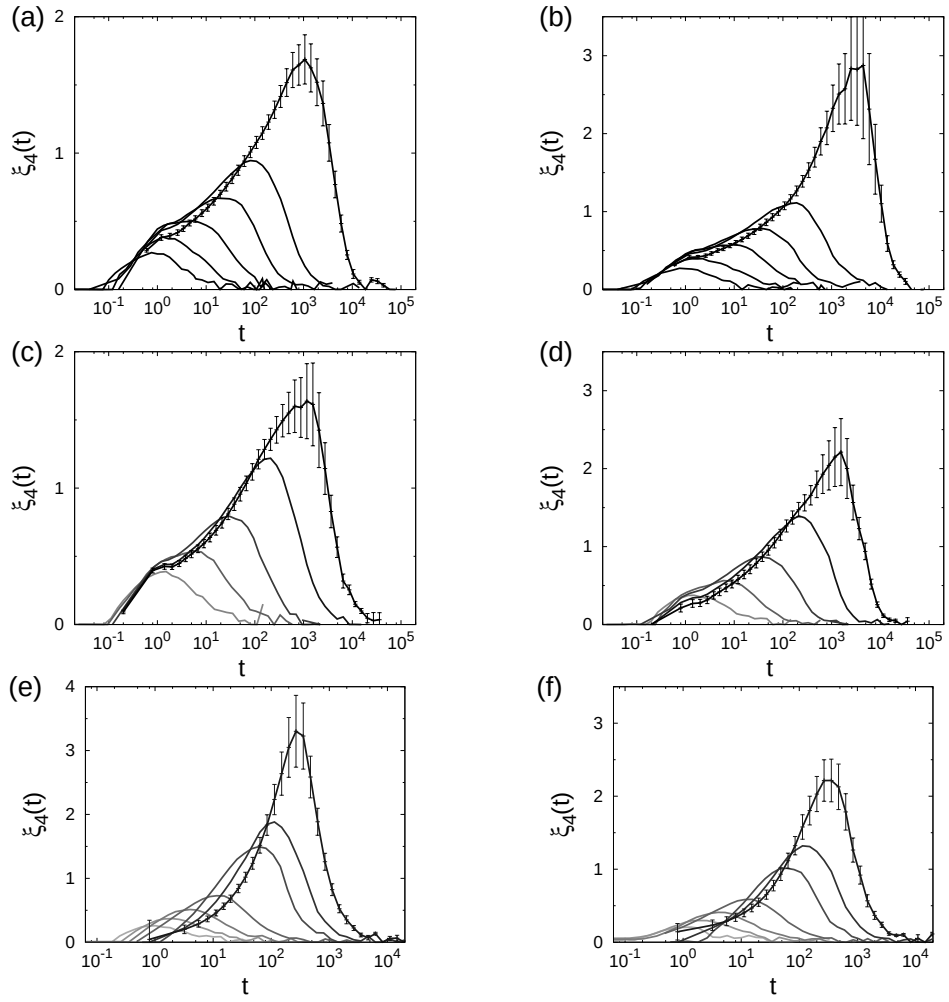

Figure 5.12: Time dependence of the dynamic correlation length, $\xi_4(t)$, at various temperatures. (a)SCM-cation, (b)SCM-anion, (c)ACM-cation, (d)ACM-anion, (e)UCM-big particle, (f)UCM-small particle. From left to right, T= 6.24, 2.49, 1.87, 1.54, 1.33, and 1.16 (SCM), T= 3.33, 2.49, 2.08, 1.87, 1.79, and 1.75 (ACM), T= 1.56, 0.94, 0.67, 0.50, 0.40, 0.37, and 0.35 (UCM). The error bars are shown only for the lowest temperature.

cal. Analogous to the previous studies on the supercooled liquids, the time for which $\xi_4(t)$ is maximum is larger than t_4^*. From this result, we find that the characteristic time scale of the correlation length is longer than the lifetime of dynamic heterogeneity.

To determine the dynamic correlation length of the system at fixed temperature, we use $\xi_4^* = \xi_4(t = t_4^*)$. ξ_4^* represents the dynamic correlation length when the dynamic heterogeneity is maximum. FIG.5.13 illustrates that all the dynamic structure factors collapse into single functional form of $f(x) = 1/(1 + x^2)$, when the x-axis is $q\xi_4^*$ and y-axis is $S_4(q, t_4^*)/S_4(0, t_4^*)$. The definition of the dynamic correlation length can be varied using different empirical functions. We compare various correlation length obtained by fitting $S_4(q, t_4)$ into functions: $(1)S_4(q, t_4^*) = S_4(0, t_4^*)/(1 + (q\xi_4^{(1)})^2)$; $(2)S_4(q, t_4^*) = (S_4(0, t_4^*) - C)/(1 + (q\xi_4^{(2)})^2) + C$; $(3)S_4(q, t_4^*) = (S_4(0, t_4^*) - C)/(1 + (q\xi_4^{(3)})^\zeta) + C$; $(4)S_4(q, t_4^*) = (S_4(0, t_4^*) - C)/(1 + (q\xi_4^{(4)})^2 + (q\xi_4^{(4)})^4) + C$. Here, the C and ζ are fitting parameters and C is included to improve the fitting against the baseline problem. The fitted function to the data is shown in the FIG.5.14(a) for cation in SCM at T=1.16.

FIG.5.14(b) shows the temperature dependence of these length scales for the cation in SCM. Among these correlation lengths, $\xi_4^{(1)}$ grows faster than the other lengths and shows clear crossover behavior. Moreover, the scaling behavior of $\xi_4^{(1)}$ and t_4^* reveals most reasonable power law exponent. In this sense, we use $\xi_4^{(1)}$ as a dynamic correlation length ,ξ_4^* , in the rest part of this article.

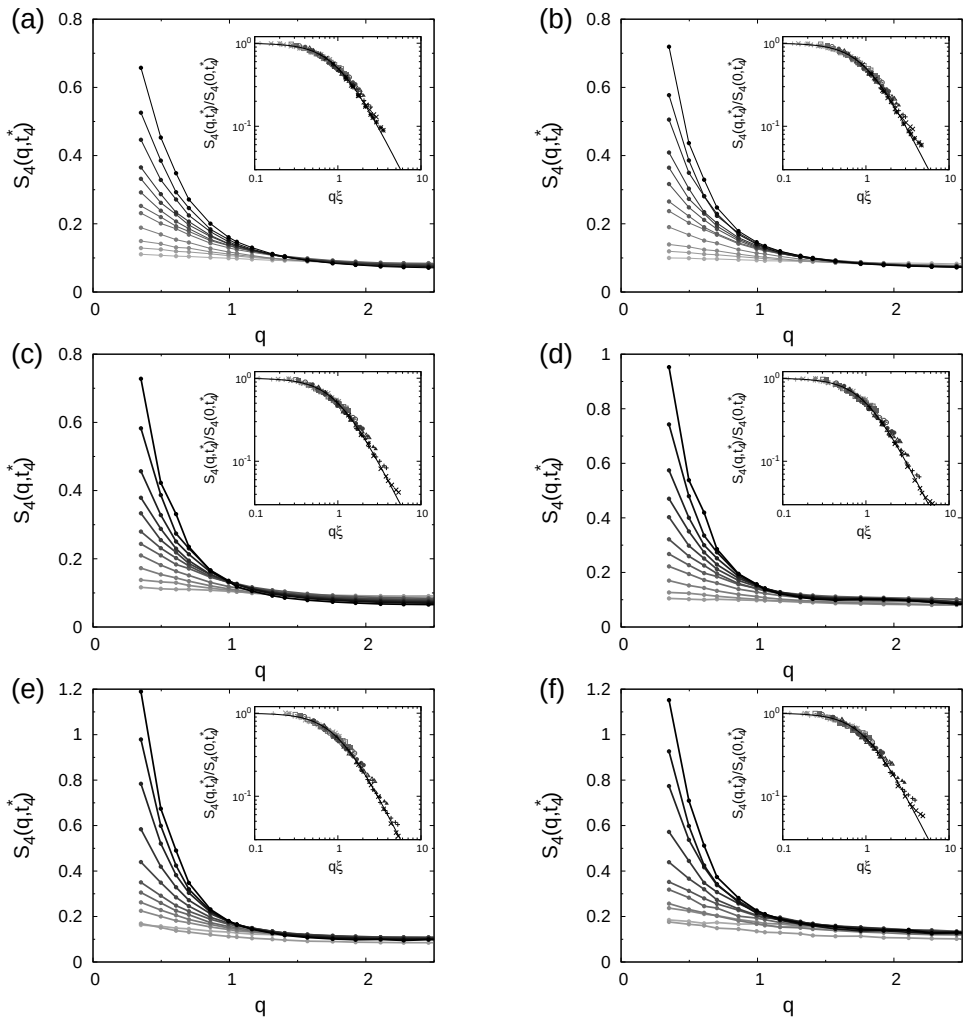

Figure 5.13: Collapse of dynamic structure factor for SCM, ACM and UCM. (a)SCM-cation, (b)SCM-anion, (c)ACM-cation, (d)ACM-anion, (e)UCM-big particle, (f)UCM-small particle. Every data shows good agreement with the function $f(x) = 1/(1 + x^2)$ (solid line).

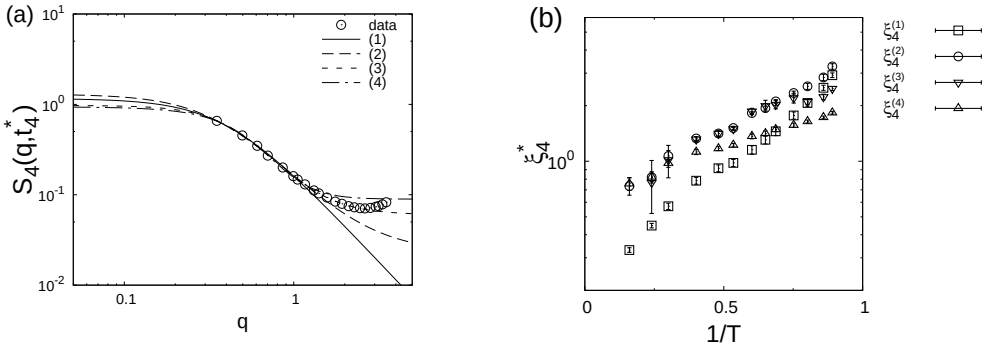

Figure 5.14: Comparison of dynamic length scales obtained from different fitting schemes. (a)Various fitting schemes on the data of cation in SCM, at $T = 1.16$. (b)Temperature dependence of the dynamic correlation lengths.

5.3.3 Scaling laws

We now investigate the power law relations between the dynamic physical quantities we calculated. In various model systems of the supercooled liquids, the scaling law has been found for the dynamic length and time scales.[23,51,61,89,106] It is noticeable that these kinds of relations are originally found in the critical behavior of phase transitions. In our ionic liquid model system, a similar power law relation is discovered. First, we show the relation between t_4^* and χ_4^* in FIG.5.15 For all three systems, the power law relation, $t_4^* \sim \chi_4^{*\delta}$ is found. Another power relation for t_4^* and ξ_4^* is also found, $t_4^* \sim \xi_4^{*\gamma}$, FIG.5.16. As previously observed, there is clear crossover behavior. Interestingly, this crossover behavior is prominent in SCM and ACM which include the charge on the particles. Kim et al. also found the crossover behavior for a glass-forming binary soft-sphere mixture, and addressed that this is due to different physical behaviors at different time scales, which are β-relaxation time, τ_β, and α-relaxation time, τ_α.[87] In this study, τ_β is defined by the minimum value of

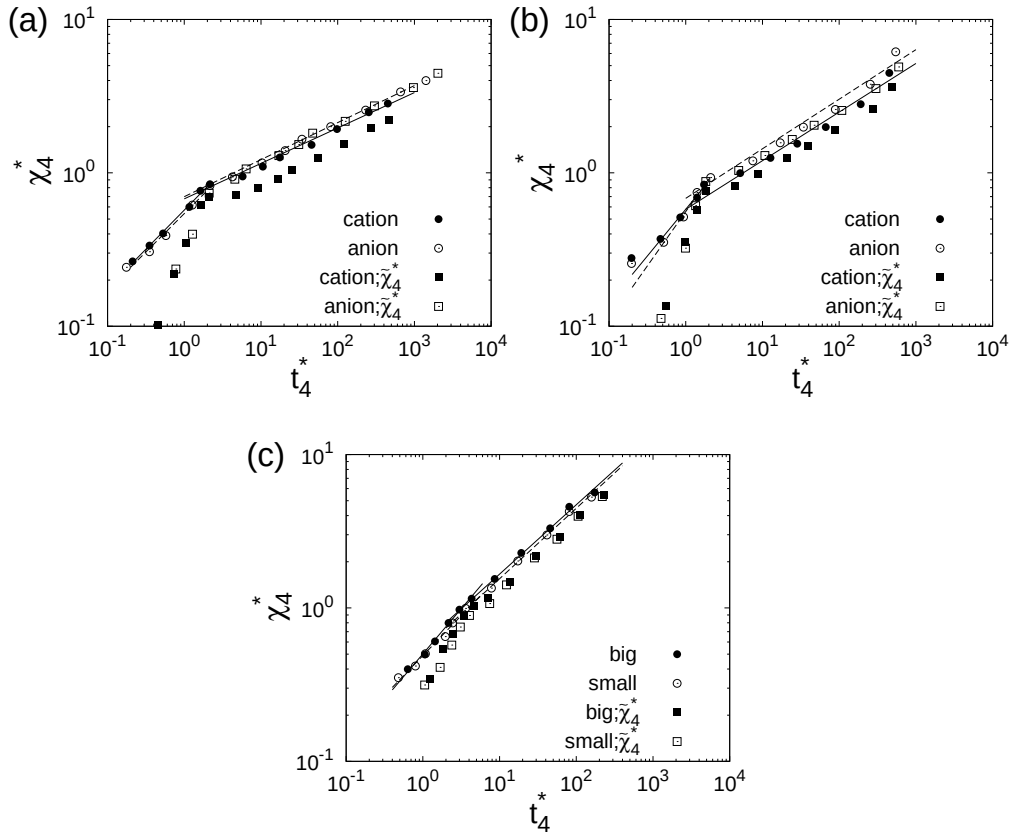

Figure 5.15: Power law relation between t_4^* and χ_4^* is shown for (a)SCM, (b)ACM and (c)UCM. Circle denotes data using χ_4^* and square is for $\tilde{\chi}_4^*$. The crossover behavior is profound in SCM and ACM. The power law exponents using χ_4^* and $\tilde{\chi}_4^*$ are similar at low temperature regime for all three models.

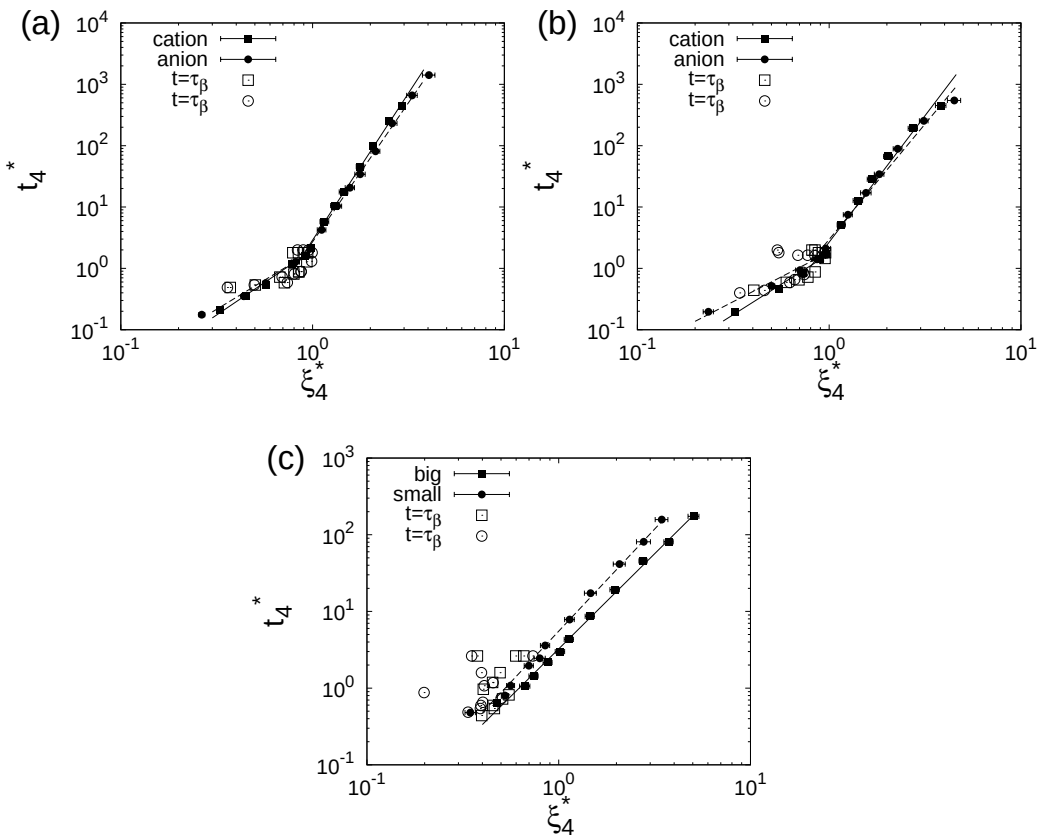

Figure 5.16: Power law relation between t_4^* and ξ_4^* is shown for (a)SCM, (b)ACM and (c)UCM. Circle denotes the data when $t = \tau_\alpha$ and square is for $t = \tau_\beta$. The data at short length scale in condition of $t = \tau_\alpha$ (circle) correspond to the data in condition of $t = \tau_\beta$ (square) in SCM and ACM. The crossover behavior is not observed in UCM.

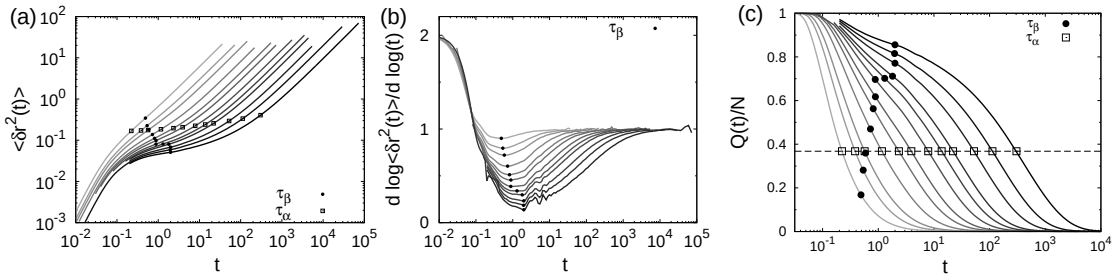

Figure 5.17: Time scales τ_α and τ_β are indicated with square and circle, respectively. The cation in SCM at various temperature (same with FIG.5.9) is used. (a)Mean-squared displacement $\langle \delta \mathbf{r}^2(t) \rangle$ is shown. In the view of mean-squared displacement, τ_β is characteristic time scale for the plateau, while τ_α is the time scale of inset of diffusive regime. (b)Derivative of mean-squared displacement is shown. τ_β is defined as the time value that makes $\mathrm{d}(\ln\langle \delta \mathbf{r}^2(t) \rangle)/\mathrm{d}(\ln t)$ minimum. (c)$Q(t)/N$ is shown. Note that τ_α is defined by the time that makes $Q(\tau_\alpha)/N = 1/e$.

$\mathrm{d}(\ln\langle \delta \mathbf{r}^2(t) \rangle)/\mathrm{d}(\ln t)$, where $\delta \mathbf{r} = \mathbf{r}(t) - \mathbf{r}(0)$. This means that τ_β is the time value of the plateau of mean-squared displacement at each temperature. The mean-squared displacement and its derivative of the cation in SCM is shown in FIG.5.17. As the temperature is lowered, τ_β increases until it reaches maximum value of $t = 2$. Beware that our definition of τ_α and τ_β allows τ_β to be longer than τ_α at high temperatures.

In this sense, τ_β can be interpreted as a characteristic time scale that particles stay in the cage. When the temperature is high, β-relaxation regime is not clearly observed in the time correlation function $Q(t)/N$. However, at low temperature system, slowing down of local dynamics due to the cage effect makes β-relaxation regime distinctive. The onset temperature of this phenomenon is related to the onset of the crossover behavior. When $\xi_4(t)$ is calculated at $t = \tau_\beta$, cations and anions of SCM and ACM have the power law exponent

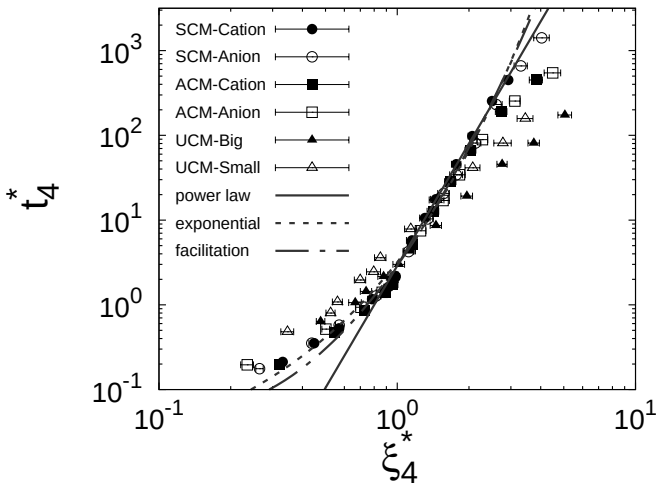

Figure 5.18: Comparison of relations between t_4^* and ξ_4^* for SCM, ACM and UCM. The power law exponent, γ, of cation and anion in SCM and ACM is much larger than the exponent of big and small particle in UCM. Three different functional form is used to fit the data of cation in SCM: (1) $t_4^* \sim \xi_4^{*\gamma}$, (2) $t_4^* \sim \exp(\xi_4^{*z})$, (3) $t_4^* \sim \exp(A(\log(\xi_4^*/B))^2)$.

$\gamma \sim 2$, FIG.5.16. However, when $t = \tau_\alpha$, the exponent is much larger at low temperatures. Such phenomenon is not found in the UCM system since the cage effect of uncharged system is weak compared to the charged systems. This crossover behavior found in SCM and ACM can be thought as a distinguishing property of ionic liquid systems.

When we compare the values of the exponent γ, we find $\gamma_{SCM}^C \sim 4.8$, $\gamma_{ACM}^C \sim 4.1$, and $\gamma_{UCM}^B \sim 2.5$. The exponent of the anion (small particle) is similar to that of the cation (big particle). The exponent values of SCM and ACM are analogous to the result of the previous studies,[24,86,99] and the exponent value of UCM is similar to the Lennard-Johns mixture studied by Lačević

et al.[34] FIG.5.18 clearly shows that the t_4^* of SCM and ACM increases much faster than the t_4^* of UCM, when ξ_4^* is increased. As we can interpret ξ_4^* as a size of the dynamic cluster, same size of the dynamic cluster is preserved longer in time for charged system. This is because the local structure of charged system is highly ordered compared to the structure of uncharged system. Meanwhile, the difference between two charged system, SCM and ACM, is not profound. In spite of the different charge distributions of the cation, the crossover behavior is very similar for two systems and the exponents of the power law between the correlation length and the life time of dynamic heterogeneity have similar values.

Finally, we demonstrate the three fitting schemes to find the relation between t_4^* and ξ_4^*. These fitting schemes have different theoretical bases. First, mode-coupling theory predicts there is a power law relation between two quantities as we already observed,[23,107,108] $t_4^* \sim \xi_4^{*\gamma}$. Second, a Random-First-Order Transition (RFOT) theory suggest the exponential relation,[6,109] $t_4^* \sim \exp(\xi_4^{*z})$. Lastly, the view of the facilitation picture suggests the following relation,[42] $t_4^* \sim \exp(A(\log(\xi_4^*/B))^2)$. FIG.5.18 shows the functions fitted on the data of the cation of SCM using different schemes. The lower fitting range is set to be 0.15 for all functional forms. It seems that the power law relation is most appropriate to describe the data at long length scale. The other two functions show similar exponential behavior. At short length scales, it seems that the exponential function well matches to the data. However, the data at short length scales are governed by a different physical environment, and it may be a coincidence that the functions agree with the data. Note that different behavior of short length regime is due to the cage effect of ionic liquid model. Flenner

et al. reported that there is an universal behavior of supercooled liquids which is a exponential relation between t_4^* and ξ_4^*.[96] In our ionic liquid models, the temperature of the system is not sufficiently low compared to their results. To verify the statement, deeper analysis would be needed.

5.4 Conclusion

In the previous works, heterogeneous dynamics have been found in RTILs using the theoretical schemes which are applied to the supercooled liquids. In this study, we find the evidences of heterogeneous dynamics in the simple ionic liquids models. As the temperature decreases, displacement distribution of the cation and the anion is getting broaden as shown in Fig.5.2. It seems that the broadening of the distribution reaches its maximum when the time is comparable to the relaxation time of each model system. Furthermore, the decoupling of the mean exchange time and the mean persistence time is observed. At low temperatures, the mean persistence time is growing much faster than the mean exchange time as expected from previous studies.[27,49] From the result, we can infer that defined excitation events are correlated each other at sufficiently low temperatures, which is caused by the correlated local motion of the particles.

We adopt four-point correlation function analysis to study how the local densities are correlated in our liquid model systems. To quantify the heterogeneous dynamics, the dynamic susceptibility is calculated based on two different time-correlation functions which are $Q(t)/N$ and $F_s(k,t)$. The time dependence and the temperature dependence of calculated dynamic susceptibility, $\chi_4(t)$ and $\tilde{\chi}_4(t)$, are investigated. Our results illustrate that the dynamic heterogeneity

found in RTILs is transient in time analogous to the situation in the supercooled liquids. Also, the length scale dependence of the dynamic susceptibility is observed by varying the wavevector $\mathbf{k}$ in the $\tilde{\chi}_4(k,t)$ and overlap cutoff a in the $\chi_4(t)$. The length scale dependence show consistence results for both functions. As the length scale is increased, the peak of the dynamic susceptibility is found in longer time and the power law exponent at short time is increased.

We also successfully extract the dynamic correlation length, ξ_4^* by fitting the dynamic structure factor, $S_4(t)$, into the Ornstein-Zernike equation. Calculated quantities such as the lifetime of the dynamic heterogeneity, t_4^*, the maximum value of the dynamic susceptibility, χ_4^*, and the dynamic correlation length ξ_4^* are connected via the power law relations at low temperatures. Interestingly, the crossover behavior around $t_4^* \sim 1$ and $\xi_4^* \sim 1$ is prominent in the charge model, SCM and ACM. We count this phenomenon on the enhanced cage effect due to the existence of charge. The crossover behavior and the peak of the dynamic susceptibility in the short time region $t \sim \tau_\beta$ are not noticeable in the UCM and the previous studies. Note that the shoulder peak is growing as the length scale used in the four-point correlation function is decreased. When the length scale is properly tuned, the crossover behavior may be found in UCM system.

As we vary the charge distribution on the cation particle, the effect of different charge distributions on the glassy dynamics is observed. When the result of UCM is compared with the charged model system, all three models show the heterogeneous dynamics at sufficiently low temperatures. Even if the particles do not have the charge in UCM, the mixture of different shape of particle shows the glassy behavior like other supercooled liquids models. The existence

of charge on the particles mainly affects two aspects of the system. First, the onset temperature of heterogeneous dynamics increases. Because the structures of the charged systems are more stable than the structure of UCM at same temperature, the dynamics is much slower and the temperature which shows heterogeneous dynamics is much higher. Second, the cage effect is enhanced. From the simulation results of dynamic susceptibility and the power law analysis, we confirm that the alternating local structure of cations and anions results strong cage effect. As a result, we find crossover behavior for the power law relation between the time scale and the length scale of the dynamic heterogeneity. Furthermore, the comparison between SCM and ACM reveals that the asymmetric charge distribution makes the system more fragile. However, two models basically show similar behaviors except the onset temperature of dynamic heterogeneity.

Chapter 6

Conclusion

In this thesis, mainly three model systems which show heterogeneous dynamics are investigated using computer simulation method. Considered systems are (1) higher dimensional generalizations of the East models, (2) fragile-to-strong crossover model, (3) simple ionic liquid model. Although the details in each model may differ, they have much in common from the view of dynamic heterogeneity. The evidences of the heterogeneous dynamics are found in each model, and analysis based upon issues on these models are done separately. We conclude the thesis by mentioning the main results of each system.

The main point of the results of higher dimensional generalizations of the East models is that the upper critical dimension of the East model is conjectured to be infinite. As predicted from previous studies, hierarchical nature of facilitation in the East model is so strong that the fragility of the East model is preserved in higher dimensions. We demonstrate that the prediction is convincing, using the power law analysis of the fractional Stokes-Einstein relation found in this model. Obtained power law exponent is decreased as the dimension is increased. In our expectation, however, the exponent would not be 0 in

the finite spatial dimension. The results highlight mainly two points. First, the facilitation condition of the East model is extremely strong that hierarchical dynamics remains in high dimensions. There may be limitation of using the East model to describe molecular systems, especially in high dimensions. The disagreement with the results of the MCT and the molecular dynamics simulation study should be examined in more detailed investigations. Second, there should be a correlation between hierarchical process and the upper critical dimension. Note that the FA model which is non-cooperative and non-hierarchical model has finite upper critical dimension. It would be worth to investigate the dimensional dependence of the model which can control the hierarchical process. The model might have finite upper critical dimension higher than that of the FA model. In the thesis, we assume that the characteristic time scale for the diffusion process exists. We calculated differently defined time scales to find which process is crucial on the movement of probe particles. Among the candidates, shortest waiting time between neighboring kinks is considered to be in good agreement with the diffusive motion of probes. It means that the movement of the probe particle is highly dependent on the fastest change of the environment. Even if the dynamic heterogeneity remains in high dimensions, various evidences of reducing heterogeneity are found. Reduced decoupling of the mean persistence times and the mean exchange times, narrow distribution of the persistence times, decreased dynamic susceptibility are the evidences.

In the 1-dimensional crossover spin facilitated model of supercooled liquids, functions related to dynamic heterogeneity make smooth fragile-to-strong crossover around a certain crossover temperature. The mean persistence time, diffusion constant, and the dynamic length scale clearly show the crossover be-

havior. When the power law behavior of the fractional Stokes-Einstein relation is investigated, crossover behavior is not found. However, we find smooth transition of the exponents from 0.67 to 0.73 when the asymmetric parameter b is reduced. The dynamic crossover is the result of the competition between entropy barrier of symmetric mechanism and energy barrier of asymmetric mechanism. Our simulation results of different physical quantities support this explanation.

Lastly, simple ionic liquid model is used to study the dependence of charge distributions on the heterogeneous dynamics of the system. Three proposed models - symmetrically charged model (SCM), asymmetrically charged model (ACM), uncharged model (UCM) - show heterogeneous dynamics at sufficiently low temperature. The evidences of the heterogeneous dynamics are investigated such as broadening displacement distribution and decoupling of the mean exchange time and the mean persistence time. To quantify the dynamic heterogeneity and to extract the correlation length of the dynamic heterogeneity, we adopt four-point correlation function analysis. The analysis makes it possible to investigate how much the local densities are correlated. The quantification of the dynamic heterogeneity through the dynamic susceptibility reveals that the lifetime of the dynamic heterogeneity increases as the temperature is decreased. The dynamic correlation length is obtained by fitting the dynamic structure factor into the Ornstein-Zernike equation. The dynamic correlation length shows the power law relation with the lifetime of the dynamic heterogeneity. Interestingly, the crossover behavior is prominent in the charged model, SCM and ACM. We attribute this phenomenon to the enhanced cage effect due to the existence of charge. The charge on the particle contributes to the alternating local structure and stabilizing the total energy. However, our simulation results

strongly support that the heterogeneous dynamics of the ionic liquids has its origin to the molecular structure, not to the existence of charge.

In conclusion, we study how the dynamic heterogeneity is appeared in different system with computational method. Using the similar physical basis, we focus on special issues in each research area. We hope that our study would contribute to the understanding of the dynamic heterogeneity and provide a guidance to future studies.

Bibliography

[1] Angell, C. A. Formation of glasses from liquids and biopolymers. *Science* **1995**, *267*, 1924–1935.

[2] Ediger, M. D.; Angell, C.; Nagel, S. R. Supercooled liquids and glasses. *J. Phys. Chem.* **1996**, *100*, 13200–13212.

[3] Angell, C. A.; Ngai, K. L.; McKenna, G. B.; McMillan, P. F.; Martin, S. W. Relaxation in glassforming liquids and amorphous solids. *J. Appl. Phys.* **2000**, *88*, 3113–3157.

[4] Ediger, M. D. Spatially heterogeneous dynamics in supercooled liquids. *Annu. Rev. Phys. Chem.* **2000**, *51*, 99–128.

[5] Debenedetti, P. G.; Stillinger, F. H. Supercooled liquids and the glass transition. *Nature* **2001**, *410*, 259–267.

[6] Lubchenko, V.; Wolynes, P. G. Theory of structural glasses and supercooled liquids. *Annu. Rev. Phys. Chem.* **2007**, *58*, 235–266.

[7] Chandler, D.; Garrahan, J. P. Dynamics on the Way to Forming Glass: Bubbles in Space-Time. *Annu. Rev. Phys. Chem.* **2010**, *61*, 191–217.

[8] Berthier, L.; Biroli, G. Theoretical perspective on the glass transition and amorphous materials. *Rev. Mod. Phys.* **2011**, *83*, 587.

[9] Stillinger, F. H.; Debenedetti, P. G. Glass transition thermodynamics and kinetics. *Annu. Rev. Condens. Matter Phys.* **2013**, *4*, 263–285.

[10] Adam, G.; Gibbs, J. H. On the temperature dependence of cooperative relaxation properties in glass-forming liquids. *J. Chem. Phys.* **1965**, *43*, 139–146.

[11] Cavagna, A. Supercooled liquids for pedestrians. *Physics Reports* **2009**, *476*, 51–124.

[12] Elmatad, Y. S.; Chandler, D.; Garrahan, J. P. Corresponding states of structural glass formers. *J. Phys. Chem. B* **2009**, *113*, 5563–5567.

[13] Goldstein, M. Viscous liquids and the glass transition: a potential energy barrier picture. *J. Chem. Phys.* **1969**, *51*, 3728–3739.

[14] Stillinger, F. H.; Weber, T. A. Hidden structure in liquids. *Phys. Rev. A* **1982**, *25*, 978.

[15] Stillinger, F. H.; Weber, T. A. Dynamics of structural transitions in liquids. *Phys. Rev. A* **1983**, *28*, 2408.

[16] Sillescu, H. Heterogeneity at the glass transition: a review. *J. Non-Cryst. Solids* **1999**, *243*, 81–108.

[17] Richert, R. Heterogeneous dynamics in liquids: fluctuations in space and time. *J. Phys. Condens. Matter* **2002**, *14*, R703.

[18] Glotzer, S. C. Spatially heterogeneous dynamics in liquids: insights from simulation. *J. Non-Cryst. Solids* **2000**, *274*, 342–355.

[19] Andersen, H. C. Molecular dynamics studies of heterogeneous dynamics and dynamic crossover in supercooled atomic liquids. *Proc. Nat. Acad. Sci. USA* **2005**, *102*, 6686–6691.

[20] Lačević, N.; Starr, F. W.; Schrøder, T.; Novikov, V.; Glotzer, S. Growing correlation length on cooling below the onset of caging in a simulated glass-forming liquid. *Phys. Rev. E* **2002**, *66*, 030101.

[21] Berthier, L.; Biroli, G.; Bouchaud, J.-P.; Cipelletti, L.; El Masri, D.; L'Hôte, D.; Ladieu, F.; Pierno, M. Direct experimental evidence of a growing length scale accompanying the glass transition. *Science* **2005**, *310*, 1797–1800.

[22] Pan, A. C.; Garrahan, J. P.; Chandler, D. Heterogeneity and growing length scales in the dynamics of kinetically constrained lattice gases in two dimensions. *Phys. Rev. E* **2005**, *72*, 041106.

[23] Biroli, G.; Bouchaud, J.-P.; Miyazaki, K.; Reichman, D. R. Inhomogeneous mode-coupling theory and growing dynamic length in supercooled liquids. *Phys. Rev. Lett.* **2006**, *97*, 195701.

[24] Flenner, E.; Zhang, M.; Szamel, G. Analysis of a growing dynamic length scale in a glass-forming binary hard-sphere mixture. *Phys. Rev. E* **2011**, *83*, 051501.

[25] Karmakar, S.; Dasgupta, C.; Sastry, S. Growing length scales and their

relation to timescales in glass-forming liquids. *Annu. Rev. Condens. Matter Phys.* **2014**, *5*, 255–284.

[26] Jung, Y.; Garrahan, J. P.; Chandler, D. Excitation lines and the breakdown of Stokes-Einstein relations in supercooled liquids. *Phys. Rev. E* **2004**, *69*, 061205.

[27] Jeong, D.; Choi, M.; Kim, H. J.; Jung, Y. Fragility, Stokes–Einstein violation, and correlated local excitations in a coarse-grained model of an ionic liquid. *Phys. Chem. Chem. Phys.* **2010**, *12*, 2001–2010.

[28] Biroli, G.; Bouchaud, J.-P. Critical fluctuations and breakdown of the Stokes–Einstein relation in the mode-coupling theory of glasses. *J. Phys.: Condens. Matter* **2007**, *19*, 205101.

[29] Franz, S.; Parisi, G.; Ricci-Tersenghi, F.; Rizzo, T. Field theory of fluctuations in glasses. *Eur. Phys. J. E* **2011**, *34*, 102.

[30] Franz, S.; Jacquin, H.; Parisi, G.; Urbani, P.; Zamponi, F. Quantitative field theory of the glass transition. *Proc. Natl Acad. Sci.* **2012**, *109*, 18725–18730.

[31] Charbonneau, P.; Ikeda, A.; Parisi, G.; Zamponi, F. Dimensional study of the caging order parameter at the glass transition. *Proc. Natl Acad. Sci.* **2012**, *109*, 13939–13943.

[32] Del Pópolo, M. G.; Voth, G. A. On the structure and dynamics of ionic liquids. *J. Phys. Chem. B* **2004**, *108*, 1744–1752.

[33] Wang, Y.; Jiang, W.; Yan, T.; Voth, G. A. Understanding ionic liquids through atomistic and coarse-grained molecular dynamics simulations. *Acc. Chem. Res.* **2007**, *40*, 1193–1199.

[34] Lačević, N.; Starr, F. W.; Schrøder, T.; Glotzer, S. Spatially heterogeneous dynamics investigated via a time-dependent four-point density correlation function. *J. Chem. Phys.* **2003**, *119*, 7372–7387.

[35] Ritort, F.; Sollich, P. Glassy dynamics of kinetically constrained models. *Adv. Phys.* **2003**, *52*, 219–342.

[36] Garrahan, J. P.; Sollich, P.; Toninelli, C. Kinetically constrained models. *Dynamical heterogeneities in Glasses, colloids and granular media and jamming transitions, International series of monographs in physics (Oxford University Press, Oxford, 2011) Chap* **2011**, *10*, 341–369.

[37] Jackle, J.; Kronig, A. A kinetic lattice-gas model for the triangular lattice with strong dynamic correlations. I. Self-diffusion. *J. Phys.: Condens. Matter* **1994**, *6*, 7633.

[38] Hedges, L. O.; Garrahan, J. P. Dynamic propensity in a kinetically constrained lattice gas. *J. Phys.: Condens. Matter* **2007**, *19*, 205124.

[39] Kob, W.; Andersen, H. C. Kinetic lattice-gas model of cage effects in high-density liquids and a test of mode-coupling theory of the ideal-glass transition. *Phys. Rev. E* **1993**, *48*, 4364.

[40] Fredrickson, G. H.; Andersen, H. C. Kinetic Ising model of the glass transition. *Phys. Rev. Lett.* **1984**, *53*, 1244.

[41] Jäckle, J.; Eisinger, S. A hierarchically constrained kinetic ising model. *Zeitschrift für Physik B Condensed Matter* **1991**, *84*, 115–124.

[42] Keys, A. S.; Hedges, L. O.; Garrahan, J. P.; Glotzer, S. C.; Chandler, D. Excitations are localized and relaxation is hierarchical in glass-forming liquids. *Phys. Rev. X* **2011**, *1*, 021013.

[43] Donati, C.; Douglas, J. F.; Kob, W.; Plimpton, S. J.; Poole, P. H.; Glotzer, S. C. Stringlike cooperative motion in a supercooled liquid. *Phys. Rev. Lett.* **1998**, *80*, 2338.

[44] Teboul, V.; Monteil, A.; Fai, L.; Kerrache, A.; Maabou, S. An investigation of string-like cooperative motion in a strong network glass-former. *EPJ B* **2004**, *40*, 49–54.

[45] Zhang, H.; Khalkhali, M.; Liu, Q.; Douglas, J. F. String-like cooperative motion in homogeneous melting. *J. Chem. Phys.* **2013**, *138*, 12A538.

[46] Aldous, D.; Diaconis, P. The asymmetric one-dimensional constrained Ising model: rigorous results. *J. Stat. Phys.* **2002**, *107*, 945–975.

[47] Chleboun, P.; Faggionato, A.; Martinelli, F. The influence of dimension on the relaxation process of East-like models: Rigorous results. *Europhys. Lett.* **2014**, *107*, 36002.

[48] Sollich, P.; Evans, M. R. Glassy time-scale divergence and anomalous coarsening in a kinetically constrained spin chain. *Phys. Rev. Lett.* **1999**, *83*, 3238.

[49] Jung, Y.; Garrahan, J. P.; Chandler, D. Dynamical exchanges in facilitated models of supercooled liquids. *J. Chem. Phys.* **2005**, *123*, 084509.

[50] Berthier, L.; Chandler, D.; Garrahan, J. P. Length scale for the onset of Fickian diffusion in supercooled liquids. *Europhys. Lett.* **2005**, *69*, 320.

[51] Berthier, L.; Garrahan, J. P. Numerical study of a fragile three-dimensional kinetically constrained model. *J. Phys. Chem. B* **2005**, *109*, 3578–3585.

[52] Buhot, A.; Garrahan, J. P. Crossover from fragile to strong glassy behaviour in the spin facilitated chain model. *J. Phys.: Condens. Matter* **2002**, *14*, 1499.

[53] Blondel, O.; Toninelli, C. Is there a fractional breakdown of the Stokes-Einstein relation in kinetically constrained models at low temperature? *Europhys. Lett.* **2014**, *107*, 26005.

[54] Charbonneau, B.; Charbonneau, P.; Jin, Y.; Parisi, G.; Zamponi, F. Dimensional dependence of the Stokes–Einstein relation and its violation. *J. Chem. Phys.* **2013**, *139*, 164502.

[55] Bortz, A. B.; Kalos, M. H.; Lebowitz, J. L. A new algorithm for Monte Carlo simulation of Ising spin systems. *J. Comput. Phys.* **1975**, *17*, 10–18.

[56] Ashton, D. J.; Hedges, L. O.; Garrahan, J. P. Fast simulation of facilitated spin models. *J. Stat. Mech.: Theor. Exp.* **2005**, *2005*, P12010.

[57] Hedges, L. O.; Maibaum, L.; Chandler, D.; Garrahan, J. P. Decoupling

of exchange and persistence times in atomistic models of glass formers. *J. Chem. Phys.* **2007**, *127*, 211101.

[58] Elmatad, Y. S.; Keys, A. S. Manifestations of dynamical facilitation in glassy materials. *Phys. Rev. E* **2012**, *85*, 061502.

[59] Léonard, S.; Berthier, L. Lifetime of dynamic heterogeneity in strong and fragile kinetically constrained spin models. *J. Phys.: Condens. Matter* **2005**, *17*, S3571.

[60] Glotzer, S. C.; Novikov, V. N.; Schrøder, T. B. Time-dependent, four-point density correlation function description of dynamical heterogeneity and decoupling in supercooled liquids. *J. Chem. Phys.* **2000**, *112*, 509–512.

[61] Whitelam, S.; Berthier, L.; Garrahan, J. P. Renormalization group study of a kinetically constrained model for strong glasses. *Phys. Rev. E* **2005**, *71*, 026128.

[62] Jack, R. L.; Mayer, P.; Sollich, P. Mappings between reaction–diffusion and kinetically constrained systems: A+A↔A and the Fredrickson–Andersen model have upper critical dimension $d_c = 2$. *J. Stat. Mech.: Theor. Exp.* **2006**, *2006*, P03006.

[63] Eaves, J. D.; Reichman, D. R. Spatial dimension and the dynamics of supercooled liquids. *Proc. Natl Acad. Sci.* **2009**, *106*, 15171–15175.

[64] Sengupta, S.; Karmakar, S.; Dasgupta, C.; Sastry, S. Breakdown of the Stokes-Einstein relation in two, three, and four dimensions. *J. Chem. Phys.* **2013**, *138*, 12A548.

[65] Buhot, A.; Garrahan, J. P. Crossover from fragile to strong glassy behavior in kinetically constrained systems. *Phys. Rev. E* **2001**, *64*, 021505.

[66] Pan, A. C.; Garrahan, J. P.; Chandler, D. Decoupling of Self-Diffusion and Structural Relaxation during a Fragile-to-Strong Crossover in a Kinetically Constrained Lattice Gas. *ChemPhysChem* **2005**, *6*, 1783–1785.

[67] Garrahan, J. P.; Chandler, D. Coarse-grained microscopic model of glass formers. *Proc. Natl. Acad. Sci. U.S.A.* **2003**, *100*, 9710–9714.

[68] Ito, K.; Moynihan, C. T.; Angell, C. A. Thermodynamic determination of fragility in liquids and a fragile-to-strong liquid transition in water. *Nature* **1999**, *398*, 492–495.

[69] Faraone, A.; Liu, L.; Mou, C.-Y.; Yen, C.-W.; Chen, S.-H. Fragile-to-strong liquid transition in deeply supercooled confined water. *J. Chem. Phys.* **2004**, *121*, 10843–10846.

[70] Chen, S.-H.; Liu, L.; Chu, X.; Zhang, Y.; Fratini, E.; Baglioni, P.; Faraone, A.; Mamontov, E. Experimental evidence of fragile-to-strong dynamic crossover in DNA hydration water. *J. Chem. Phys.* **2006**, *125*, 171103.

[71] Zhang, C.; Hu, L.; Yue, Y.; Mauro, J. C. Fragile-to-strong transition in metallic glass-forming liquids. *J. Chem. Phys.* **2010**, *133*, 014508.

[72] Mallamace, F.; Branca, C.; Corsaro, C.; Leone, N.; Spooren, J.; Chen, S.-H.; Stanley, H. E. Transport properties of glass-forming liquids suggest that dynamic crossover temperature is as important as the glass transition temperature. *Proc. Natl. Acad. Sci. U.S.A.* **2010**, *107*, 22457–22462.

[73] Berthier, L.; Biroli, G.; Bouchaud, J.-P.; Cipelletti, L.; van Saarloos, W. *Dynamical heterogeneities in glasses, colloids, and granular media*; Oxford University Press, 2011.

[74] Garrahan, J. P.; Chandler, D. Geometrical explanation and scaling of dynamical heterogeneities in glass forming systems. *Phys. Rev. Lett.* **2002**, *89*, 035704.

[75] Darst, R. K.; Reichman, D. R.; Biroli, G. Dynamical heterogeneity in lattice glass models. *J. Chem. Phys.* **2010**, *132*, 044510.

[76] Kumar, S. K.; Szamel, G.; Douglas, J. F. Nature of the breakdown in the Stokes-Einstein relationship in a hard sphere fluid. *J. Chem. Phys.* **2006**, *124*, 214501.

[77] Kumar, P.; Buldyrev, S.; Becker, S.; Poole, P.; Starr, F. W.; Stanley, H. Relation between the Widom line and the breakdown of the Stokes–Einstein relation in supercooled water. *Proc. Natl. Acad. Sci. U.S.A.* **2007**, *104*, 9575–9579.

[78] Xu, L.; Mallamace, F.; Yan, Z.; Starr, F. W.; Buldyrev, S. V.; Stanley, H. E. Appearance of a fractional Stokes–Einstein relation in water and a structural interpretation of its onset. *Nat. Phys.* **2009**, *5*, 565–569.

[79] Kim, K.; Saito, S. Multiple length and time scales of dynamic heterogeneities in model glass-forming liquids: A systematic analysis of multi-point and multi-time correlations. *J. Chem. Phys.* **2013**, *138*, 12A506.

[80] Klameth, F.; Henritzi, P.; Vogel, M. Static and dynamic length scales

in supercooled liquids: Insights from molecular dynamics simulations of water and tri-propylene oxide. *J. Chem. Phys.* **2014**, *140*, 144501.

[81] Jung, Y.; Kim, S.; Garrahan, J. P.; Chandler, D. Comment on "Is there a breakdown of the Stokes-Einstein relation in Kinetically Constrained Models at low temperature?" by O. Blondel and C. Toninelli, arXiv:1307.1651. 2013.

[82] Holbrey, J.; Seddon, K. Ionic liquids. *Clean Prod. Process.* **1999**, *1*, 223–236.

[83] Wasserscheid, P.; Keim, W. Ionic liquids-new "solutions" for transition metal catalysis. *Angew. Chem.* **2000**, *39*, 3772–3789.

[84] Weingärtner, H. Understanding ionic liquids at the molecular level: facts, problems, and controversies. *Angew. Chem. Int. Ed.* **2008**, *47*, 654–670.

[85] Charbonneau, P.; Tarjus, G. Decorrelation of the static and dynamic length scales in hard-sphere glass formers. *Phys. Rev. E* **2013**, *87*, 042305.

[86] Berthier, L. Time and length scales in supercooled liquids. *Phys. Rev. E* **2004**, *69*, 020201.

[87] Kim, K.; Saito, S.; Miyazaki, K.; Biroli, G.; Reichman, D. R. Dynamic Length Scales in Glass-Forming Liquids: An Inhomogeneous Molecular Dynamics Simulation Approach. *J. Phys. Chem. B* **2013**, *117*, 13259–13267.

[88] Toninelli, C.; Wyart, M.; Berthier, L.; Biroli, G.; Bouchaud, J.-P. Dy-

namical susceptibility of glass formers: Contrasting the predictions of theoretical scenarios. *Phys. Rev. E* **2005**, *71*, 041505.

[89] Stein, R. S.; Andersen, H. C. Scaling analysis of dynamic heterogeneity in a supercooled Lennard-Jones liquid. *Phys. Rev. Lett.* **2008**, *101*, 267802.

[90] Wang, C.-Y.; Ediger, M. How long do regions of different dynamics persist in supercooled o-terphenyl? *J. Phys. Chem. B* **1999**, *103*, 4177–4184.

[91] Cicerone, M. T.; Ediger, M. Relaxation of spatially heterogeneous dynamic domains in supercooled ortho-terphenyl. *J. Chem. Phys.* **1995**, *103*, 5684–5692.

[92] Schmidt-Rohr, K.; Spiess, H. Nature of nonexponential loss of correlation above the glass transition investigated by multidimensional NMR. *Phys. Rev. Lett.* **1991**, *66*, 3020.

[93] Heuer, A.; Wilhelm, M.; Zimmermann, H.; Spiess, H. W. Rate memory of structural relaxation in glasses and its detection by multidimensional NMR. *Phys. Rev. Lett.* **1995**, *75*, 2851.

[94] Dasgupta, C.; Indrani, A.; Ramaswamy, S.; Phani, M. Is there a growing correlation length near the glass transition? *Europhys. Lett.* **1991**, *15*, 307–312.

[95] Chandler, D.; Garrahan, J. P.; Jack, R. L.; Maibaum, L.; Pan, A. C. Lengthscale dependence of dynamic four-point susceptibilities in glass formers. *Phys. Rev. E* **2006**, *74*, 051501.

[96] Flenner, E.; Staley, H.; Szamel, G. Universal features of dynamic heterogeneity in supercooled liquids. *Phys. Rev. Lett.* **2014**, *112*, 097801.

[97] Flenner, E.; Szamel, G. Dynamic heterogeneities above and below the mode-coupling temperature: Evidence of a dynamic crossover. *J. Chem. Phys.* **2013**, *138*, 12A523.

[98] Flenner, E.; Szamel, G. Dynamic heterogeneity in a glass forming fluid: Susceptibility, structure factor, and correlation length. *Phys. Rev. Lett.* **2010**, *105*, 217801.

[99] Flenner, E.; Szamel, G. Anisotropic spatially heterogeneous dynamics on the α and β relaxation time scales studied via a four-point correlation function. *Phys. Rev. E* **2009**, *79*, 051502.

[100] Young, A. P. *Spin glasses and random fields*; World Scientific, 1997.

[101] Malvaldi, M.; Chiappe, C. From molten salts to ionic liquids: effect of ion asymmetry and charge distribution. *J. Phys. Condens. Matter* **2008**, *20*, 035108.

[102] Roy, D.; Patel, N.; Conte, S.; Maroncelli, M. Dynamics in an idealized ionic liquid model. *J. Phys. Chem. B* **2010**, *114*, 8410–8424.

[103] Weeks, J. D.; Chandler, D.; Andersen, H. C. Role of repulsive forces in determining the equilibrium structure of simple liquids. *J. Chem. Phys.* **1971**, *54*, 5237–5247.

[104] Pronk, S.; Páll, S.; Schulz, R.; Larsson, P.; Bjelkmar, P.; Apostolov, R.; Shirts, M. R.; Smith, J. C.; Kasson, P. M.; van der Spoel, D. GRO-

MACS 4.5: a high-throughput and highly parallel open source molecular simulation toolkit. *Bioinformatics* **2013**, *29*, 845.

[105] Park, S.-W.; Kim, S.; Jung, Y. Relation between the dynamic heterogeneity time scale and the structural relaxation length scale in ionic liquids systems. *Phys. Chem. Chem. Phys.* **2015** (submitted).

[106] Whitelam, S.; Berthier, L.; Garrahan, J. P. Dynamic criticality in glass-forming liquids. *Phys. Rev. Lett.* **2004**, *92*, 185705.

[107] Biroli, G.; Bouchaud, J.-P. Diverging length scale and upper critical dimension in the Mode-Coupling Theory of the glass transition. *Europhys. Lett.* **2004**, *67*, 21.

[108] Szamel, G. Divergent four-point dynamic density correlation function of a glassy suspension. *Phys. Rev. Lett.* **2008**, *101*, 205701.

[109] Kirkpatrick, T.; Thirumalai, D.; Wolynes, P. G. Scaling concepts for the dynamics of viscous liquids near an ideal glassy state. *Phys. Rev. A* **1989**, *40*, 1045.

국문초록

동력학적 불균일성은 과냉각액체의 특이한 성질들을 잘 설명할 수 있고, 이로 인해 많은 주목을 받아왔다. 본 학위논문에서는, 전산모사 방법을 통해 동력학적으로 불균일한 계에 대한 연구결과를 소개한다.

첫 번째로, 동적 구속 모형을 이용하여 구현한 과냉각액체의 차원에 따른 동력학적 불균일성의 변화를 살펴보았다. 약한 과냉각액체를 구현하기 위하여 1차원 이스트 모델과 이의 고차원 확장 모델을 사용하였다. 또한, 상위 임계 차원을 구하기 위하여 스토크스-아인슈타인 관계의 깨짐 현상을 살펴보았다. 본 연구에 따르면, 기존에 수행되었던 강체 모형이나 평균장 이론 연구들과는 달리, 이스트 모델은 무한한 상위 임계 차원을 가질 것으로 예상된다.

두 번째로, 비대칭 계수 b를 이용하여 강한액체의 행동과 약한액체의 행동을 조율하는 교차모델에서의 동력학적 불균일성을 연구하였다. b의 변화에 따른 스토크스-아인슈타인 관계의 변화에 대한 연구가 수행되었다. b가 고정되면, 온도의 변화에 따라 일정한 멱법칙 상수를 가지며, 그 값은 강한 액체와 약한 액체 중간의 값을 가진다. 비대칭 계수 b가 작아짐에 따라 멱법칙 상수의 값이 0.66 에서 0.73 으로 부드럽게 변화하는 것이 관측되었다.

마지막으로, 이온성 액체의 대단위 모형에서 나타나는 동력학적 불균일성과 그 길이 축척에 대한 연구를 수행하였다. 이온성 액체는 두 개의 구로 이루어진 양이온과 한 개의 구로 이루어진 음이온을 사용하여 모델링되었다. 전하의 분포에

따른 영향을 살펴보고 위하여 다른 전하분포를 가지는 두가지 이온성 액체 모델이 제안되었으며, 대조군으로 전하를 띠지 않는 모델 또한 고려되었다. 온도가 낮아짐에 따라, 세가지 이온성 액체 모델에서 모두 동력학적 불균일성이 급격하게 증가하는 것이 관측되었다. 나아가, 잘 알려진 네-점 감수율을 통하여 동력학적 불균일성을 정량화하였다. 동력학적 상관 길이 또한 동력학적 구조 인자를 온스타인-제르니케 함수로 근사하여 계산되었다. 얻어진 시간 축척과 길이 축척간에는, 과냉각액체에서 비슷한, 멱법칙이 발견되었다. 특히, 전하가 존재하는 모델에서는 다른 모델과 달리 교차 거동의 양상이 발견되었다. 이러한 교차 거동은 전하의 존재로 인해 향상된 바구니 효과 때문인 것으로 생각된다.

주요어 : 동력학적 불균일성, 동적 구속 모형, 스토크스-아인슈타인 관계, 상온이온성 액체, 몬테-카를로 전산모사, 분자 동력학 전산모사

학번 : 2008-20308